Pulse Shape Discrimination

with Liquid Organic Scintillators.

thesis

submitted by

Alasdair Stewart Hall, B.Sc.

for the degree of

Master of Science.

University of Edinburgh

August, 1971.

EDINBURGH

ABSTRACT

The techniques of gamma-neutron pulse shape discrimination are reviewed in detail and the problems associated with assessing their performance considered. The experimental procedures and precautions necessary to obtain good discrimination are established. Results are obtained from an experimental comparison of four techniques used in conjunction with three photomultipliers and various scintillators. Conclusions are reached regarding the relative merits of these techniques, tubes and scintillators and the best combinations for good pulse shape discrimination.

CONTENTS.

CHAPTER 1.

Introduction and Review of past work in Pulse Shape Discrimination. Page 1.

CHAPTER 4.

Pulse Shape Discrimination by the timing technique.

CHAPTER 1.

Introduction and Review of past work in Pulse Shape Discrimination.

1-1 Introduction and Objectives.

In general, pulse shape discrimination is a process whereby one may distinguish between differently formed signals, independently of the size of , or the area under the pulse (fig.1). The identity of a particle passing through a detector may thus be revealed if the excitations in its track give rise to a distinctive pulse shape. Certain scintillation detectors using either organic or inorganic scintillators are very well suited for this function because the light they emit decays differently according to the identity of the initiating radiation. The choice of scintillator in most experiments is governed by several factors of varying importance; below are listed examples of these: light output relative to anthracene, the decay time constant of the major light components (τ_s), and in each case the particle discrimination obtained by exploiting their pulse shape properties.

Type	Scintillator	Light O/P	τ_s(ns)	P'cle Disc.
Inorganic crystal	NaI(Tl)	230	250	e-p e-α
Organic	Anthracene	100	32	α-e p-e
crystal	Stilbene	50	~6.2	e-p
Liquid	NE213	80	~3.6	e-p
Plastic	Naton136,NE102	50	~2	e-p

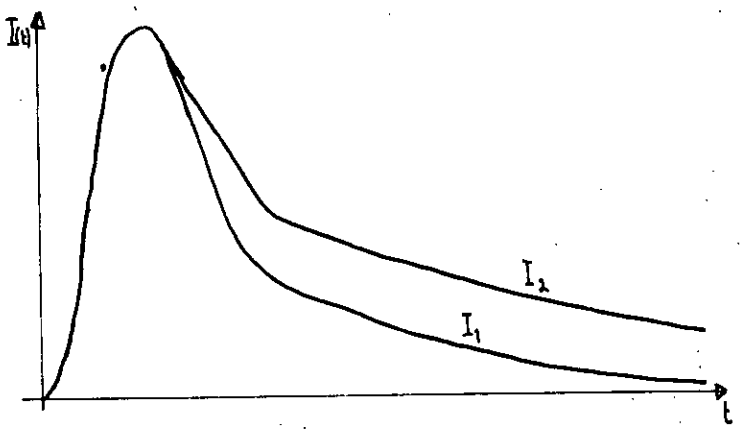

Fig.1: Two pulses distinguishable by pulse shape discrimination.

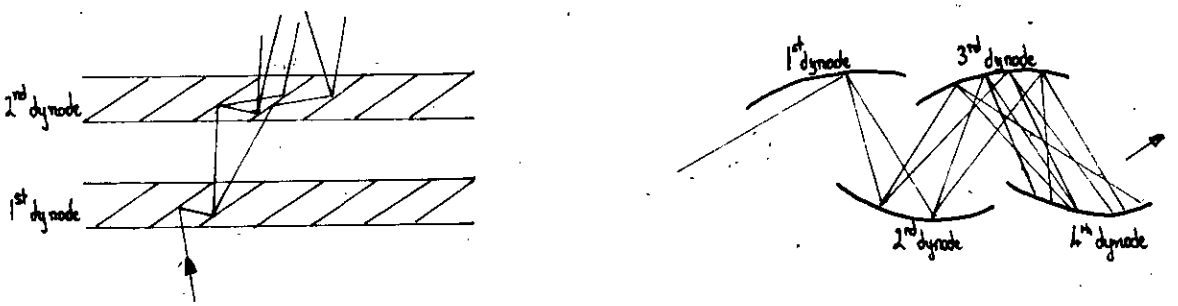

Venetian-blind dynodes

linear structure

Fig.2: Two types of dynode construction.

Note that while NaI (Tl) has the best light output and the plastics give the best timing resolution, it is NE213 that provides the best compromise between these characteristics of importance.

The choice of photomultiplier is governed by the required face diameter, timing resolution and gain, and, particularly in multidetector systems, the cost is most important. These parameters are noted below for two 2" diameter tubes of different structure.

Table 2.

Type(fig.2)	No. of stages.	Variance of pulse transit time.	Gain	Cost
Unfocussed Venetian Blind (6097B)	11	14ns	10^6	£35
Focussed Linear (56AVP)	14	4ns	10^8	£100

1-1.1 Objectives.

After reviewing the previous work in the field of pulse shape discrimination (P.S.D.), consideration is given to the basic limitations of the system to be used with particular reference to an eleven-stage venetian-blind tube. The performance of P.S.D. is then compared using different techniques, tubes and organic scintillators in order to determine the best combination from the points of view of discrimination obtained and economy. Organic scintillators are used for their comparatively high neutron

efficiency and the discrimination techniques are applied to distinguish between these and the invariably attendant gamma-rays. The objective is thus to increase neutron acceptance and gamma rejection ratios over as large an energy range as possible.

In particular cases the dependence on source energy spectrum, count rate, energy threshold, scintillator size, and the effect of light guides is ascertained. Incidental measurements are also made on the relative light output of various scintillators and and the P.S.D. properties of a variety of plastic scintillators.

1-2 REVIEW:

The techniques of pulse shape discrimination (P.S.D.) were reviewed by Owen in 1962 (1) and more recently by McBeth (2). A clear distinction may be drawn between those techniques which compare the charge collected in various parts of a scintillation pulse and those involving some form of timing on the shaped detector pulse (3). Into a third category fall those methods involving some special filtering or sampling of the detector pulse. The effectiveness of a scintillator for pulse shape discrimination depends on the degree to which certain modes of excitation are identifiably associated with different types of radiation. The mechanisms governing these processes have been authoritatively considered by Birks (4), and the present state of knowledge is best reviewed in the 1970 Scintillator Conference Proceedings (5); the application and development of these scintillators for shape discrimination has been considered by

Horrocks (6). No particular attention has been paid to the choice of photomultiplier apart from remarks by Owen (7) concerning his own technique and some general conclusions by Gatti (8) relating to the timing technique.

1-2.1 Measuring Pulse Shape Discrimination Performance.

Reference has been made to the yardstick of gamma rejection and neutron acceptance by which performance may be judged. These figures are given as proportions of the total numbers of the gammas and neutrons detected, and as such should be distinguished from the absolute detection efficiencies which take account both of the discrimination obtained and of the efficiency of the scintillator. This absolute efficiency is only quoted when no other figures are available. Further criteria have been generally adopted for methods producing pulse height distributions as shown (fig.3). The figure-of-merit:(9)

$$M = \frac{\text{peak separation}}{\text{gamma+neutron FWHMs}}$$

and the peak-to-valley (P/V) ratio (10) allow easy visualisation of performance, but cam be misleading if used for comparative purposes ((11) see also Sect.3-2.4). Since the discrimination performance is dependent on the pulse size, the lower limit being set by fluctuations in scintillator excitations (1), these performance figures should be quoted at or above specific energies (9,12). For similar reasons gamma rejection ratios obtained with $\sim$ 1Mev gamma sources may be significantly better than obtained in practice, say, with a Po - Be source producing

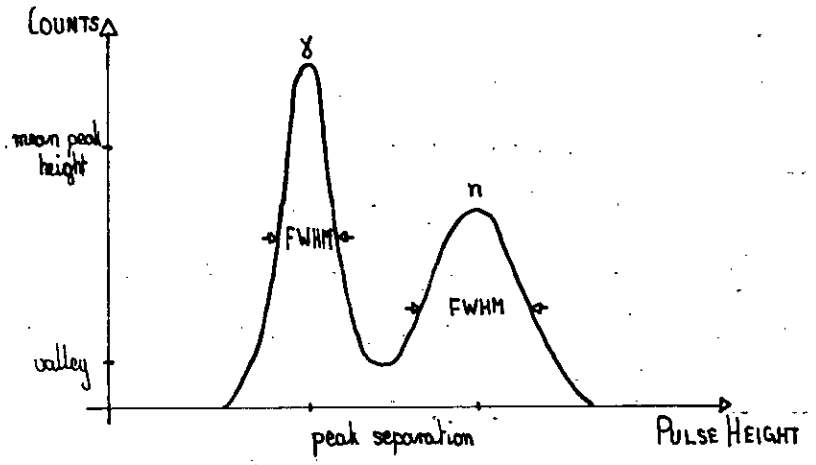

Fig. 3: To illustrate figure-of-merit definitions.

4.5 Mev gamma-rays.

The ability to distinguish pulses is also a function of count rate. Unless some form of dead-time protection circuitry is used (13) the point at which pulse overlap distortion occurs depends on a relation between count rate and circuit resolving time (14). The effect on gamma rejection has been shown by de Vries (15). In certain cases where an intense gamma-ray background vastly outnumbers the neutrons detected (16) a technique is judged by its ability to identify these few neutrons while accepting a minimum of falsely identified gamma-rays.

1-3 The Charge Comparison Technique.

The scintillators considered have two main components of decay. These may be fitted by a rapid plus a slower decay exponential with characteristic time constants (17) except for the particular case of Stilbene (18). It is however the proportions of fast and slow components which are used to identify particles in the charge comparison technique. The photomultiplier acts as a low distortion amplifier, translating the form of the light scintillation into a charge collection profile (fig.1).

1-3.1 "Fast-total" comparison.

The charge comparison technique takes several forms, the first historically being adopted in Owen's 2-dimensional display (19). Brooks (20) adapted it for detection purposes obtaining the fast portion of the pulse from a clipped anode output and a longer portion from the previous dynode. Amplification in the two branche.

was arranged such that the sum of the pulses was negative or positive according to the identity of the exciting radiation (fig.4). The shaped anode pulse acted as a radiation independent arbiter. Absolute efficiences of .007% and 9.5% were claimed for gammas and neutrons from Po-Be. Stilbene produced reasonable discrimination at a slightly lower energy than did liquid scintillator; but no difference was detected for a variety of tubes with transit times of 2 - 20ns.

Many similar techniques have been reviewed by Owen (1) variously selecting from the first ten to first 100ns as representing the fast part of the pulse. Since his survey, various developments have occurred. Jackson (21) established that the fraction of light in the fast signal would have to be at least 50% greater for gammas than for neutrons for complete separation. He reasoned also that, for best results, the resolving time required, in this case about 20ns, should be similar in magnitude to the transit time of the photo-tube used. His comparison of fast and slow tubes substantiated this. The performance obtained compares unfavourably with Reid's results (9) who also considered a range of scintillators. Typically, he obtained a figure-of-merit of 1.9 at (rather than above) 0.8Mev equivalent electron energy for an Am-Be source and NE213 scintillator. According to his assumptions, this corresponded to a neutron acceptance of 99.995% and a gamma acceptance ratio of $5 : 10^5$. Reasonable discrimination appeared feasible down to 250 kev.

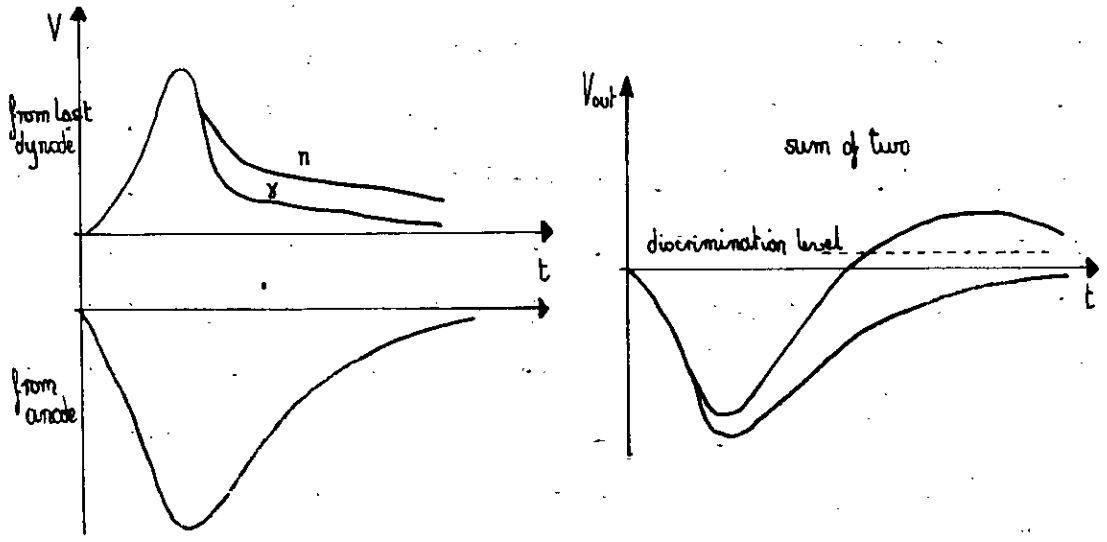

Fig.4: The processing involved in Brooks pulse shape discrimination.

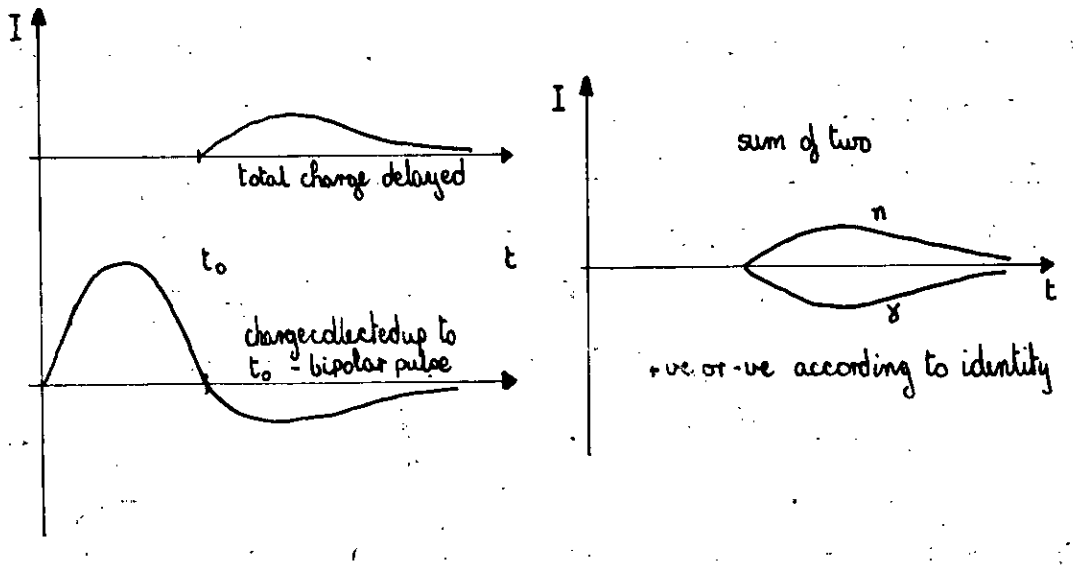

Fig.5: The technique devised by Saltah & Suhami

Hereafter, most methods used a single dynode output for processing, consequently avoiding the effect of interstage gain fluctuations. A superior circuit based on this principle was devised in 1968 (3)(fig,5). It produced 99.9% gamma rejection and virtually 100% neutron acceptance above a neutron energy of 60 kev and at a count rate of 1kcps. This was checked with gammas from Am^{241}(60kev) and D-D neutrons. The dynamic range of the circuit limits the working neutron energy range to 0 - 30 Mev.

A comparative analysis of performance with various tubes and scintillators followed shortly (22) and the circuit is now produced commercially(23,24). Various versions of this have been devised since: Jones used the anode output of an RCA6810A photomultiplier in similar fashion (14) but only obtained useful discrimination down to 200kev neutron energy with his integrated circuit version (25)(however this was for a count rate of 10^5cps). Czirr used a deuterated version of NE213 with an XP1040 tube which, although reducing neutron capture background by a factor of ten, produced unimpressive results (147). Inferior performance has also been obtained using fast, total charge comparisons with Russian tubes (26,27).

1-3.2 "Fast-slow" Comparison.

Since the fast component for electrons and protons in an organic scintillator has the same shape, an alternative approach by Daehnick and Sherr (28) compared the ratio of fast/slow amplitudes, or in practice, the fast negative and slow positive

pulses from the anode and last dynode respectively (fig.6). This corresponded to a comparison of charge collected in the first 10ns and after 100ns. A rejection ratio of 10^4 : 1 was obtained for 1 Mev gamma sources at 500cps but this deteriorated rapidly with count rate. In common with other circuits of this type, only the identified neutron pulses result in output pulses. However, Richter (29) has described modifications whereby gamma identifying pulses may also be produced from this system. Little improvement in count rate performance was obtained by Mendell (30), but a system using the commercial version of this circuit (31) was sufficiently sensitive to identify gamma-rays and neutrons correctly in a comparatively intense gamma background (1 : 10^3) (16). A faster system devised by Bertin (32) compared the charge arriving in the first 50ns with that between 60ns and 200ns; this produced a 98% gamma rejection ratio above 750kev equivalent electron energy with a 4% absolute neutron efficiency falling to 1.8% above 250kev.

1-3.3 "Slow-total" Comparison.

The obvious alternative, a comparison of the slow and total pulse amplitude was used by St.Onge and Lockwood (33,34) taking a single pulse from the anode (fig.7). The supposed advantage of this method is the avoidance of saturation and non-linearity associated with the fast component in the photomultiplier. They obtained an $M > 3.1$ at 1 Mev electron energy, and a usable P.S.D. over a range from 1 to 20 Mev neutron energy.

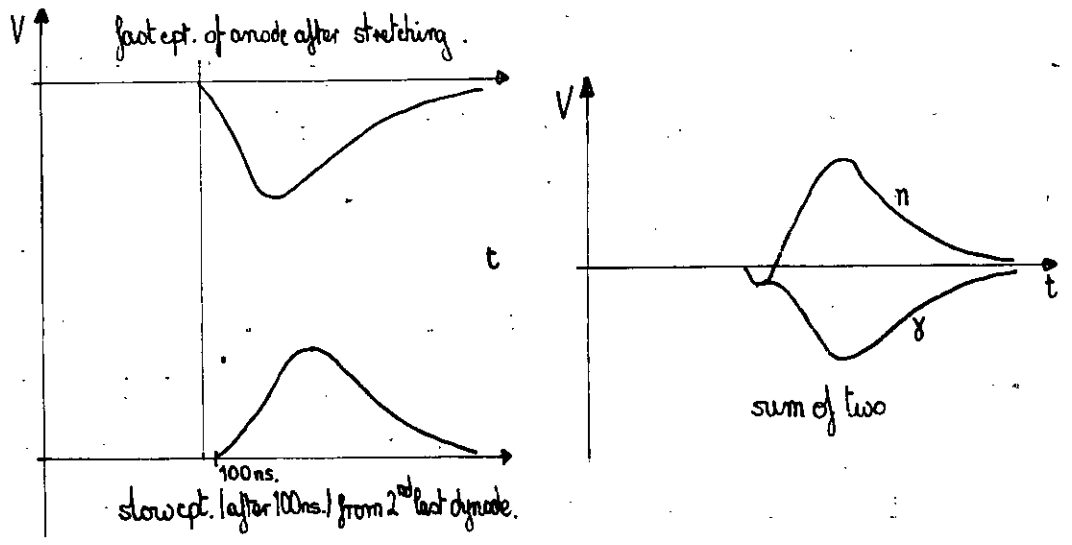

Fig.6: Schematic explanation of the Paehnick + Shenr method.

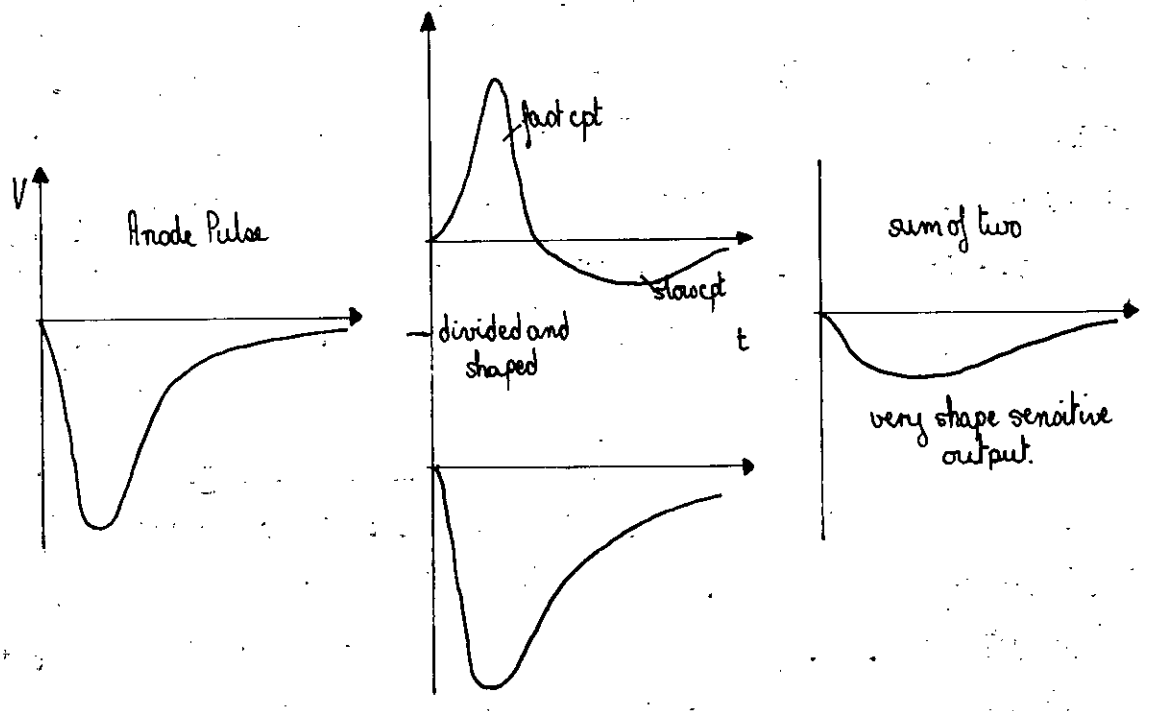

Fig.7: The single example of 'slow-total' comparison.

1-3.4 Criticisms.

Horrocks (35) has made general criticisms of these circuits on the grounds that they are based on the relative amplitude of the slow component. Thus at low neutron energies when the amplitude of this is small, discrimination is poor. It was probably in answer to such and further criticisms regarding non-linearity of stretching diodes and pulse pile-up that de Vries and Udo (15) devised their sophisticated fast-total comparison circuit. It had a 0.1μs resolving time, rejection ratios of 1 : 10^4 at 1 Mev electron energy and handled a 0.5 - 30 Mev neutron energy range. The problem of non-linearity in different branches of a comparison circuit has also been considered by Jones (25). As opposed to Horrocks' comments, Sabbah (3) has produced a mathematical argument calculating the time dispersion of the charge comparison and zero-crossing methods at various energies, and he suggested that below 600kev electron energy the charge comparison method was superior to any timing technique.

1-4 The Timing Techniques.

The timing techniques may be divided into two main groups. The first of these shapes a photomultiplier output pulse by one of a large variety of methods to produce a bipolar pulse which changes polarity at a point in time which is strongly dependent on the shape of the charge collection profile. Since the discrimination is based on the time elapsing between the start

of the pulse and the point of crossing the zero amplitude axis, these are referred to as zero cross-over timing techniques. A second group consists of those methods which obtain some measure of the rate of charge collection. This is represented as the time elapsing between the attainment of certain percentages of the integrated voltage pulse amplitude and so might be referred to as constant fractions of pulse height timing techniques. These techniques are largely independent of or take account of the amplitude of the pulse to be processed. The general remarks made previously (sect. 1-2) apply equally well here though in particular one can see more justification for Gatti's preference for fast phototubes in this context. There is some importance in determining what type of shaping allows the most significant timing information to be extracted, and, particularly for the zero cross-over technique, what circuitry allows the most accurate time-marking. Some attention must also be paid to the process of time-to-analog conversion.

1-4.1 Zero cross-over timing.

The early attempts at zero cross-over timing have again been reviewed by Owen (1) but it is worth repeating Forte's (36) observation that the use of a single dynode output avoids the effects of interstage gain fluctuations and leaves the anode free for other purposes. Roush (11) performed the first systematic appraisal of shaping techniques. With an initial short integration the optimum values were obtained for bipolar pulse forming with

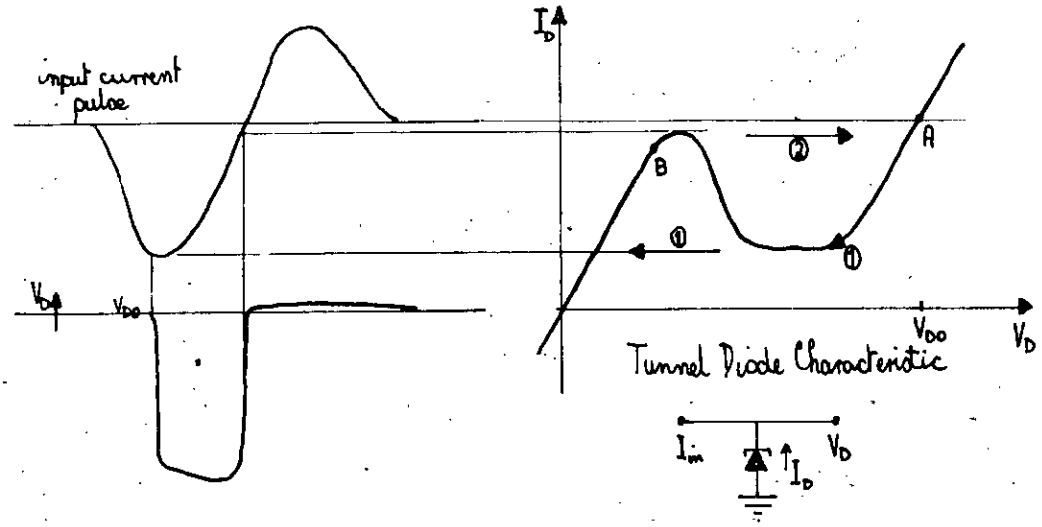

① Transition from operating point Ⓐ as input pulse decreases.

② Transition from 'low' to 'high' voltage as input pulse exceeds the threshold - the fast transition

Ⓑ The 'ready' operating point at which the diode is held for use in ②

Fig.8: Operation of an Orman zero-crossing discriminator (38)

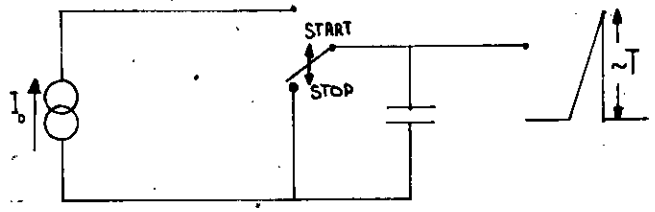

Fig.9: Start-stop converter.

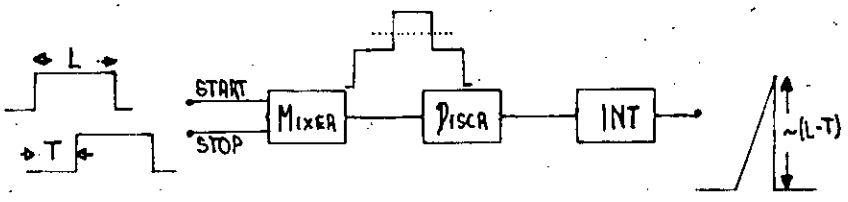

Fig.10: Overlap converter.

RC, RL and delay-line elements. The importance of a pronounced gradient for timing at the zero cross-over was stressed, and elsewhere the need for speedy discrimination and the reduction of statistical fluctuation has been underlined (37). The use of tunnel diodes and other coincidence circuit techniques (38) such as "arming" i.e. alerting the tunnel diode for rapid transition at cross-over pick-off (fig.8), these all enhanced the timing resolution.

The absolute precision of the timing measurement still depended on the time-to-analog converters. These are of two main types (see Kowalski's book (39) for an excellent review of these). First there is the start-stop converter in which a storage element, almost always a capacitor C, is connected to a constant current generator by the START signal and disconnected by the STOP signal. The resulting pulse amplitude is proportional to the time interval T between the START and STOP signals (fig.9). In the second type, the overlap converter, the START pulse must exhibit a well defined length L, and the STOP pulse must be somewhat longer. The length of their overlap is measured by a discriminator and linear integrator, INT, and the amplitude of the resulting pulse is proportional to (L-T) (fig.10). An overlap converter does not produce an output signal for a single START pulse as a basic START-STOP converter does. However, the overlap converter cannot check the correct sequence of the input pulses.

1-4.2 RC Shaping.

Roush used a start-stop converter, in fact a simple valve difference amplifier acting as a constant current generator for a small capacitor; time separation sensitivity was increased by delaying the leading edge start pulse until shortly before the expected cross-over time. He also indicated that the shaping requirements were fairly flexible and this was evidenced by subsequent papers referring to both organic (37,40) and inorganic (41,42) scintillators. These all used integrations and differentiations of different lengths but produced similar quality of P.S.D. i.e. M ≑ 1.4 above 500kev equivalent electron energy (fig.11). One or two facts are noteworthy: the use by Nadav (37) of a tunnel diode biased in its higher voltage state to allow negative triggering; and the removal of statistical fluctuation by selected integration (42). A similar circuit with temperature compensation (for space applications) (43) produced a gamma rejection ratio of 125 : 1 for 97.8% neutron acceptance above 200kev equivalent electron energy (as with other techniques when the gamma rejection ratio was increased to 450 : 1, the neutron acceptance ratio deteriorated slightly). Soucek's (44) circuit was designed with 3 critically biased tunnel diodes and obtained ± 2ns timing resolution over a 100 : 1 dynamic range, but the discrimination was poorer. This inferior performance may be partly due to the tunnel diode arming pedestal being applied only "a few ns" before transition, (more commonly the arming is done ~100ns prior to transition), but the time dispersion over this

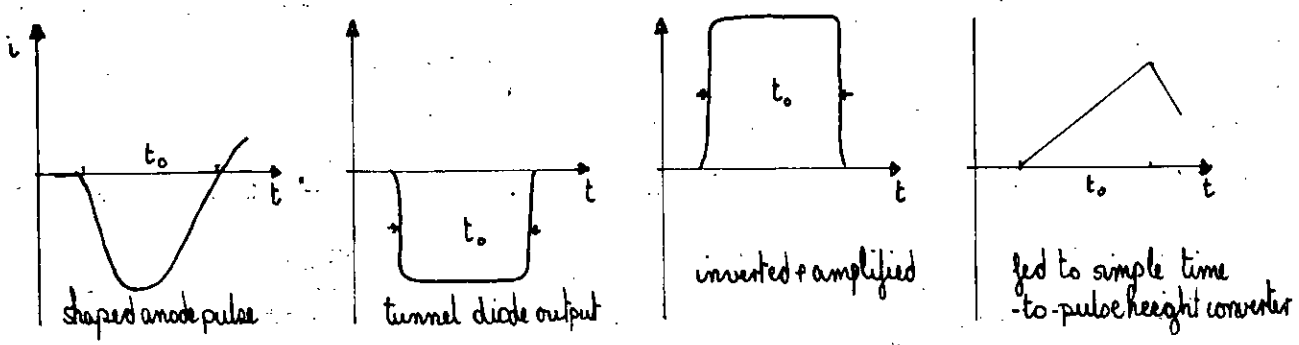

Fig. 11: Idealised picture of signal processing sequence.

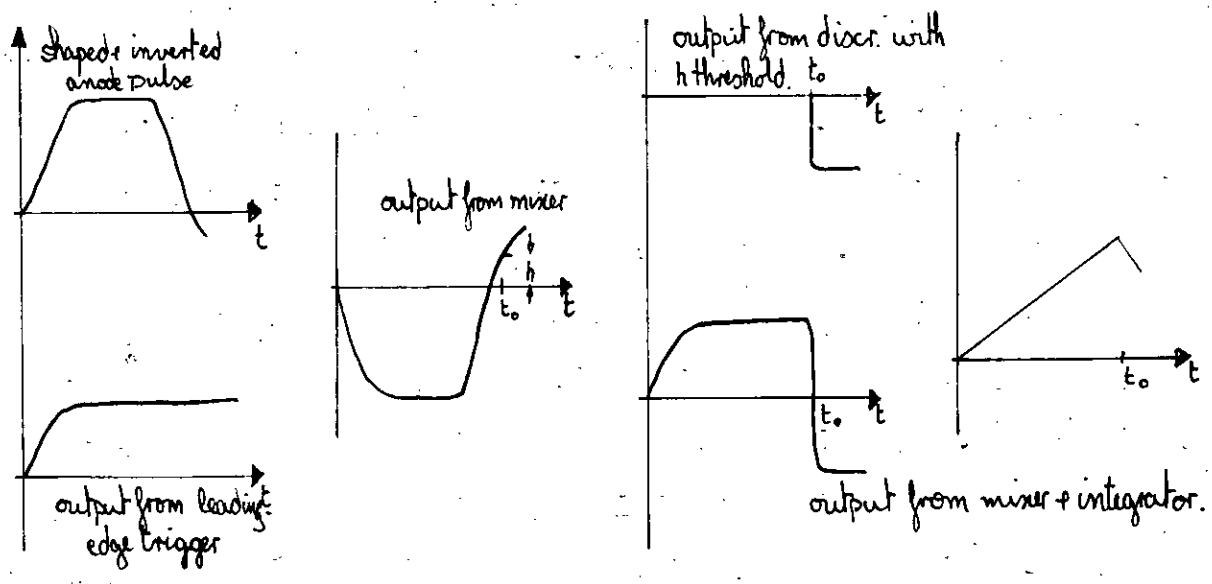

Fig. 12: An example of threshold discriminator timing discrimination.

dynamic range is also explained by Brady and Bonner (45) to be a consequence of two channel discrimination. (An additional weakness of the system is the occurence of saturation in the time to pulse height converter).

Rather superior performance was obtained by Johnson (13), the tunnel diodes in this case being biased in their 'ready' low voltage mode (fig.12). In a start-stop time-to-pulse height converter devised by Alston and Draper (46) the time separation sensitivity was increased by the same method as Roush adopted i.e. delaying the leading edge until shortly before the expected cross-over time. The threshold at 30kev equivalent electron energy sufficiently reduced the effects of statistical variation and noise to obtain 99% gamma rejection for a 1 Mev source and M = 1.06 (P/V = 38) for a Po-Be source, at 1300cps. Almost as good performance was obtained by Kozlowski (47) at a count rate of 3×10^4 cps. Much poorer performance using this technique with large volume scintillators (12,48) may be related to deteriorations in timing resolution. Some of the possible sources of this have been dealt with by the second research team (49). The other bipolar pulse shaping techniques dealt with by Roush have not been so widely used. Only Kahane (50) and Gatti (51) appear to have had success with RCL shaping. Kahane obtained 99.5% neutron acceptance at 1 to 10kcps above a 150kev equivalent electron energy bias, a quality factor of 1.5.

1-4.3 DL Shaping.

The use of delay line clipping was mentioned in Owen's review and has been frequently used since with varying amounts of shaping prior to the clipping.

Alexander (52) devised the first such circuit with only slight but critical shaping of the clipped pulse (fig.13), and despite the use of Schmitt triggers (working at a 5mv threshold with ± 3ns accuracy) obtained 50% neutron acceptance at 1kcps. with a 200 : 1 gamma rejection above a 300kev. equivalent electron energy bias. This performance was slightly improved on by Peele (53) using tunnel diodes. (A previous article describes the application of this principle to noise signal rejection (54)). Similar results were obtained by Miller (55) and Cialella (56). The trend was to the use of a separate later electrode for the start signal (a time pick-off unit was used to obtain both a start and a bipolar pulse from the anode, in Cialella's paper) and clipping times of $\leq 1\,\mu s$. The same philosophy was adopted by Bucher (10) but performance was far better because of the superior discriminator he used (based on a series of articles in (57)) which produced <0.26ns "walk" (fig.14) over a 1 : 500 dynamic range, and the output was suitable for use in either start-stop or overlap converters. Gamma rejection ratios of 2000 : 1 at 360cps and 350 : 1 at 10^4cps over a neutron energy range of 0.1 - 1 Mev. were maintained when a further sophistication (58) extended the energy range to 15 Mev. and the P/V ratio to 10^3 : 1. An integrated circuit version of this (59) gave similar results,

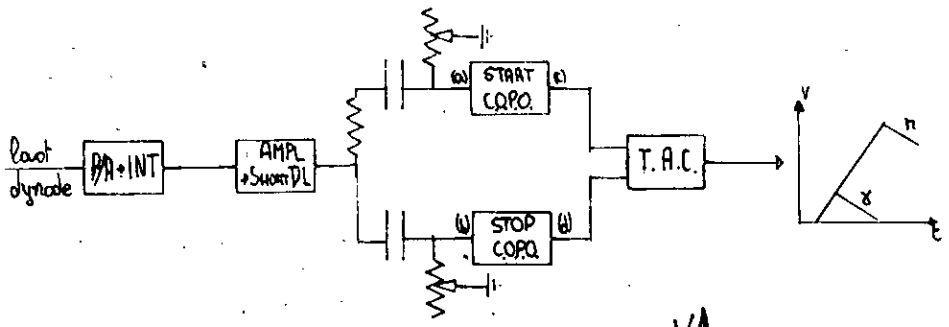

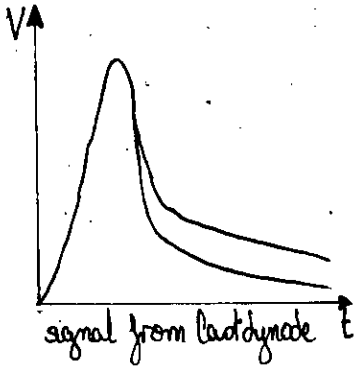

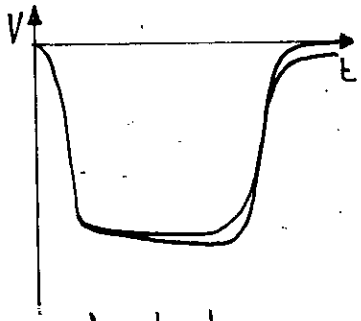

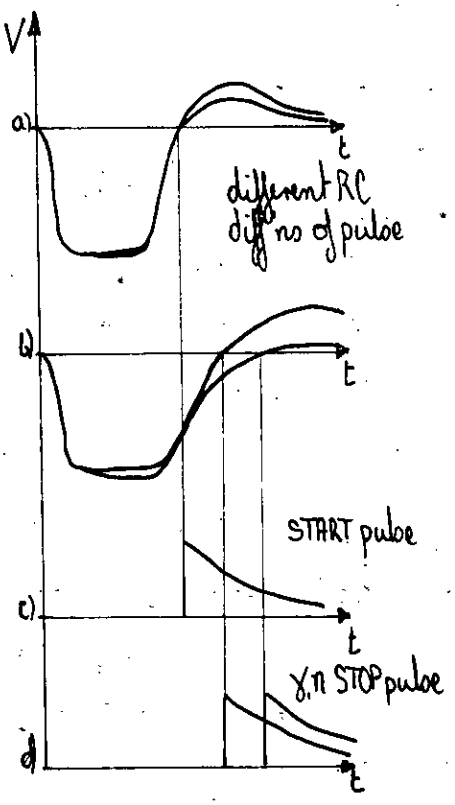

Fig. 13: Block circuit diagram and pulse shapes for the Alexander+Goulding method.

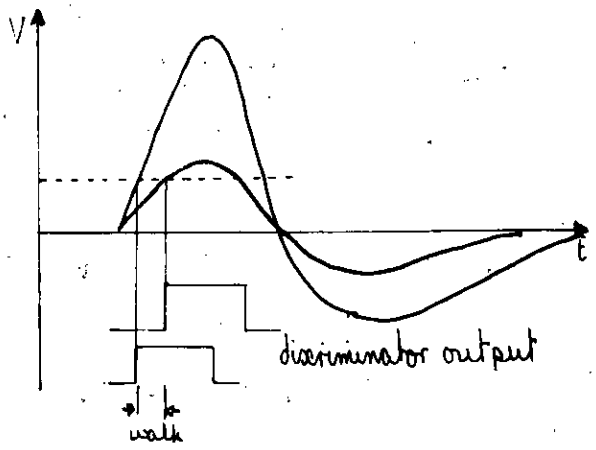

The amplitude dependent delay of discriminator pulses is referred to as 'walk'. As shown in an appendix the point of zero-crossing is amplitude independent but the time of crossing some non-zero level does depend on pulse size.

Fig. 14: To indicate the meaning of 'walk'.

but because of additional pile-up rejection circuitry its count-rate capability might be slightly superior. Ingenious use of delay lines has also been made in order to fabricate filters with special characteristics - these will be considered separately.

Mention should also be made of the use of long double differentiation. This has been applied by Johnson (13), Burrus (60) and by McBeth (61) but only in the last paper is sufficient detail given to allow performance to be assessed. The drastic reduction in gamma rejection ratio for a 1 Mev. source from 10^5 : 1 at 100cps to 135 : 1 at 1500cps is obviously a result of the long start to cross-over time of 3.7 s. This problem was overcome by Johnson with the use of dead-time protection circuitry.

1-4.4 Constant fraction of pulse height timing techniques.

According to Bell (62), leading-edge timing provides far superior timing resolution to that obtained with zero cross-over timing, the sole justification for using the cross-over method being the avoidance of amplitude dependence. The best resolution is obtained by taking the measurement after n of the total R photoelectrons have been collected, such that: $\eta/R = \sigma_{ph}/\tau_e$ where σ_{ph} represents the variance of arrival time of photoelectrons at the electrode and τ_e refers to the relevant fluorescence decay time. In addition, Jones (63) has shown that threshold discriminators create smaller time variances because they register on a centroid of part of a microscopically irregular pulse whereas a cross-over pick-off triggers at a single electron or

rather, in practice, a small number of electrons. Hence the use of gating pedestals in Bucher's (10) tunnel diode circuitry and the method of Bass (64) using non-zero tunnel-diode thresholds on the leading-edge and cross-over, thresholds being adjusted to account for different rise times.

The advantage of leading-edge timing and wide dynamic range were combined in a constant fraction of pulse height discriminator devised by Gedke (65,66) and applied to P.S.D. (67) to give a dynamic range of 100 : 1 for a cross-over "walk" of $\pm$ 1.2ns. They were concerned with maximum timing precision at 10% of the pulse height. In fact the most significant point on the integrated neutron or gamma pulse lies at $\sim$85% of the pulse height according to Kuchnir and Lynch (68) (fig.15). They obtained a zero cross-over at a corresponding point using asymmetrical double delay-line shaping but the results were fairly typical. However two Japanese groups have devised integrated circuits with wide dynamic range. Kimbara devised (69) and applied (70) such a circuit measuring between 10% and 90% points to get 2 : 1000 gamma rejection below 500kev neutron energy and M = 1.29 (P/V = 70) for an Am^{241} - Be + Co^{60} source. While Furuta (71) obtained similar performance over a 50 - 500kev neutron energy range and a value of M = 1.4 (P/V = 200) over a 50 : 1 dynamic range (fig.16). There is now a commercially available unit (72) which measures the 90 - 10% fall time of a delay-line shaped pulse.

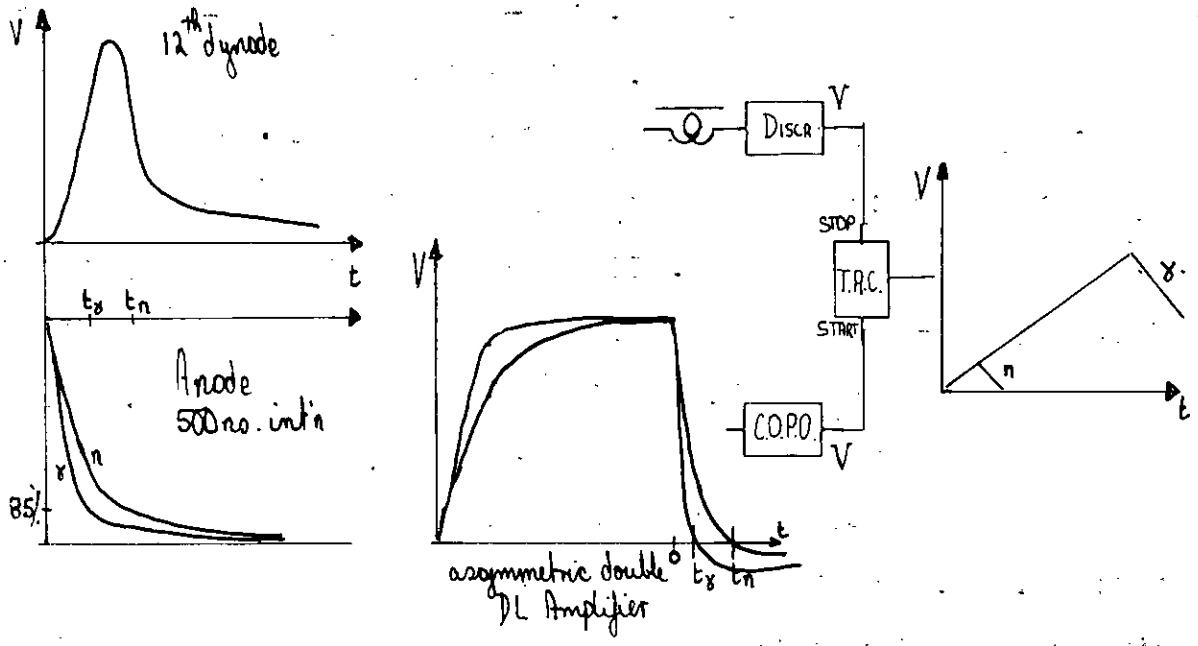

Fig.15: Schematic presentation of the Kuchnir + Lynch method.

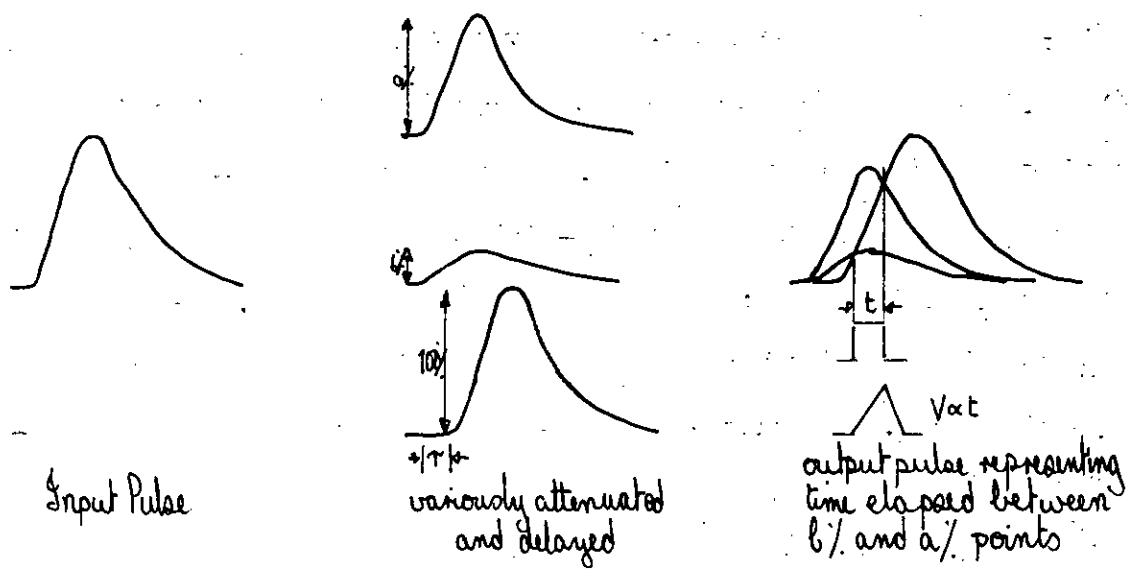

Fig.16: Operation of Furuta's 'rise-time to pulse height converter.

This last technique bears a strong resemblance to the technique developed by Johnson (73) which involved an idealised trapezoidal single delay shaped pulse which crosses zero at the 85% charge collection point identified by Kuchnir and Lynch. The performance does not come up to expectation: one is reminded of Johnson's remarks in an earlier paper (13) suggesting that the simple processing with minimal circuitry is more likely to retain the most pulse shape information.

1-5 Filter and hybrid techniques.

1-5.1 Delay-line filters.

In the above mentioned discrimination techniques, only a part of the available information can be used. Gatti and de Martini (74) reported a technique for which the information yield is optimum. They devised a time-dependent linear filter which processed the current pulse from the photomultiplier by applying to it a time-varying attenuation P(t) - a weight function which emphasises the more pronounced differences in the pulse shapes of the scintillations to be distinguished between (fig.16). Figure 17 shows the realisation of a network having the required response, with the aid of two delay lines of length $T_{1/2}$ and $T_{2/2}$ which are terminated by two small resistors $R_1 < Z_o$ and $R_2 < Z_o$ respectively. (Z_o denotes the characteristic line impedance). The identity of the radiation is indicated by the polarity of the processed signal at the sampling point $t = T$. Gatti applied this

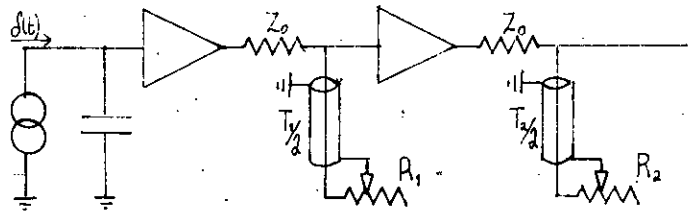

Fig. 17: Realisation of Gatti's filter

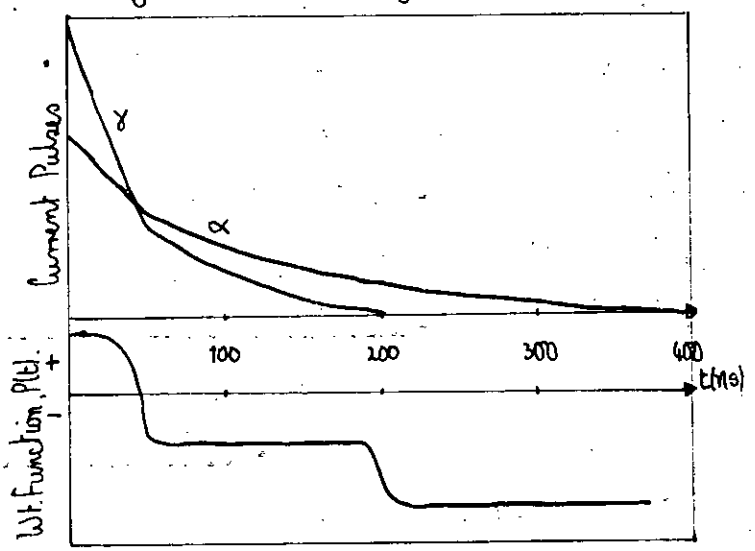

Fig. 18: The weight function according to Gatti
+ 19: The current pulses for α, γ in anthracene.

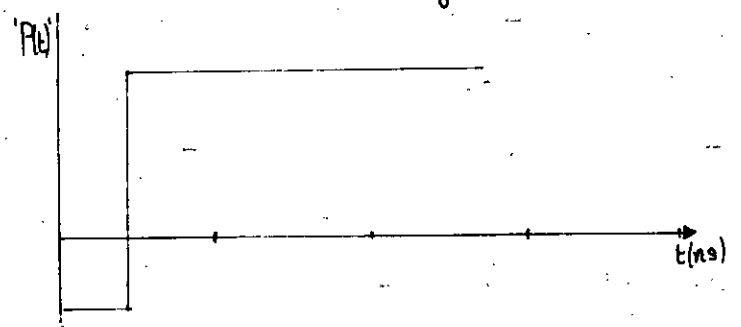

Fig 20: The analogous charge comparison filter.

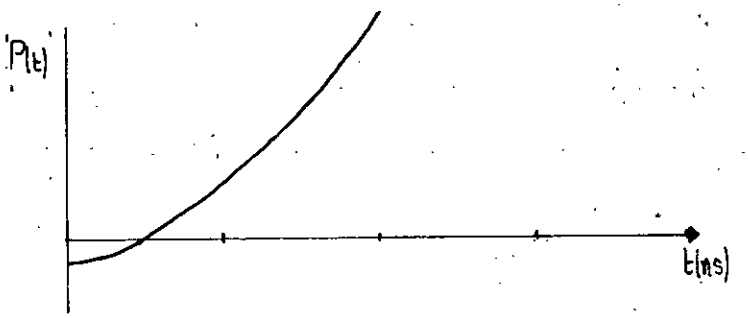

Fig. 21: The effective filter function of a cascade of RC and CR networks.

principle to alpha-gamma discrimination in anthracene. Both Williamson (18) and Adam (15) have used the technique in neutron-gamma discrimination. The former created a pulse shaper from a shorted and small resistance terminated delay lines which produced a gamma cross-over but a wholly positive neutron pulse. The reflecting length of the second delay-line was 0.1 μ s, the time required for 87% of the gamma light and 70% of the neutron light to be collected. The only indication of performance is a reference to the gammas being distinguishable down to 30kev. Adam also shaped the pulse with an unmatched delay line but then integrated it giving discrimination down to 150kev neutron energy - almost the equivalent performance.

In fact both the charge comparison and timing techniques can be interpreted as a form of filtering. Sabbah and Suhami (3) have derived the analogous filter function in the charge comparison case (fig.20) and demonstrated that in terms of Gatti's discrimination factor - the fractional variance of the pulse differences, this technique is $\sim$2 times worse. Gatti himself (76) has deduced the idealised equivalent filter function for the timing technique (fig.21) and compared it with the actual filter formed by Roush's (11) shaping technique, but only in a more recent paper (51) has he taken into account non-statistical effects and the photomultiplier dark current. With this additional rigour one can appreciate that there are optimum RC shaping values, but that they still give discrimination 25% worse than the original optimised circuit.

1-5.2 Space-charge filters.

One of the earliest circuits devised discriminated (7) between neutron and gamma pulses according to their ability to overcome saturation in the last stage of the photomultiplier. Although this technique is normally classified as a charge comparison because the saturation recovery is related to the proportions of the pulse in the fast and slow components, it seems more appropriate to consider this rapidly saturating final stage of the tube as an active filter. A mathematical derivation of the form of this filter appears in an appendix and the resulting wave forms are shown in Figure 22. This technique was applied to the analysis of pulse spectrum distortion effects (77) over a 1 - 10.7Mev neutron energy range with gamma rejection set at 99.9% for a 2.5Mev ThO_2 source, and with a similar performance in a muon capture experiment (78).

There are two possible drawbacks to such a system: firstly, as can be seen (fig.22) simple pulse height discrimination on the processed output may identify the strong overswing of high energy gammas as associated with neutrons; a further criticism is the long time (several microseconds) required to obtain sufficient information for radiation discrimination, though an advantage of this technique according to Owen is that cheaper slow tubes may be used. Circuitry to tackle this first problem was devised by Batchelor (79) who utilised the late cross-over of high energy gamma pulses as a means of gating against them (fig.23). This lowered the threshold considerably allowing 10% neutron detection

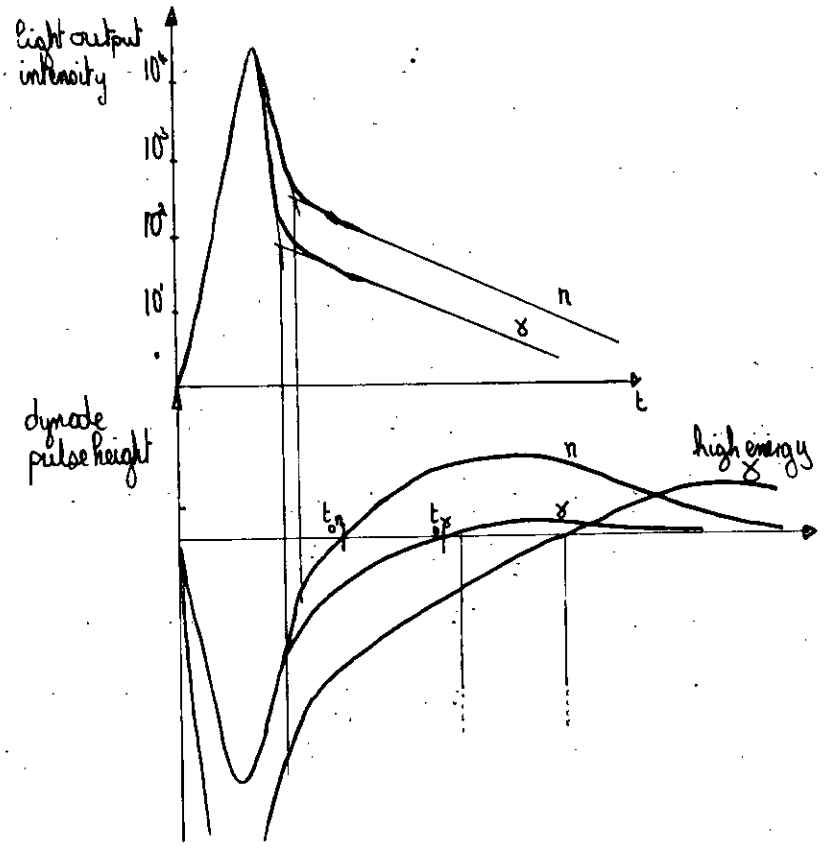

Fig 22: To indicate the relation between scintillator light intensity var'n and the saturated output voltage pulse.

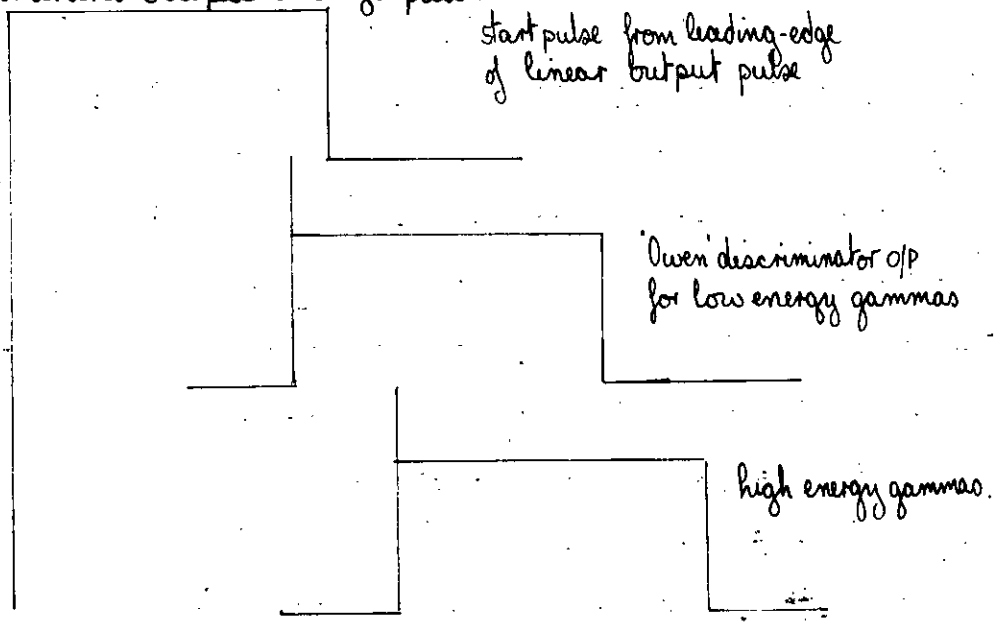

Fig 23: The absence of overlap between linear and 'Owen' discriminator pulses allows high energy gamma pulses to be rejected.

(See Sect. 1-2.1) at 500kev neutron energy and a 300 times reduction in counting of 1 Mev. gammas. The commercial version of Owen's circuit (80) cancelled the positive gamma overshoot using a delay-line (81) but performance was not specified in terms of energy.

Johnson's circuit (82) overcame both problems, i.e. long resolving time and high energy gamma-neutron pulse similarity, by the use of a 0.8μs gating pulse and slight integration which accentuated the gamma-neutron pulse height differences. This led to a further improvement - 99.7% rejection of gammas at 800cps above a neutron energy threshold of 400kev with 98% neutron counting above 500kev.

The restriction imposed on energy range by hard saturating neutron pulses or restricted tube gain has been relieved by the methods of Doke (83) and Hiramoto (84) using an adjusted capacitance over the saturating stage. This reduced the threshold to neutrons and increased the range of gamma energies tolerated to 50kev to 7Mev. (fig.24).

Rather than extract the information from the filtered pulse by means of pulse height discrimination, one may use the cross-over point which also, as implied above, allows radiation to be distinguished. This effectively uses Batchelor's idea (fig.23) as a timing technique in its own right. No performance figures are given in Hsu's paper (85) but Fabiani (86) quoted a ~99% gamma rejection ratio using this technique; this was for a 140kev equivalent electron energy bias. The neutron acceptance rose to ~80% at 1Mev neutron energy - but this was at very low count rates.

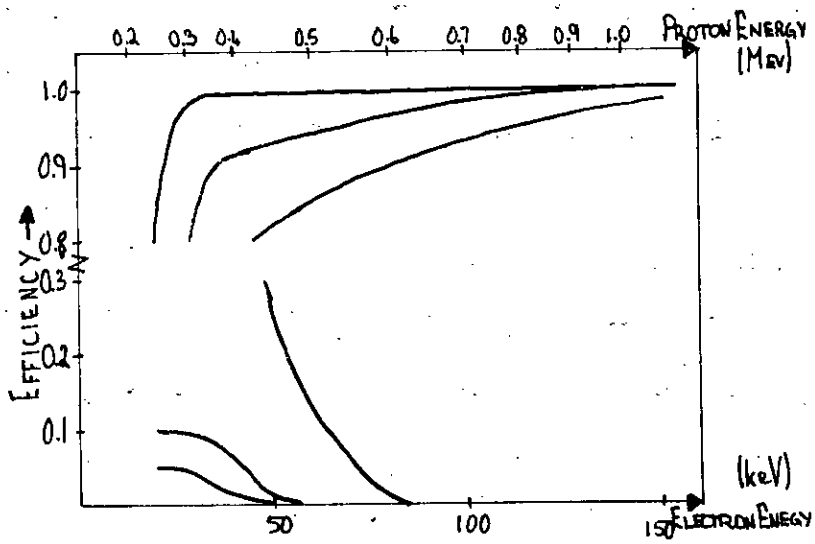

Fig 24: Hiramoto's graph of relative efficiencies to electron + proton.

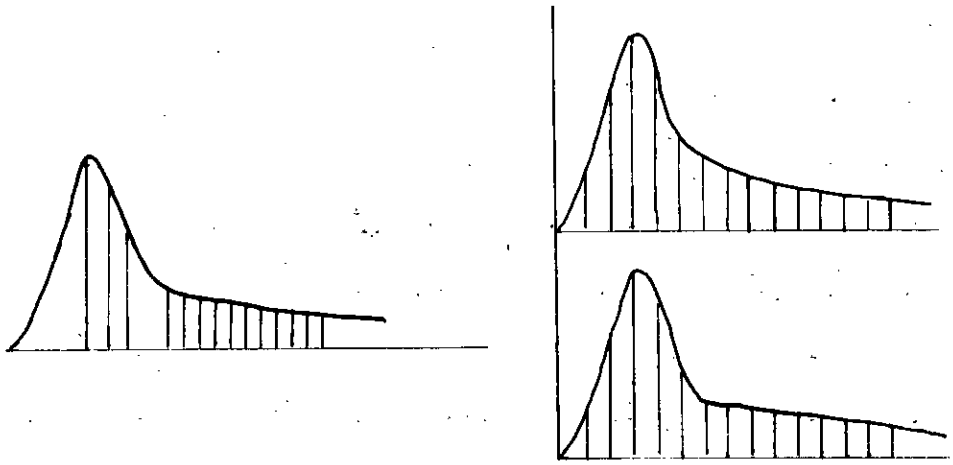

Fig. 25a Pulse shape parameter derived by multiplying samples by appropriate values of P(t) (fig 18)

Fig 25b) Correlation coefficient for similarity to standard pulse derived by multiplying samples by corsp. value of standard

1-5.3 Sampling technique.

Finally, mention should be made of a sampling method of pulse shape observation devised by Tojo (87) which can be applied to pulse shapeddiscrimination. It appears possible to derive a parameter characteristic of a pulse in terms of variously weighted samples of pulse height at selected points; or alternatively, to make a similar point by point comparison with some standard pulse shape (fig.25). Although such a technique promises excellent performance and very short resolving times, there has been no attempt to produce such a unit.

1-6. Conclusions.

In attempting to draw conclusions from the vast array of techniques and performances, it may be realised why no single method of P.S.D. has been adopted. (Table 3 selects the best examples of the various techniques). Firstly, although in the majority of cases the efficiency of the scintillators and tubes does not vary appreciably, the quality of discrimination obtained by different workers using the same technique often differs considerably. In addition, any comparative assessment is severely hampered by a shortage of performance data or by its presentation in an unintelligible form.

However, some general statements may be made. The theoretically based assertions of Sabbah and Gatti regarding the superiority of charge comparison and timing techniques respectively appear contradictory. In practice equally good performance has

been obtained with either, down to the same threshold. Of the charge-comparison techniques, the best appears to be the fast-total comparison. Regarding the timing techniques, there is both theoretical and practical evidence that threshold timing is superior. In general poorer performance is obtained with the filtering technique, the best being from the unmatched delay cable circuits, but Tojo's shape analyser shows promise of very good discrimination.

Table 3: The best examples of the various techniques.

Technique	Ref	Threshold (Eq.e⁻ en)	Count rate (cps)	Range (n energy)	P/V	M	Gamma acc.	Neutron rej.
Charge Comparison								
Fast/total	3	50kev	1k*	0.06-14Mev			$1:10^4$	2:10
Slow/total	33	500kev*		1-20Mev		3.1*	$1:10^4$	
Fast/slow	28	300kev?*	500				$1:10^3$	
Timing								
Without DL								
1- or pedestal	13	10kev	1300		38	1.06	$1:10^2$	
2-with pedestal	36	300kev?	low	1-14Mev	50*	1.5		
With DL								
1-without pedestal	59	60kev	500	0.4-12Mev	10^3	2*	1:200	
2-with pedestal	58		10k*	0.1-15Mev	10^3	2.5*	1:350	
Long double Diff'n	61	50kev	100 1500	0.15-20Mev	10^3	2.0	$1:10^5$ 1:135	
True rise time	71			0.05- 5Mev	200	1.4		
Filter								
Owen								
1-Amplitude difference	84	50kev		0.15-20Mev				
2-Cross-over difference	86	140kev	low*				1:100	1:5 at 1Mev
Contrived DL filter	75	50kev		0.15-15Mev			1:100	

* Information not specifically quoted, but derived by inspection.

CHAPTER 2.

The experimental assemblage.

In designing the experimental assembly, particular attention was paid to factors relating to stability and uniformity of detector response as these are of the utmost importance in obtaining truly representative performances in various systems to be compared. Of the many factors affecting linearity, the voltage divider design is considered first.

2-1 The voltage divider theory.

To work efficiently, the voltage divider must provide interdynode potentials of maximum stability. To achieve this firstly its high tension power supply should be largely unaffected by variations of mains voltage or load, and must have an excellent long term stability, temperature independence, and low hum (the Fluke High Voltage Supply used had a ripple of less than $100\mu V_{rms}$ and a stability of 0.002% per hour).

Secondly, when the tube is used for pulse operation, there are abrupt changes of electron current between the dynodes and hence also in the parallel chain of resistors. (The theory of this has been extensively dealt with by Lush (88)). Since the electron current increases geometrically up the tube, (assuming a constant photoemmissive multiplication factor, δ), this effect is of more consequence at the anode end where the dynodes draw more on the standing current in the resistor chain, thus reducing the

inter-dynode potentials here so that an increased proportion of the overall potential is dropped over the lower part of the tube. The net result is an increase in gain as is demonstrated in a Mullard publication (89)

$$\frac{\Delta\bar{A}}{\bar{A}} - \frac{\bar{\delta}^{n} I_k}{I_s}\left(1 - \frac{1}{n+1}\frac{\bar{\delta}}{(\bar{\delta}-1)}\right)$$

where I_s is the standing current, I_k is the current drawn by the cathode, n is the number of stages and A the overall gain. The relative gain variation is thus reduced as I_s is increased (though focussed tubes are not so susceptible to such distortion). In addition, stability is further assured by placing capacitors across the last dynode sections to carry high peak pulse currents (a common method in amplification techniques).

Thirdly, although the use of by-pass capacitors may reduce the need for high currents in the resistor chain, it can introduce a count rate dependent distortion. It can be shown that gain variations are minimised by making $R_nC_n \gg T_{fl}$ (the fluorescence decay time), but as R_nC_n is increased so does the likelihood of overlap between following pulses (R_n and C_n refer to the resistance and capacitance between the n^{th} and $(n+1)^{th}$ dynode). Kowalski (39) shows that the mean deviation of $\bar{A}$ is given by:

$$\sqrt{\left\langle\left(\frac{\Delta\bar{A}}{\bar{A}}\right)^2\right\rangle} = \frac{\bar{A}e\bar{N}}{I_s R_nC_n}\sqrt{\frac{1}{2}rR_nC_n}$$

For a given maximum pulse rate r, maximum number of electrons $\bar{N}$ arriving at the anode, and mean gain $\bar{A}$, optimum choices are $R_nC_n \approx 1/r$, and $I_s \gg \frac{\bar{A}e\bar{N}}{R_nC_n a_{max.}}$ where $a_{max.}$ denotes the maximum

permissible root-mean-square deviation. For instance for a typical 11-stage photomultiplier with $\bar{A} = 10^6$, $\delta = 3.5$, $r = 10^4$ counts per second, $\bar{N} = 10^3$ electrons and $a_{max} = 0.1\%$, the second requirement for stability implies that $I_s > 10^9 I_k$ or $I_s > 10^3 I_a$ (anode current), while the third requirement indicates $R_n C_n \approx 100\mu s$ and $I_s \approx 1.6mA$ as preferable choices. With such limitations it only remains to choose the components of the chain subject to the manufacturers recommendations as to overall working voltages. Painstaking optimisation of the chain as performed by Bellettini(90) is undesirable as the resulting gain, though vastly improved, is critically dependent on the resistor values and the particular tube used. However, it being essential to avoid any tendency for unwanted tube saturation to occur, most researchers initially select the manufacturers' 'B' type recommended chain (12) but finally adopt something between that and type 'A'. A technique developed by Gibson (91) produces a satisfactory non-critical dynode chain with pulses free of saturation distortion and ringing. The method involves selecting the ratio of resistor values in accordance with the upper limit of overall voltage (for which saturation is most likely to occur at the final dynodes) leaving the last stage resistor adjustable for working optimisation. Such a procedure has been adopted with the additional precaution of placing a Zener across the cathode - first dynode stage to provide a stable inflated potential difference at a point where the collection losses of photocathode electrons must remain negligible. It was also borne in mind that discrimination techniques using a

single dynode output should not be influenced to the same extent by changes in interstage gain (36). Numerous papers have been written discussing the use of voltage regulator tubes (92), diodes (93-5), voltage dependent resistors (96) or, most successfully, transistor stabilisation (97,98) but in the present experimental set-up such precautions were not considered necessary. As mentioned above, capacitive by-passing is required for stability, but it is found that, particularly at high count rate, heavy by-passing is also required if the integrated signals taken from the dynodes are not to be subject to slow baseline shifts.

2-2 The dynode chains to be used in the investigation.

The dynode chain circuit for the 6097B photomultiplier is shown in Figure 26. Its construction and layout was strongly influenced by suggestions made in Gibson's (91) paper: all leads were kept as short as possible and Radiospares EHT cable (14/36SWG) was used for all signal lines and for high tension supply to keep capacitive coupling and pick-up to a minimum. Insulation was also used to remove the possibility of corona sparking. A single heavy ground plane was provided by brass casing of the whole assembly. It was decided to make the cathode earthed, for although making the anode earthed reduces the output insulation problems, it also increases the noise problems of possible contact of negative potential with the tube envelope (4).

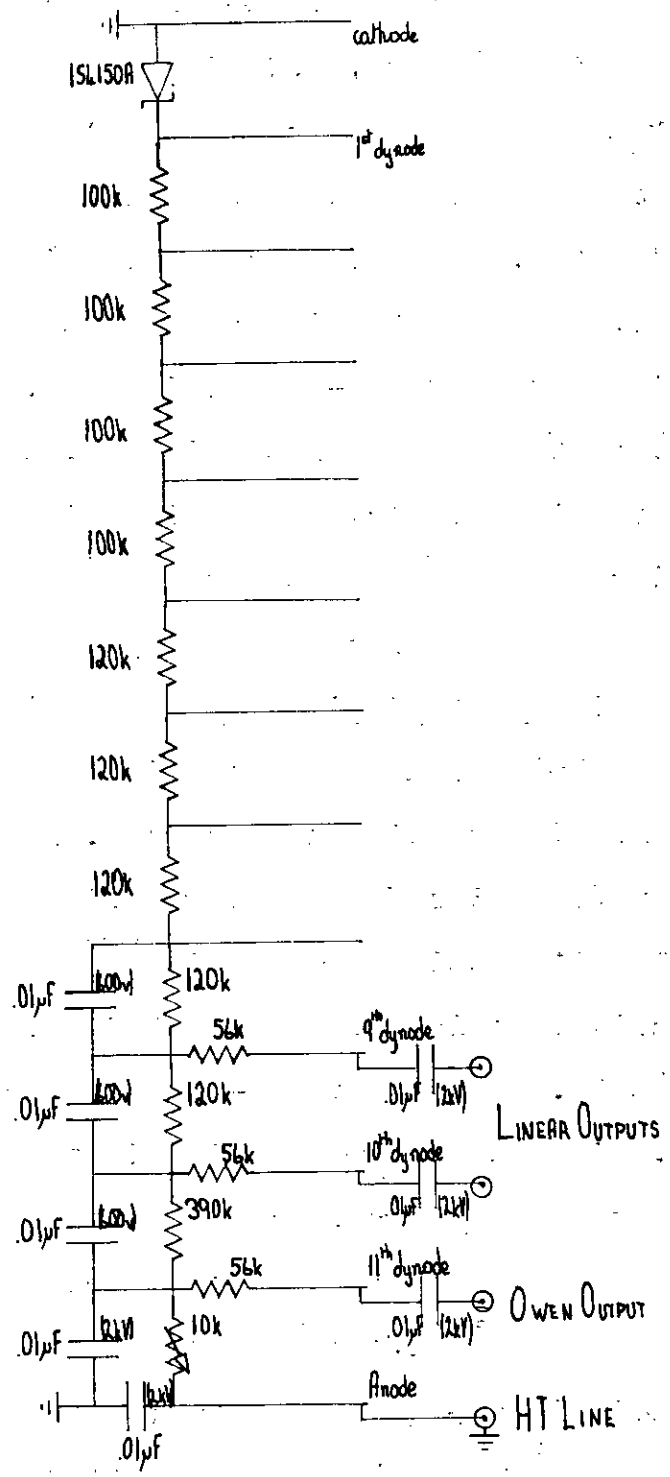

Fig. 26: Dynode chain designed for use with the 6097B photomultiplier tube.

While adhering to the same general principles, the construction of the 56AVP dynode chain (circuit shown in fig.27) differed in that the voltage divider could be made completely accessible for working adjustments. This facilitated alteration of the focus control and saturation voltage "Helipots" (low inductance cermet potentiometers (99)) and the close coupling of oscilloscope probes to the dynode outputs. The design also featured a spring-loaded light-tight coupling to the photomultiplier base and a perforated zinc safety shield which was locked in place over the voltage divider when not under test. This faster tube is more susceptible to ringing and although by-passing capacitors were placed direct on the dynode base, sufficient precautions were not initially taken in connecting the output signal cables. The causes and avoidance of these problems by close coupling of well screened cable is discussed in an RCA publication (100).

The precise form of the potential divider owes much to that described in Vass' thesis (101) and also bears some similarity to the Ashkin voltage divider (102). The form of the latter has the additional advantage of rapid recovery, i.e. the next pulse is identifiable in a third or less of the time taken with a recommended dynode chain.

Details should also be given of the dynode chain (fig.28) for the XP1040 phototube (a fast tube with 5" photocathode). The chain was primarily designed (103) for use in a multidetector system applied to the analysis of the products in the ternary mode of thermal neutron induced fission. In addition to the adjustable

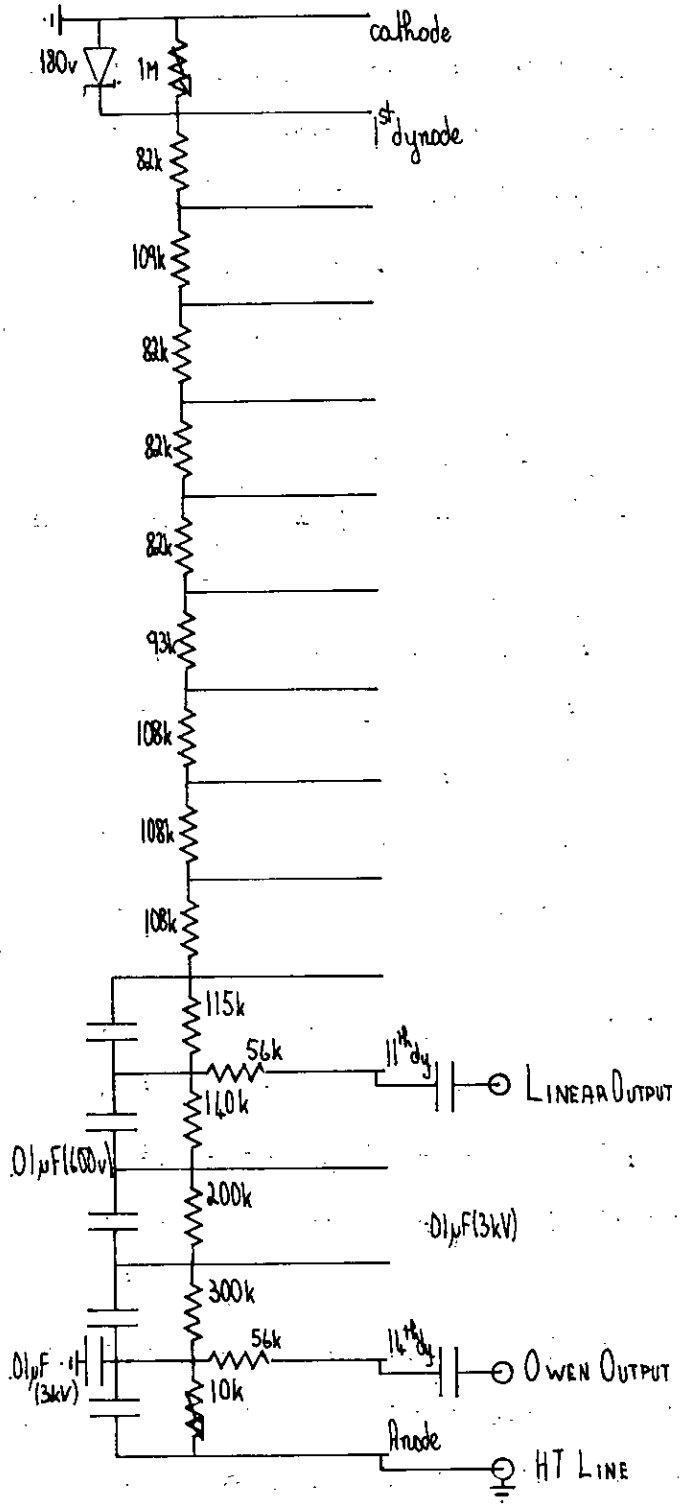

Fig 27: Dynode chain designed for use with the 56 AVP photomultiplier tube

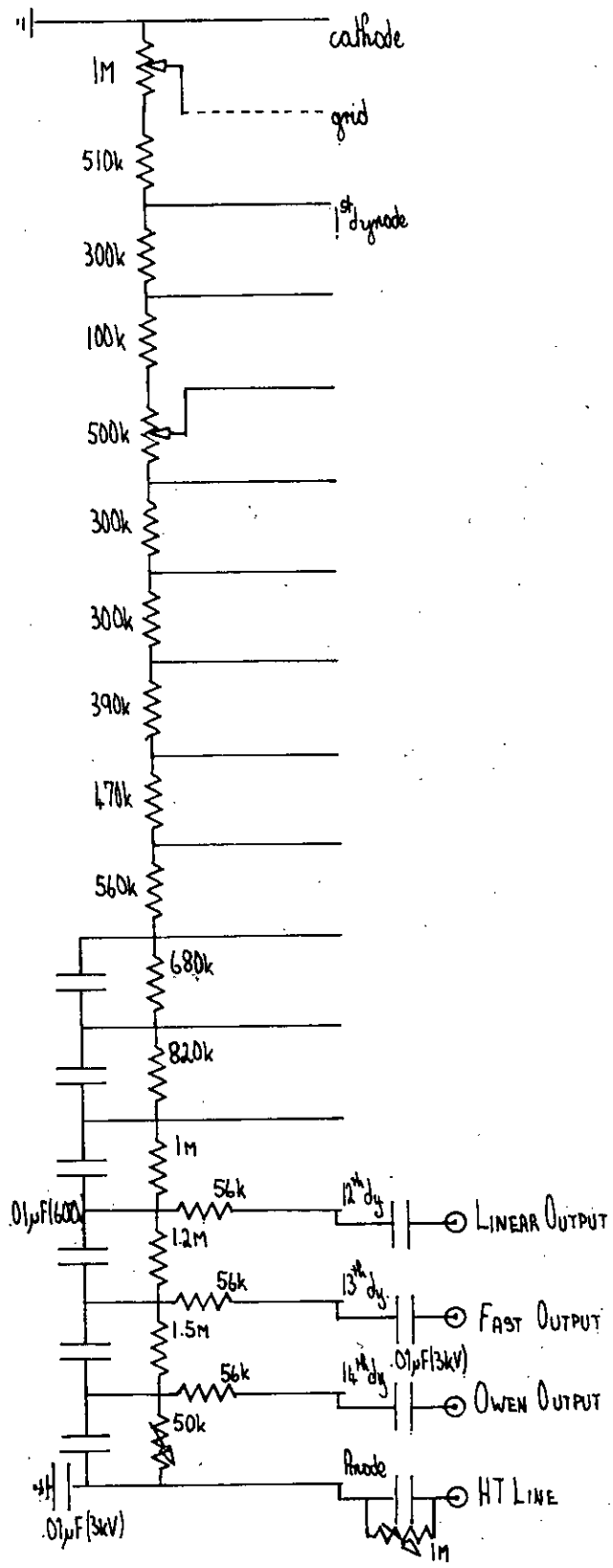

Fig 28: Dynode chain designed for use with the XP1040 photomultiplier tube.

focus and saturation voltage potentiometers, control is also maintained over the applied H.T., and an additional potentiometer enables the voltage distribution to be optimised for maximum gain and minimum transit time spread. An additional "fast" output is also available for timing purposes.

2-3 Factors affecting linearity and optimum performance.

Besides the dynode chain features required for good stability, the particular scintillator, the tube and their optical coupling, the associated electronics and multi-channel analyser - these all introduced factors affecting the linearity and the reproducability of performance. In the following, consideration is given to these influences, particularly as they affect venetian-blind type tubes and in their application to neutron-gamma P.S.D.

Birks (4) has dealt extensively with the characteristics of organic and inorganic scintillators. NaI (Tl) for example has a linear response to gamma-rays to within 7% over the energy range 0.2-2.0Mev. and an efficiency that peaks at a temperature of 20°C. Temperature dependence is negligible in most organic scintillators (104) and the linearity of their energy response down to 100kev. gamma-ray energy has been demonstrated (105). The use of liquid and plastic scintillators overcomes complications arising from crystal anisotropy. The response of the scintillator also depends on its size and shape because the forms and proportion of various excitations depend on the radiation and the

range of its energy spectrum which determine the preferred interactions. Geometrical theories (106-7) have been developed which take account of the possible sites of scintillations; neutron spectrum unfolding techniques are largely concerned with the various interactions occuring and the importance of wall effect and interaction product escape probabilities (108-10). This knowledge has led to the choice of scintillator size and shape giving optimum neutron detection at a particular (77) or over a range of energies, i.e. by enhancing the neutron detection efficiency by comparison with the detection of the accompanying gammas (111). It appears that stilbene crystals taller than 2" offer no advantages in detection of a 0-14Mev range of neutron energies while a 2 : 1 length to diameter ratio appears to be the optimum for an NE213 capsule in such an application.

2-3.1 Linearity checks.

The conditions for linear performance were obtained with a 1" NaI (Tl) crystal coupled directly onto the phototube, and standard 3μCi gamma sources (Na^{22}, Co^{60}, Cs^{137}). These sources do not produce calibration peaks in the range below 400Kev in which the non-linearity of NaI (Tl) becomes more apparent. The count rate for each source was adjusted to be approximately the same (about 10^3 counts per second). All unused dynode outputs were shorted out and care was taken that the amplifier output was itself truly linear over the voltage range used. The pulses were analysed in 100 channels of a 'Laben'

400 channel pulse height analyser. The calibration curve shown (fig.29) indicates linearity at the tenth dynode of the 6097B up to 1300v. (tube EHT). The same EHT limit applied at the ninth dynode, presumably because of the rapid onset of saturation with the chain designed to give a strong space charge effect over the last dynode-anode stage. A similar procedure was adopted with the other tubes used, the 56AVP producing a linear output from the 11th dynode at 2000v. and the XP1040 from the 12th dynode at 2,500v.

It is possible to calibrate the system with an organic scintillator, but in this case the gamma interactions are predominantly by Compton scattering for energies less than 1.02Mev, since in low Z materials the photoelectric effect, which varies approximately as Z^5, is about 10^4 times less probable than in NaI (Tl). Richter (29) has produced Gaussian 'smeared' computer compiled spectra based on the Klein-Nishina formula, from which he has derived that the theoretical Compton edge occurs at 0.72 of the maximum height. The energy at the Compton edge corresponding to the maximum kinetic energy of recoil electrons is given by:

$$T_{max} = \frac{E_o}{1+(1/2\alpha)}$$ where $\alpha = \frac{E_o}{0.51}$ and E_o, the energy of the incident gamma-ray, is in Mev. (112).

As can be appreciated from Figure 30, such a calibration is less accurate than for the organic scintillators, but had none the less to be performed for each organic scintillator in order that measurements be recorded for the same energy range of incident radiation. Such calibration data would incidentally

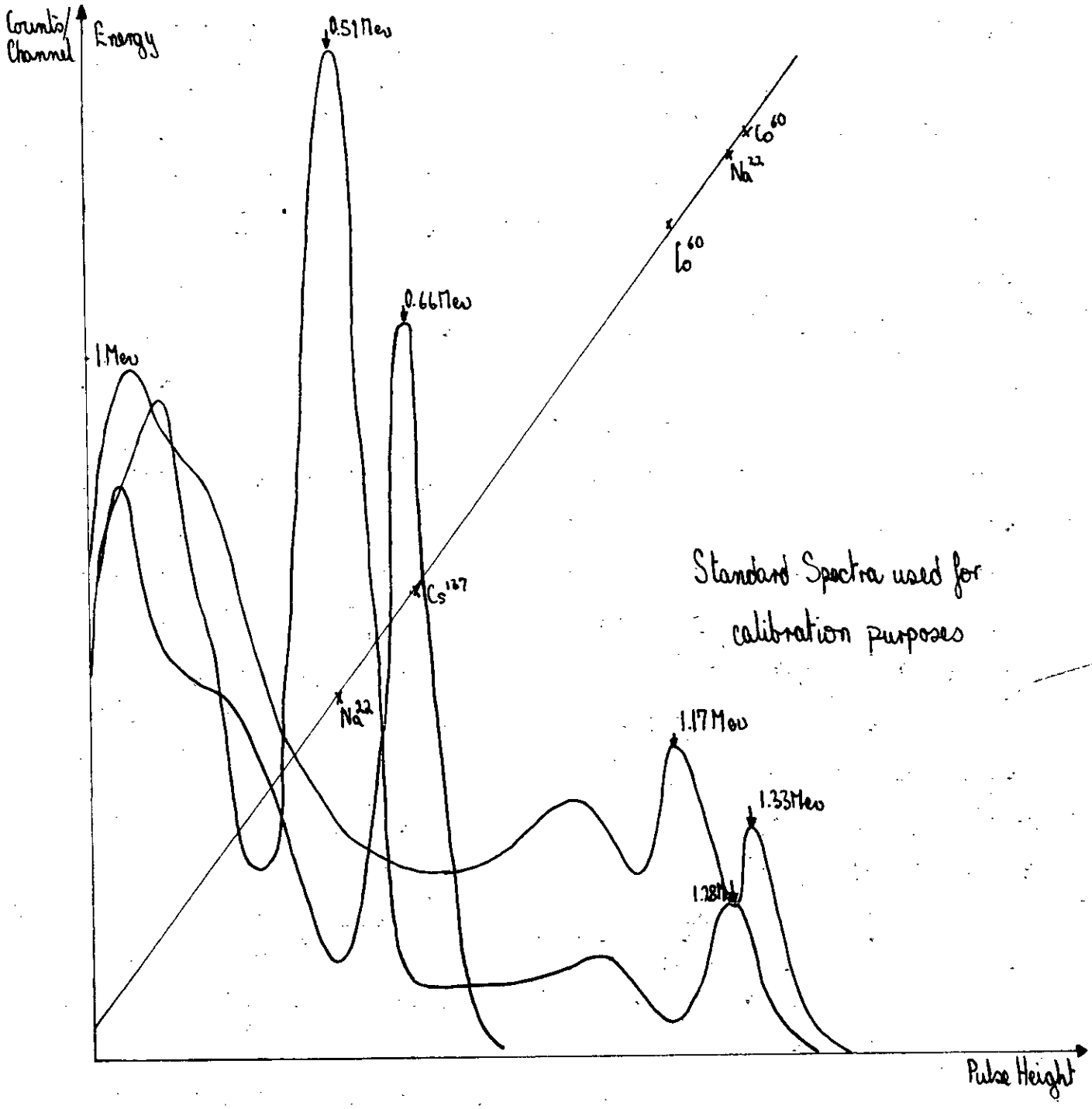

Fig 29: Calibration and linearity Check: 10th dynode of 6097B, at 1300v., 1" NaI(Tl) crystal.

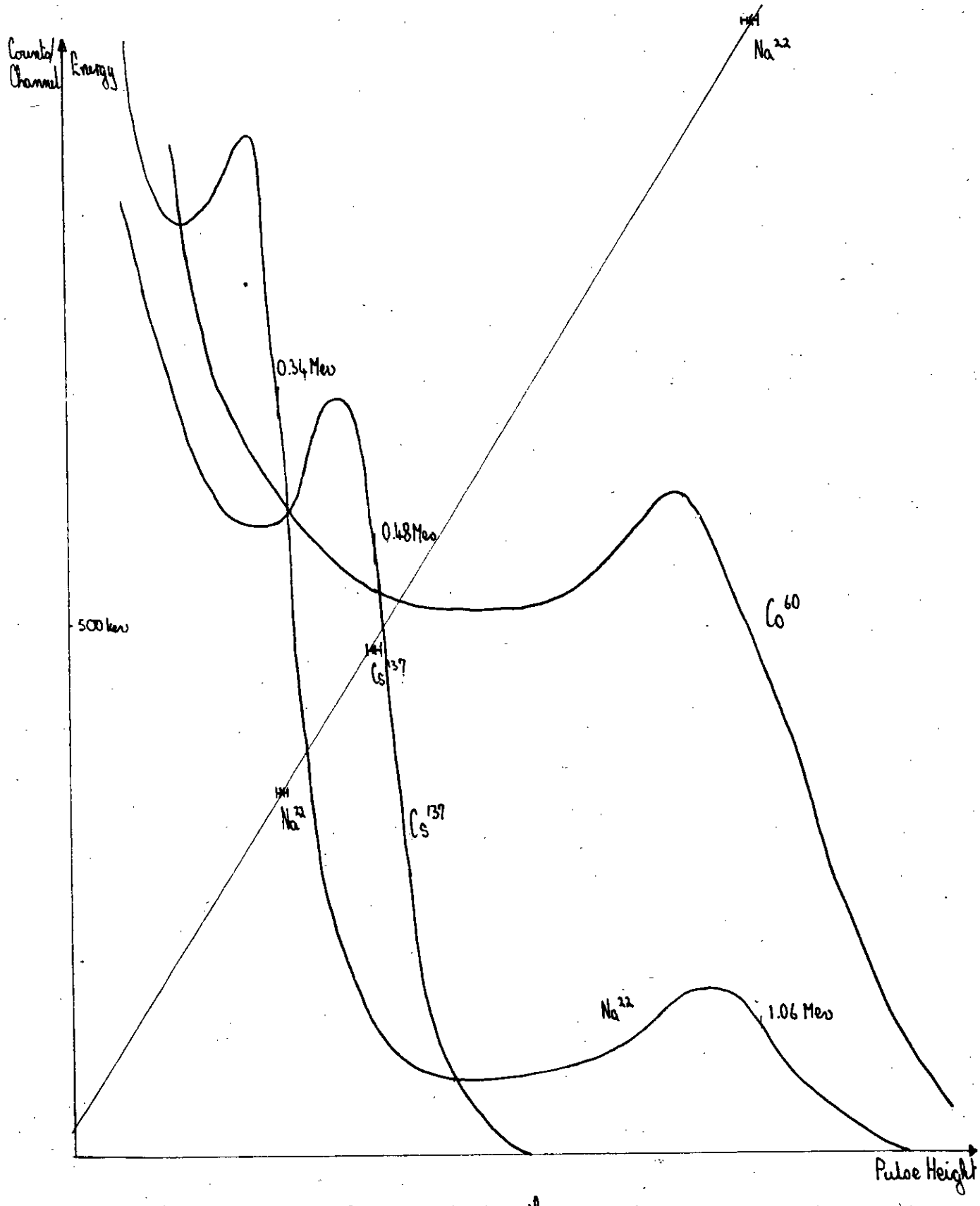

Fig. 30. Calibration and linearity Check: 10th dynode of 6097B, at 1300v, 2" NE 213 cell.

enable a comparison of light outputs from various scintillators to be made and in order that these results should be independent of the size and shape of the active scintillating volume a further experiment was performed to establish the required geometric conversion factors.

2-3.2 Shape - Light output dependence.

The main source of error in this experiment is associated with fluctuations in light collection efficiency. This is dependent on both the quality of reflectance from the scintillator walls, and the optical coupling with the photo-detector. Numerous comparisons of reflective coatings and surface preparations have appeared (113-117). The suggestions appearing in the last of these papers were adhered to.

Three 2" tall cylinders of NE102A plastic scintillators with diameters of nominally 1.0", 1.4", and 1.85" diameter were hand roughened on all but the viewing end with fine sand-paper. They were then spray painted with several thin layers of TiO paint (NE560), each coating being allowed ample time to dry in a warm atmosphere. The total thickness of paint was at minimum 0.02". Each scintillator was then mounted vertically on the cathode face of the 56AVP tube using an inert optical coupling grease (118). The samples of NE102A, initially of 2" length, were lathe turned to heights of 1.4" and 1.0" so that comparisons could be made on decreased sizes of precisely the same material. The pulse height distribution was recorded for scintillations

from the two gamma sources Na^{22} and Y^{88}. These sources provided four Compton edges on the resulting spectra and these were used as reference points from which to derive relative changes in light output. The fractional changes were found to be consistent (for these sets of four reference points) to within $\pm$ 2% - a surprising degree of agreement considering the sources of error previously mentioned. The figure (31) shows both qualitative and, for the thin cylinder, quantitative agreement with the findings of Kaiser (119). It should be noted that the light output is also a function of the scintillator diameter. The difference between the small and medium diameter scintillators may be understood in terms of light trapping in a long thin rod. This problem may be relieved by placing a specular reflector on the remote end of the cylinder (117). The slightly lower light output of the large diameter scintillator is associated with the overlap of the face on the phototube, the resulting unmatched annulus representing a surprisingly large area. For instance, a 2½mm overlap on a 56AVP represents 20% of the scintillator face. This mismatched coupling duplicated the arrangement occurring when (nominally) 2" scintillators are coupled to, say, a 56AVP.

2-3.3 Tube instabilities.

The gain stability of the photomultiplier has been considered, but other agencies may affect the reproduction of the cathode response. The precautions previously mentioned allow handling of a range of count rates; however, the tube may take from a few minutes to several hours to adjust to a change in the count rate (120-22).

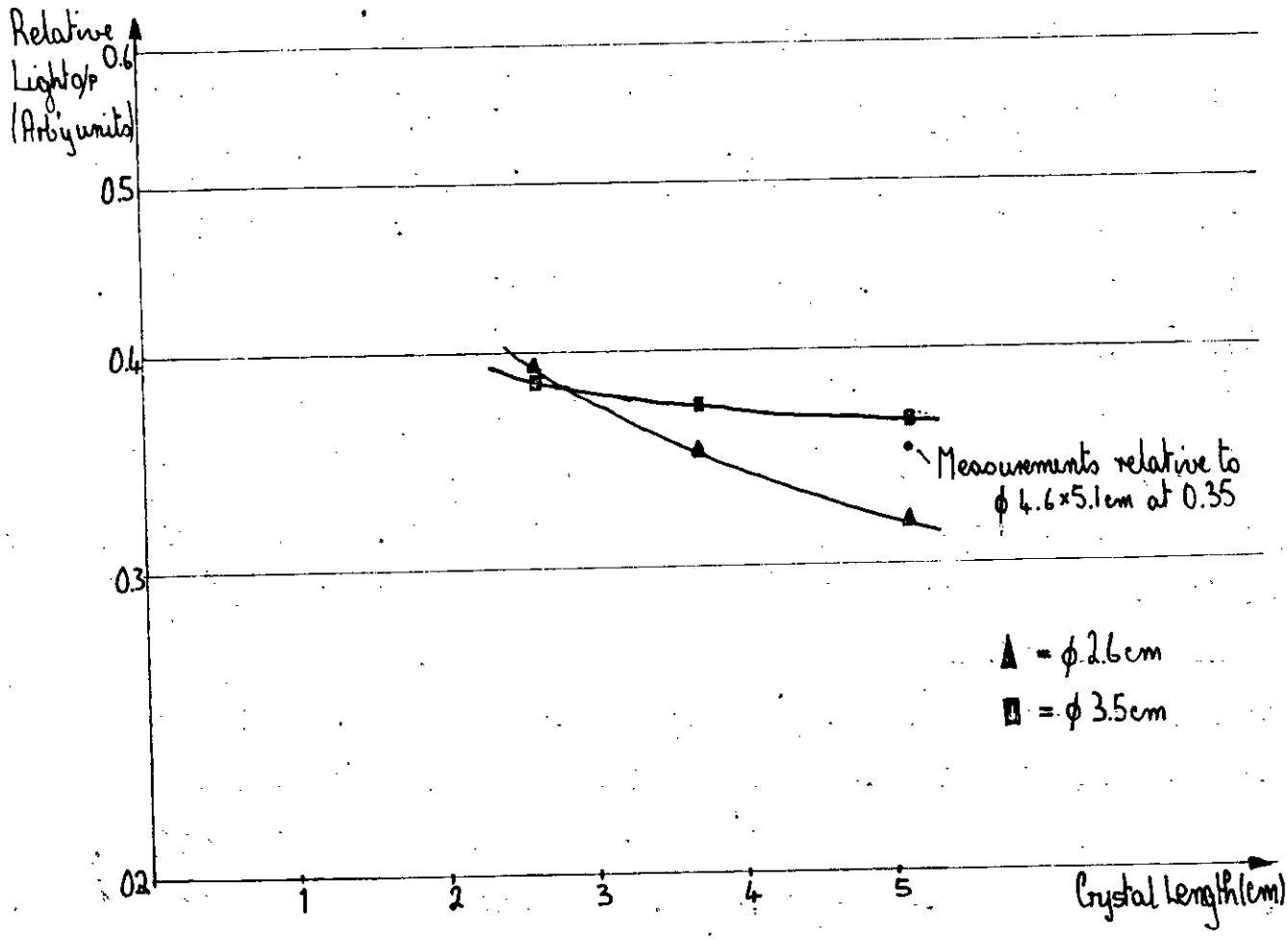

Fig. 31: Light output conversion factors for various sizes of scintillator.

Several small undesirable effects are present in photomultipliers. The temperature dependent thermonic emission (dark current) from the cathode may be shown to be negligible in comparison with the signal pulse (142). There is, however, a substantial change in the spectral sensitivity of the photocathode with temperature, in addition to the drop in response for decreasing temperature as a consequence of increasing resistance in the Cs-Sb photocathode. Recent papers have also indicated considerable fluctuations in sensitivity across the photocathode (123) and examined these fluctuations at various wavelengths (124). Since the optimum focussing and transit times are a function of the sensitivity variation (49), this behaviour has obvious relevance to pulse shape discrimination. Natural radio-activity in all glasses but fused silica produce a cathode response as do weak radiation-triggered scintillations in the tube envelope. Pre-pulsing (125) and after-pulsing (126) are associated with properties of the tube electrodes. Certainly the latter may be diminished by ageing the tube (68).

2-3.4 Field-induced effects in photomultipliers: On linear outputs.

Interference by external electrostatic or magnetic fields has more important repercussions. EMI (127) caution users that material in contact with the tube envelope should be at cathode potential. Charpak has considered the magnetic effect of small coils (128) and the electric effect of charged meshes (129)

in the neighbourhood of the end window. Very small magnetic fields of meshes held at 70v with respect to the cathode seriously perturb the current pulse.

Engstrom (130) has shown the importance of small external magnetic fields on the response of photomultipliers with a cage dynode structure and a similar effect is found in venetian-blind structures. The magnitude of the effect is very dependent on the interdynode voltages and is also increased by any misal ignment of the dynode mounting (Pietri (131) has considered the effect of this on transit time dispersion as well). External fields are particularly important when minimum transit time spread is required or if the cathode diameter exceeds that of the dynode structure (4).

A series of experiments was performed to determine the importance of external fields on the photomultiplier output pulses. Particular incentive for such enquiries was provided by the experiences of Davie (132) with 6262B tubes. His experimental procedure involved the rotation of a rig containing these photomultipliers to remove the effect of structural and efficiency asymmetries in a polarisation experiment. It was discovered that the space-charge saturated pulses at the Owen outputs (used for neutron-gamma discrimination (see sect.3-1)) suffered large orientation dependent changes in magnitude. Accordingly a tube of similar construction - the 6097B, has been thoroughly investigated.

First investigations considered the gain variations of the unshielded 6097B tube with rotation in the earth's field. For this purpose the detector was so positioned that the field associated with power lines and high voltage transformers was minimal. Coupled to this venetian-blind tube was a NaI (Tl) crystal with a Na^{22} source bound so as to be stationary with respect to the detector during rotation. The linear pulse height distribution was recorded in 200 channels of a 400 channel analyser, the 1.28 and 0.51Mev spectrum peaks being used as reference markers.

Figure 32 shows typical spectral shifts for rotations through 180°; reproductability was verified. If this is to be interpreted as a magnetic effect, reference to the EMI catalogue (127)(fig.33) would suggest that since rotations were performed between 'two downwards' and 'four downwards', the relevant components of the earth's field were responsible. In addition, it was found that the spectral shifts obtained, for rotations by 45° steps, were compatible with the interpolated curves shown. If it is granted that, as suggested by Birks (4), the effect of the field on the cathode to first dynode electron trajectory is of major consequence, then when the tube is al igned N - S the vertical component of the earth's field only is effective, while for the tube al igned E - W both components of the field act on the electrons - subject to them being emitted perpendicular to the cathode. Figure 33 also shows the variation of the shift magnitude with EHT, but because of small residual instabilities of the

Fig 32: To indicate linear spectrum shift with rotation

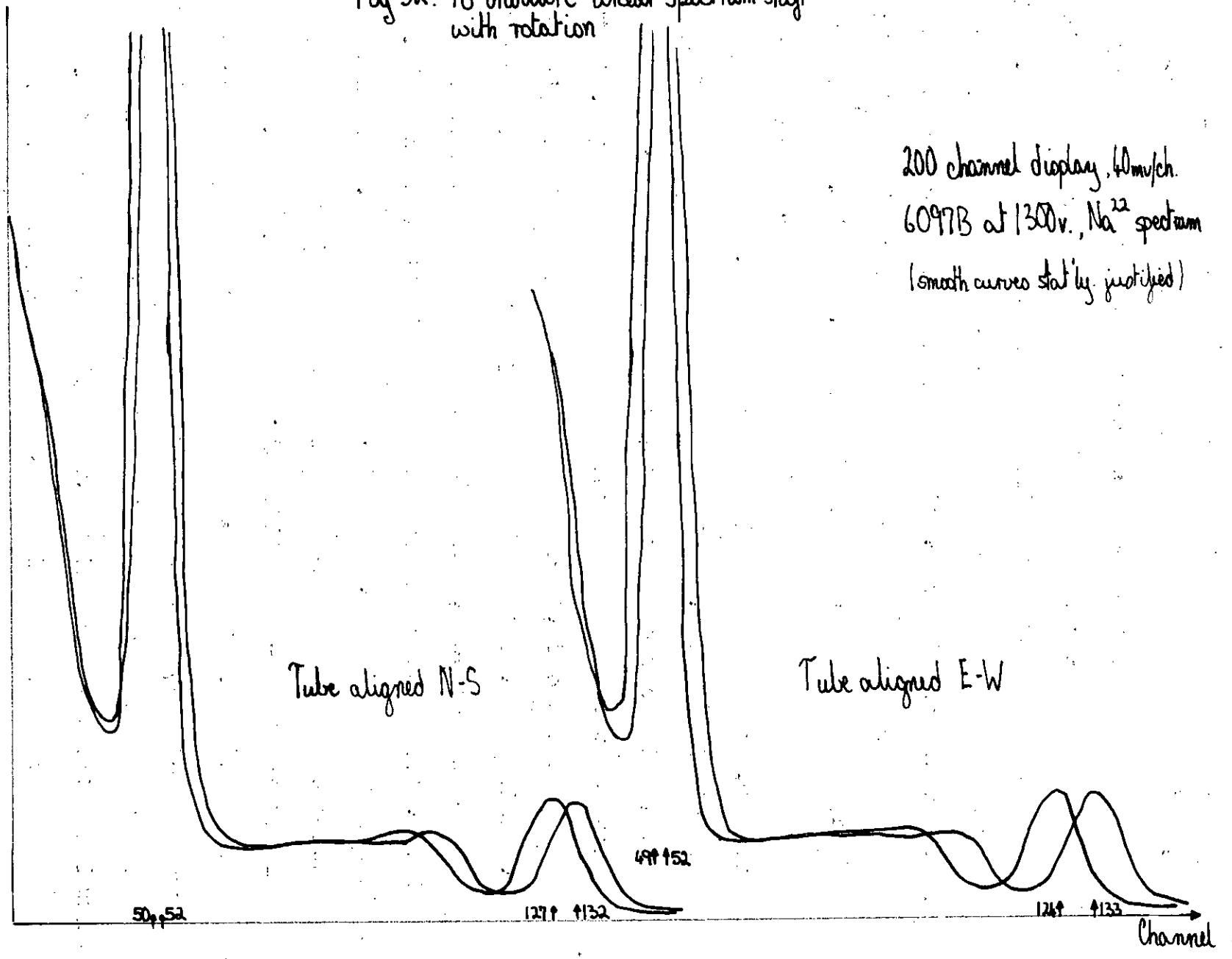

Figure 33.

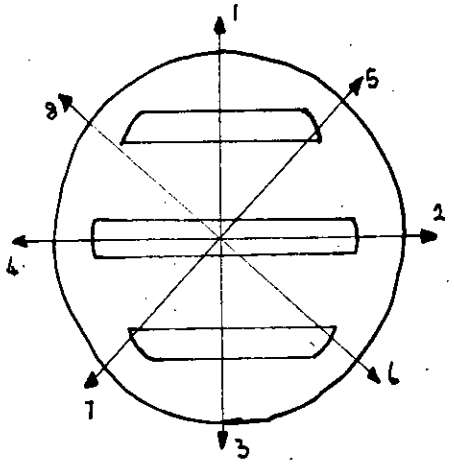

tube cross-section

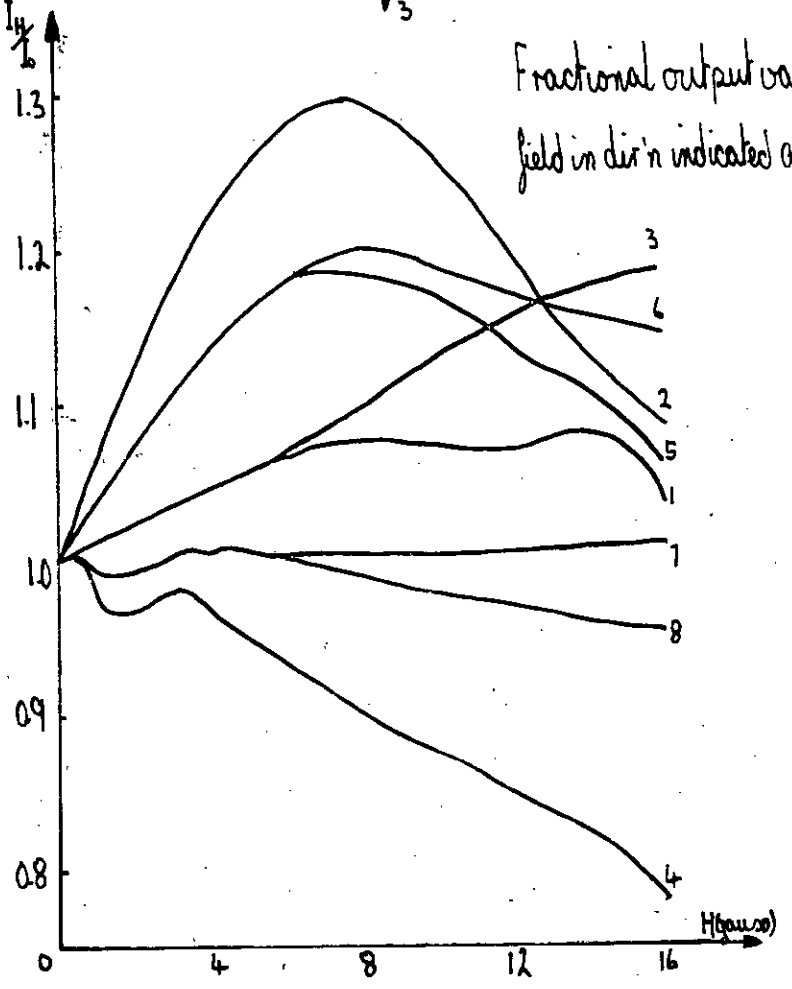

Fractional output vair with field in dir'n indicated above (127)

Effect of increasing EHT on the spectrum shift

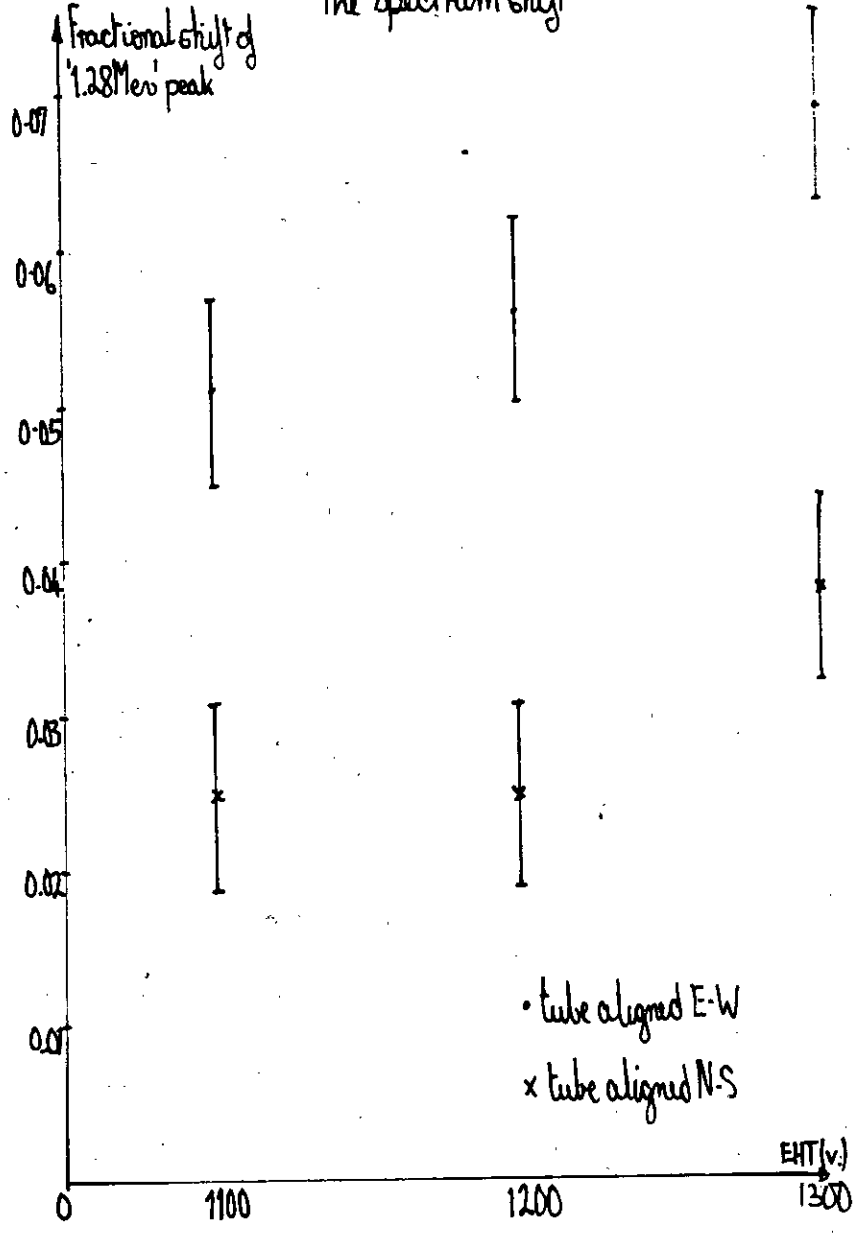

system and limitations to the reading accuracy, even these 'best' results do not allow a meaningful separation of the effects of the horizontal and vertical field components. Bearing in mind that the cathode-first dynode potential is held constant by a Zener diode, it might be expected that any distortion occuring at this stage would be amplified linearly by the rest of the tube. In practice the graph indicates that increasing the EHT, and hence interdynode potentials, actually increases the effect. There was also a slight tendency for larger pulses to be disproportionately more affected than small pulses.

A series of tests were performed to establish whether these effects could be associated with any other unknown. In an effort to eliminate any cable pick-up, the cables were bound together so as to prevent relative motion and a charge-sensitive preamplifier (133) was used to rule out capacitive effects. These and other checks on pick-up from unused outputs, count rate dependence and multi-channel analyser gain variation failed to produce any evidence of association with the above orientation-dependent effect.

It is worth noting at this stage that the changes in pulse height distribution are fairly small so that in particular integral discriminator pulses derived from such a spectrum, and intended for use in gating against signals corresponding to lower energy events, will have an associated threshold which is accurate for, say, 400Kev equivalent electron energy events to within $\pm$20Kev.

A sheet of mu-metal was tested for its shielding properties using a permanent magnet and a flux-meter. The

measurements indicated an average reduction of flux density by a factor of ten. When the sheet was formed into an external shield round the brass cylinder casing of the detector a marked increase (fig.34) in distortion was noted (the tube-shield air-space was approximately 3"). This could be understood as the result of partial screening altering the effective line of action of the magnetic field. A close fitting mu-metal shield prevented the appearance of this phenomenon; it was held at cathode-earth potential (134-5).

2-3.5 Field induced effects in photomultipliers: On Owen P.S.D.

Although anticipating to some extent the full discussion of the Owen technique (Chapter 3), it seems appropriate at this stage to consider the effect of external fields on the output of the last dynode when the last dynode-anode space is subject to saturation. In these experiments the liquid organic scintillator NE213 was used; it was contained in a specially designed bubble free encapsulation to simplify orientation tests. This was optically coupled to the 6097B phototube and irradiated by a 100mCi (nominal) Po^{210}- Be source.

This scintillator is particularly noted for its pulse shape properties and the method of such a scintillator's application has already been touched on (Sect.1-5.2). The positive overswing of the Owen pulses previously referred to has a pulse height distribution as shown (fig.35) and by applying a gating signal to the analyser, the noise and low energy event contributions

Fig. 34 : To indicate the effect of a mu-metal shield on rotational spectrum shift

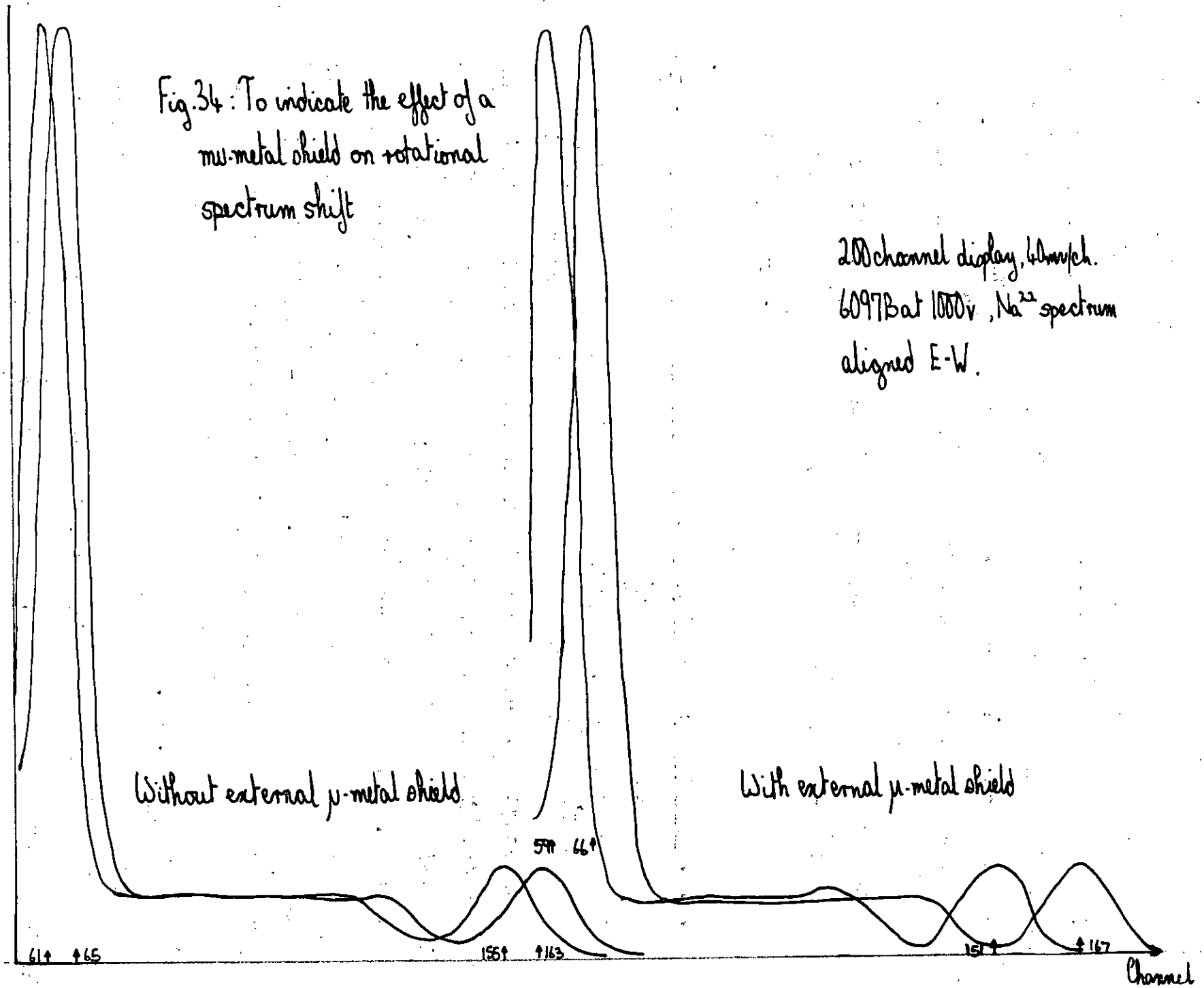

Fig. 35: Pulse height distribution of Owen output pulses.

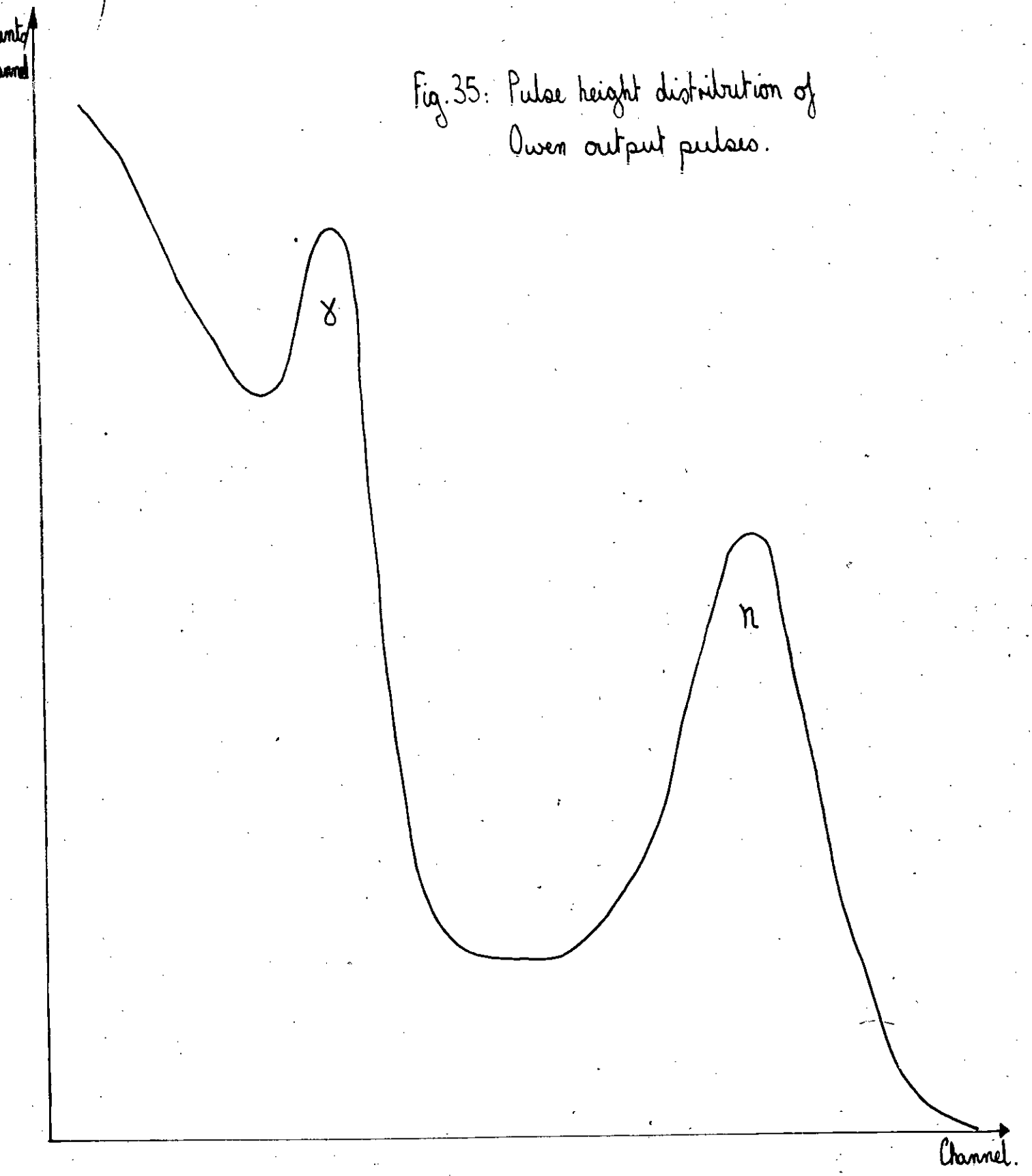

Fig. 36: Owen pulse height distribution
with low energy pulses inhibited.

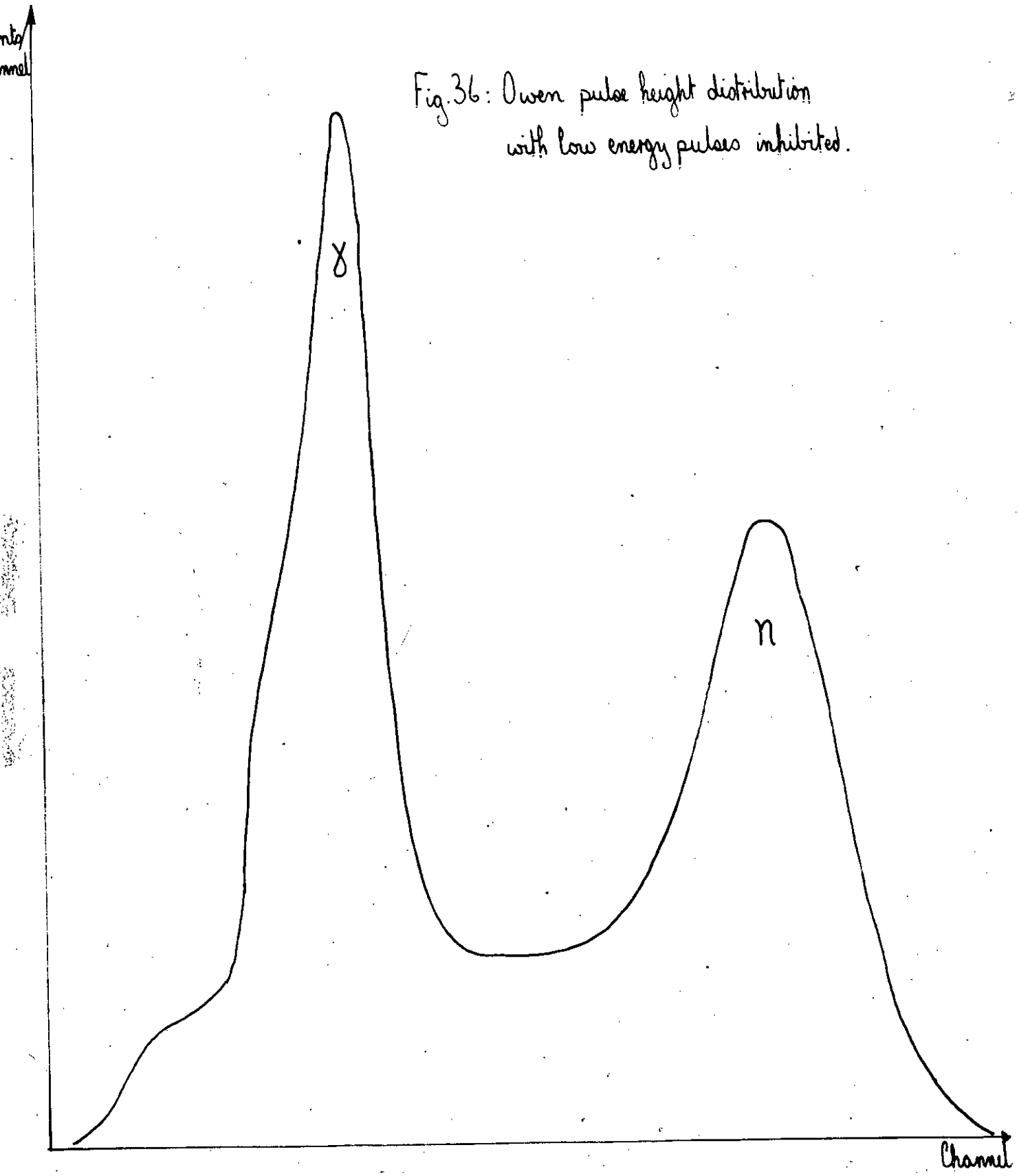

may be removed from the spectrum (fig.36). Such a gating signal may be obtained from a discriminator operating on the linear output of a dynode further down the same tube. The peaks of this spectrum correspond to the amplitudes of the gamma and neutron overswings and to obtain logic pulses identifying a pulse as that of a neutron, a discriminator threshold should be set at some point in the valley. It is obvious that if this amplitude distribution is subject to variation the setting of the discriminator will change with respect to the gamma and neutron peaks.

For this experiment the tube was centrally placed in the homogeneous field of a pair of Helmholtz coils (136). The detector mounting and coil assembly could also be tilted up to an angle of 70° to the horizontal. Such an arrangement allowed almost complete freedom of orientation and magnitude for the applied field. The discriminator operating on the linear output was set for a threshold at 400Kev Compton recoil electron energy, to provide a gating signal as explained above. The count rate above this threshold was about 4,000cps. The peaks of the gated pulse shape discrimination spectrum provided reference markers. From the dimensions of the coils and the formula

$$B_{centre} = \mu_0 \left(\frac{4}{5}\right)^{3/2} \frac{nI}{a/2}$$

the field over the neighbourhood of the tube may be deduced (137). Working in m.k.s. units $\mu_0 = 4\pi \times 10^{-7} \frac{\text{volt.sec.}}{\text{amp.metre}}$, n (the number of turns per coil) = 130 and $a/2$ (the coil radius) = 0.15m. so that for a current of 1 amp., $B_{centre} = 0.7814 \times 10^{-3}$ weber/m^2.

The effect of this applied field is shown (fig.37) for currents of 0.1 to 1.0 amp. In this case the tube was sheathed with mu-metal and the applied field was horizontal and directed towards magnetic North. The shift observed for the smaller currents cannot be caused by effective gain changes because the linear output was shown (Sect.2-3.4) to be little affected at the level of the discriminator. However, at fields of the order mentioned above (i.e. for a current of 1 amp.) it is quite feasible that the gain would be appreciably increased and the consequent lowering of the effective energy threshold would account for the worsening in P.S.D. observed. It may be shown that (138) since the electrostatic intensity (E) and flux density (D) are related, the current density (J) is given by:

$$J = k \frac{V_b^{3/2}}{d^2}$$

where in m.k.s. units, K (a constant of proportionality)$=2.34 \times 10^{-6}$, V_b is the interelectrode potential, and d the electrode spacing. Hence one may appreciate that external fields, even weak ones, may affect the space charge saturation. Furthermore, the large differences (e.g.20%) in V_b required to get optimum pulse shape distinction in different 6097B tubes may be explained by slight differences in the last dynode-anode spacing, according to this formula.

It is more difficult to explain the shift of the peaks on rotation when a large field is applied. The absence of such a shift at lower currents is indicative of the cylindrical symmetry one might expect. When the tube is placed at right angles to the

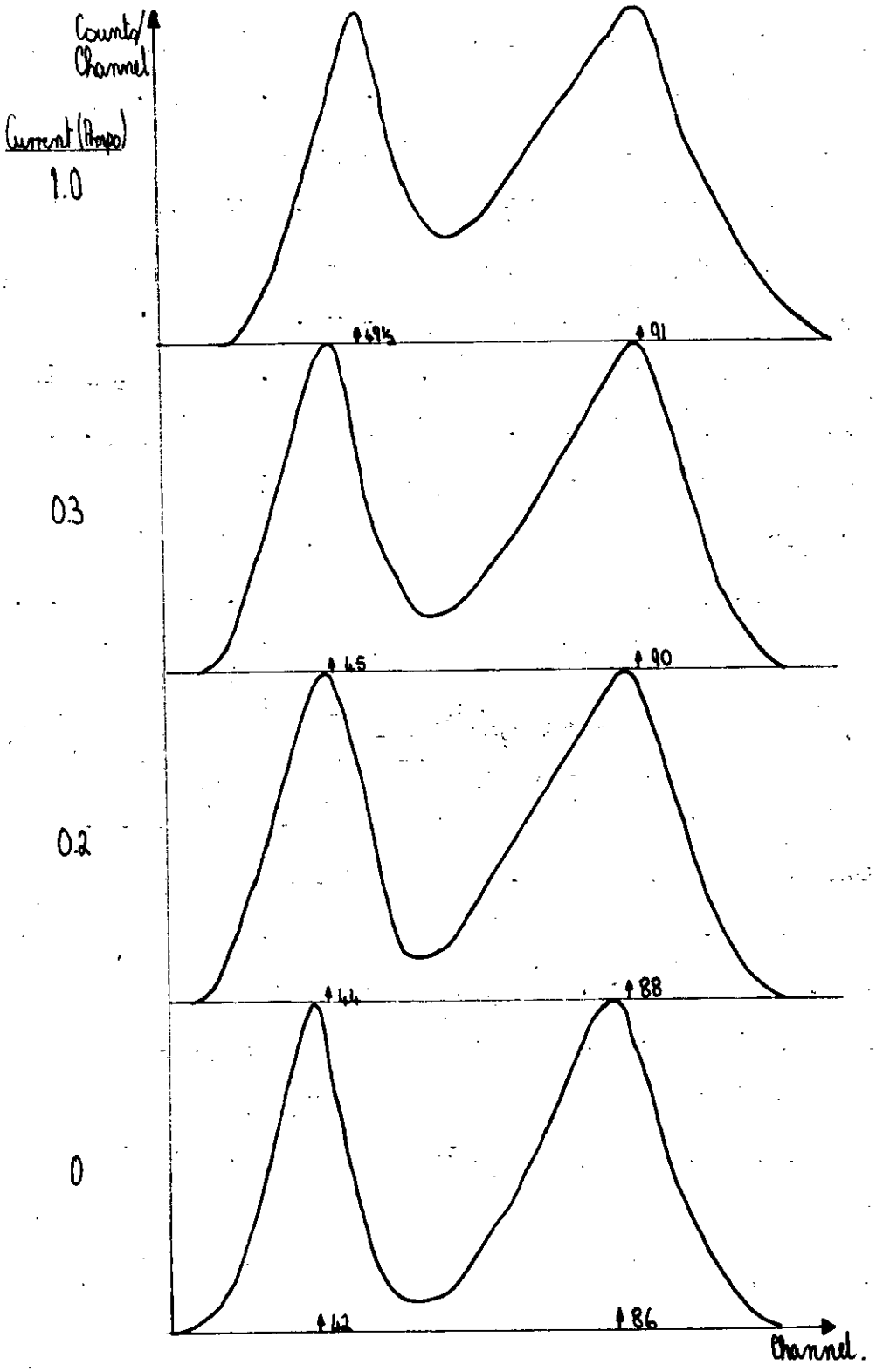

Fig. 37: The effect of applied field on pulse shape discrimination.
(pointing north, horizontal)

field the effects are more difficult to interpret precisely. The shifts are much smaller (Table 4) but the direction of shift is, even for the small currents, noticeably orientation dependent. This may be interpreted by reference to Figure 38 where in this case the angle of inclination of the resultant field (residual earth's plus applied) is a function of the strength of the applied field until the current reaches 0.3 amp; by this stage the residual earth's field is a factor of 10 times weaker. Although these shifts were small, reliance may be placed on their significance as the trends were repeatable and the reference peak numbers consistent to within less than ± 2%.

Table 4: Percentage shift on rotation of the shielded tube through 180° in various fields.

	Current amps	gamma 0°	neutron 0°	gamma 180°	neutron 180°
Parallel to field.	0.1	2%	3%		
	0.2	4.5%	2%	5.5%	2%
	0.3	7.5%	6.5%	9.5%	6.5%
	1.0	16%	8.5%	7.5%	9.5%
Perpendicular to field.	0.1		Negligible		
	0.2	0%	0.5%	2%	1%
	0.3	0%	0.5%	1.5%	1.5%

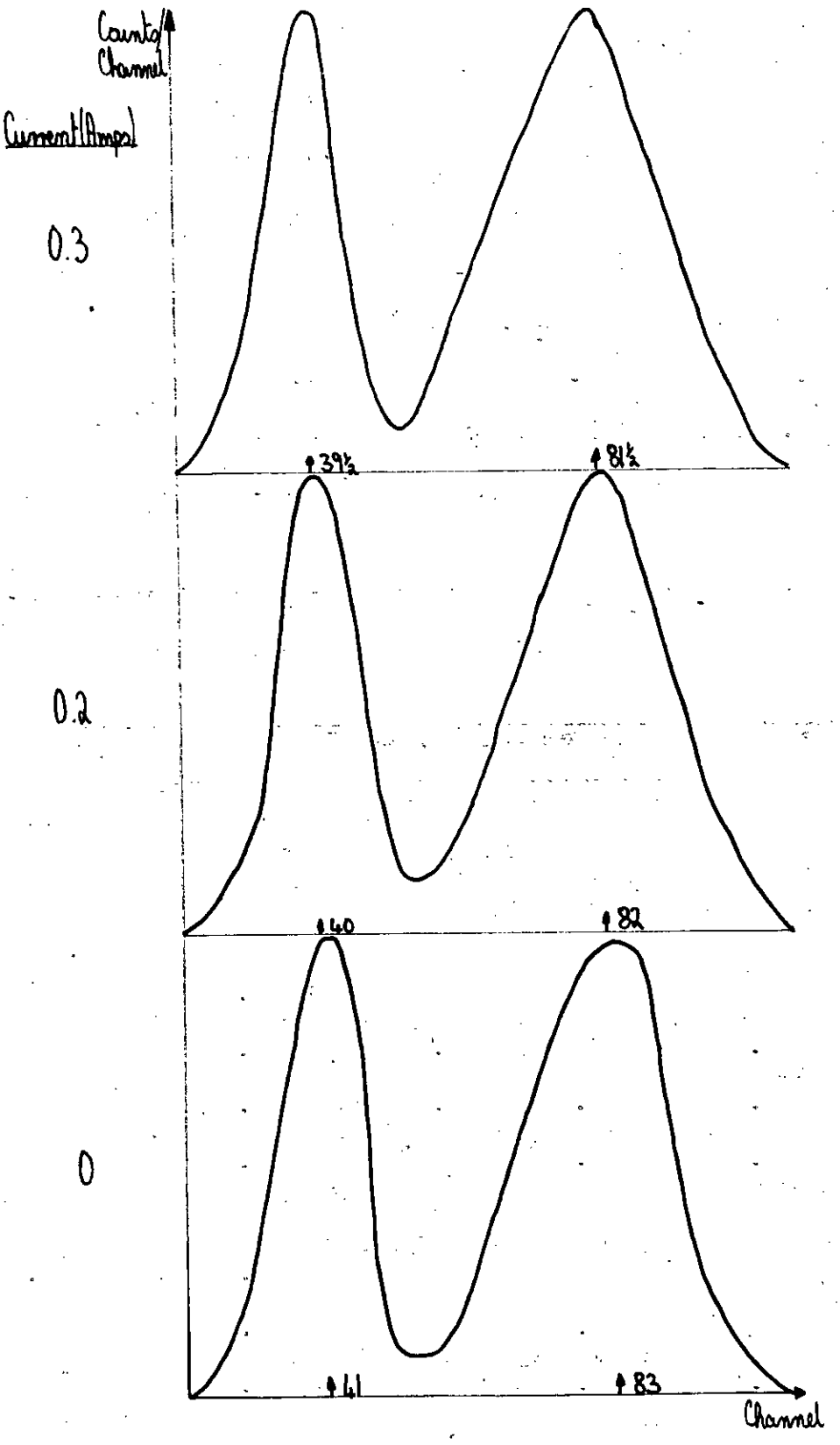

Fig. 38: The effect of applied field on pulse shape discrimination.
(pointing east, horizontal)

A final investigation was performed on the unshielded tube, Table 5 shows the shifts in the peaks on rotation with the tube pointing North and without applied field. It is interesting to note that the magnitude of the shifts is comparable to that obtained with the shielded tube and a coil current of 0.3 amps. This current corresponds to an applied field of 2.3×10^{-4} webers/m^2 as compared with the horizontal component of 1.8×10^{-5}. This shielding factor of 12.5 tallies reasonably with previous measurements on the mu-metal in sheet form (Sect 2-3.4)

Table 5: Percentage shift on rotation of the unshielded tube in 90° steps pointing North in the earth's field.

	gamma 0°	neutron	gamma 90°	neutron	gamma 180°	neutron	gamma 270°	neutron
% shift	0%	1.5%	2%	1.5%	0%	1.5%	2%	1.5%

Finally it was calculated that a current of 61 milli-amps was required to create at the centre of the coils a field equal to that of the earth. The tube and coils were aligned precisely parallel with the direction of the earth's field (a declination of 70°). When the calculated current was passed in such a direction as to create a cancelling field, no shift of the reference peaks was detected on rotation through 360° in steps of 90° (cf.139).

The magnitude of distortion found with this tube is much less than that found in the 6262B. The shifts mentioned above were of the order of a 1/20th of a volt, whereas Davie's were subject to shifts of at least a volt. It has been

conclusively shown that the major cause of the shift in the 6097B is due to magnetic field interactions.This affects the linear output as well as the saturated output pulse height distribution, at small fields the former being distorted by interactions with the cathode - first dynode focussing properties and the latter with the conditions of space charge saturation in the last dynode-anode region. Such interactions may be guarded against by the use of mu-metal or by providing a cancelling field, but shielding appears to be the simplest method.

2-3.6 Stability and Linearity of Electronics.

Further care has to be taken in designing the electronics if linearity and system stability are to be attained. A description of the various modules used and of the tests performed on them appears in Davie's thesis (132). The chief requirements of the system are independence of temperature under normal laboratory conditions, line voltage fluctuations and changing experimental conditions, e.g. count rate, dynamic voltage range. These requirements naturally apply also to the Multi-channel Analyser where in addition there must be stability of the Analog-to-Digital Converter 'zero' and the production of count rate independent spectral shapes. A series of tests was performed therefore to determine the linearity and 'subtract step' of the 400 channel analyser mainly used. Measurements of the voltage multiplication factor, differential linearity and subtract step are compared with the nominal values in Table 6.

Table 6: Differential and Integral Linearity of the Multi-channel Analyser.

Scale factor	nominal actual(±0.1)(mv/ch)		20 21.1	40 41.8	80 80.6
Integral linearity *	nominal <0.2%	actual	1±0.25%	0.6±0.1%	2.2±0.3% (at low end of conversion)
Differential linearity	nominal <2%	actual	<2%	<4%	<9%

Subtract step nominal 0.1v actual 0.14v

*Defined according to Kowalski (39) in the absence of intelligible definition in Laben handbook (fig.39).

These tests were performed with a 'Solatron' measuring oscilloscope and pulse generator, the output of the latter being shaped as shown (fig.40) to approximate closely to the pulse shapes to be analysed in practice.

The process adopted for checking the linearity of the whole system has been dealt with previously (Sect.2-3.4).

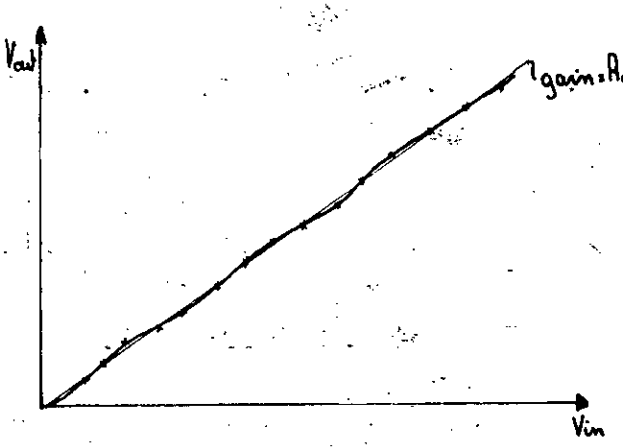

integral non-linearity $\epsilon_i(V_{out})$: $V_{out} = V_{in} \cdot A_0 [1 + \epsilon_i(V_{out})]$

differential non-linearity $\epsilon_d(V_{out})$: $dV_{out} = dV_{in} \cdot A_0 [1 + \epsilon_d(V_{out})]$

Fig. 39: Definitions of linearity.

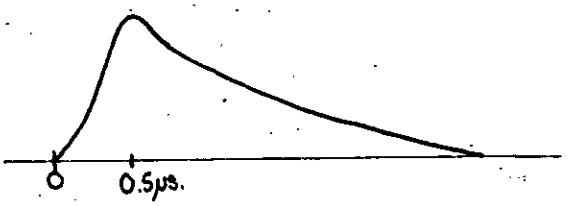

Fig. 40: Pulse shape used to check analyzer.

CHAPTER 3

Pulse Shape Discrimination by the Owen-Batchelor technique.

3-1 Theory of the Owen-Batchelor technique:

Two P.S.D. methods have been considered in detail. The first method, the Owen-Batchelor technique, essentially examines the proportion of slow component in the light output of the organic scintillator. Suhami and Ophir (140) have shown that this proportion is energy as well as particle dependent.

Consider the last dynode circuit (fig.41); assuming that the photomultiplier faithfully reproduces the light pulse shape $I_{n-1} = I_o e^{-t/\tau}$ and $I_n = \delta I_{n-1}$ where τ is the decay constant and δ the multiplication factor at the last dynode. The signal voltage is given by:

$$C\frac{dV}{dt} + \frac{V}{R} = I_n - I_{n-1} = (\delta - 1)\, I_o e^{-t/\tau}$$

If $V = -V_o$ when $t = 0$ then:

$$V_p = RI_o(\delta-1)\left(\frac{\tau}{RC} + \left(\frac{\tau}{RC} - 1\right)\cdot\frac{V_o}{RI_o(\delta-1)}\right)^{-\frac{RC}{\tau-RC}} \qquad 1.$$

and

$$t_o = \frac{\tau RC}{\tau - RC}\ln\left(1 + \left(\frac{\tau - RC}{\tau}\right)\frac{V_o}{RI_o(\delta-1)}\right) \qquad 2.$$

or

$$= \frac{\tau RC}{\tau - RC}\ln\frac{RC}{\tau} + \tau\ln\frac{RI_o(\delta-1)}{V_p} \qquad 3.$$

(See appendix for complete derivation).

1. and 2. imply that both V_p and t_o are related to V_o/I_o and both V_o and I_o must be proportional to the energy associated

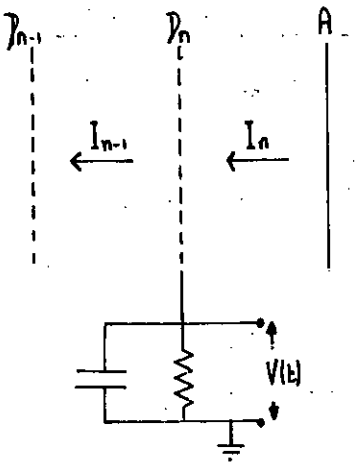

Fig. 41 : The last dynode circuit

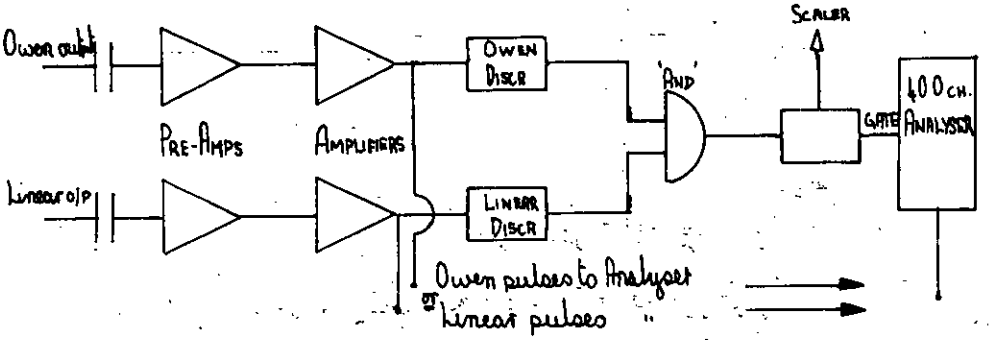

Fig. 42 : Pulse Shape Discrimination - Block Diagram.

with the pulse. Thus V_p is proportional to I_o and hence to E. On the other hand t_o will only depend on τ . Figure 22 shows how the value of τ determines the output voltage amplitude. A block circuit diagram of the P.S.D. assembly is shown in Figure 42, conventional voltage preamplifiers, delay/discriminators and amplifiers being used throughout in this rather qualitative assessment.

3-2 Application of Owen P.S.D. with various tubes.

3-2.1 Application with a slow tube.

Linearity of the 6097B photomultiplier assembly having been verified up to 1350v at the tenth dynode, this output was used as the source of linear signals though, as remarked by Bucher et al. (58), the properties of the scintillator create marked nonlinearity of proton pulses for energies of 1 to 10Mev. The scintillator used in this experiment was NE213 (151) in a glass side-bulb cell (2" x 2" height). It was held stationary with respect to the photocathode by formers, sponge wadding and cord Optical bonding with silicon grease (118) gives minimum changes of refractive index between the glass cell and the lime soda photomultiplier window. The voltage over the last dynode-anode stage was adjusted over a wide range by means of a high quality linear 10k potentiometer (141). Further particulars of the dynode chain have already been given (Sect.2-2). The voltage preamplifier was a compound common emitter with inverted output available from the collector of the second stage. Sufficient explanation of the electronics appears elsewhere (132).

With the 'linear' amplifier coupled to the analyser, the 'linear' discriminator may be adjusted to supply pulses to the 'coincidence gate' input for those linear pulses above a certain amplitude. Using a standard gamma source the discriminator could thus be set to veto pulses corresponding to Compton electron recoil energies below a chosen value. Since the analyser used had been adjusted for another purpose so that the logic level at the gate input was not examined until 6 μs after the pulse received at the input, (rise-time protection) such a delay had to be placed in the discriminator - logic converter branch. In calculating the correspondence between voltage and energy, the corrected values of subtract step and voltage scaling factor (Sect.2-3.6) were noted.

The gamma source was replaced by a gamma - neutron source and the output of the 'Owen' amplifier analysed. If these pulses were 'gated' at the analyser by the above 'linear' discriminator pulses, the 'Owen' spectrum was obtained for energy events above a set threshold, but irrespective of the time the 'overswing' crosses the base-line. As in the Batchelor (79) method, discrimination against signals crossing the zero axis after large ($\sim$2 μs) intervals of time (mostly high energy gammas) can be achieved by requiring coincidence between the variably delayed Owen discriminator output and the linear discriminator output. The occurence of such a coincidence was signalled by a pulse from the 'and' gate and similarly treated as a gating pulse. In practice, the gating pulse was such as to inhibit pulses associated with

noise and low energy gammas (a threshold corresponding to 100Kev Compton electron recoil energy) and those high energy gamma pulses which cross the base-line 1.5 μs or longer after the 'linear' discriminator is triggered. However, the timing condition was not usually enforced as the saturation conditions could be adjusted to give very small positive overshoots for all gamma pulses.

The various stages in the processing of the Owen output are illustrated by Figure 43. This shows the pulse height distribution of signals at the output when a gamma-neutron source is placed near the detector. The separation of the gamma and neutron peaks is then increased by the rejection of pulses from recoil events in the scintillator below a certain threshold, and then further improved by dismissing from consideration those gamma pulses which tend to be mistaken for neutrons.

3-2.2 Optimising and performance rating.

Figure 44 indicates the procedure adopted in selecting the best last dynode-anode voltage for distinction between neutrons and gammas. The case illustrated involves comparison of spectra obtained above a certain threshold, though ungated spectra were sometimes compared for this purpose. The criteria on which these comparisons were based involved the peak separation and the relative depth of the gamma-neutron valley. Also shown is the technique whereby gamma rejection and neutron acceptance ratios were deduced. Some justification for such extrapolations of the

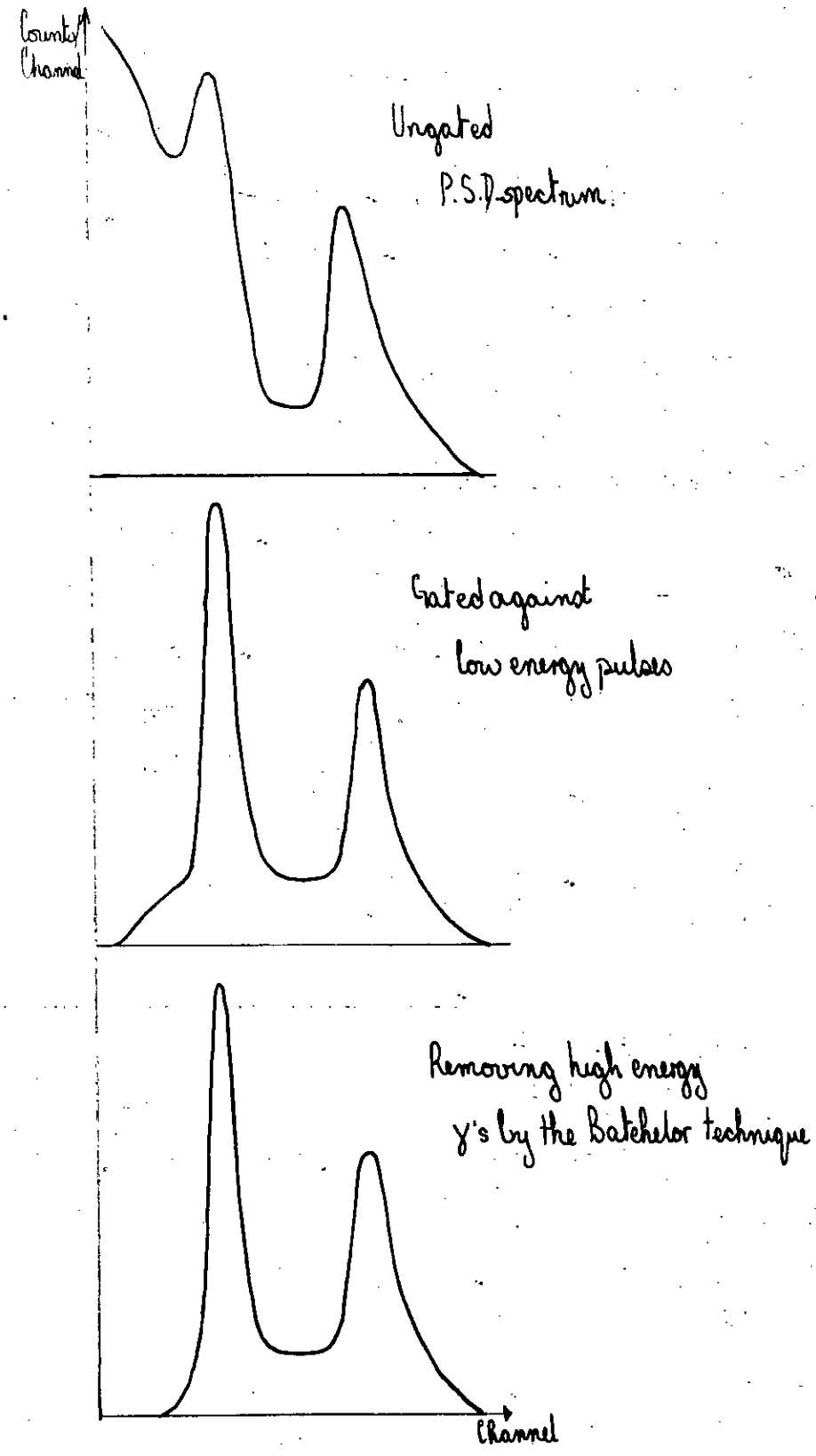

Fig. 43: The stages in processing of the Owen output.

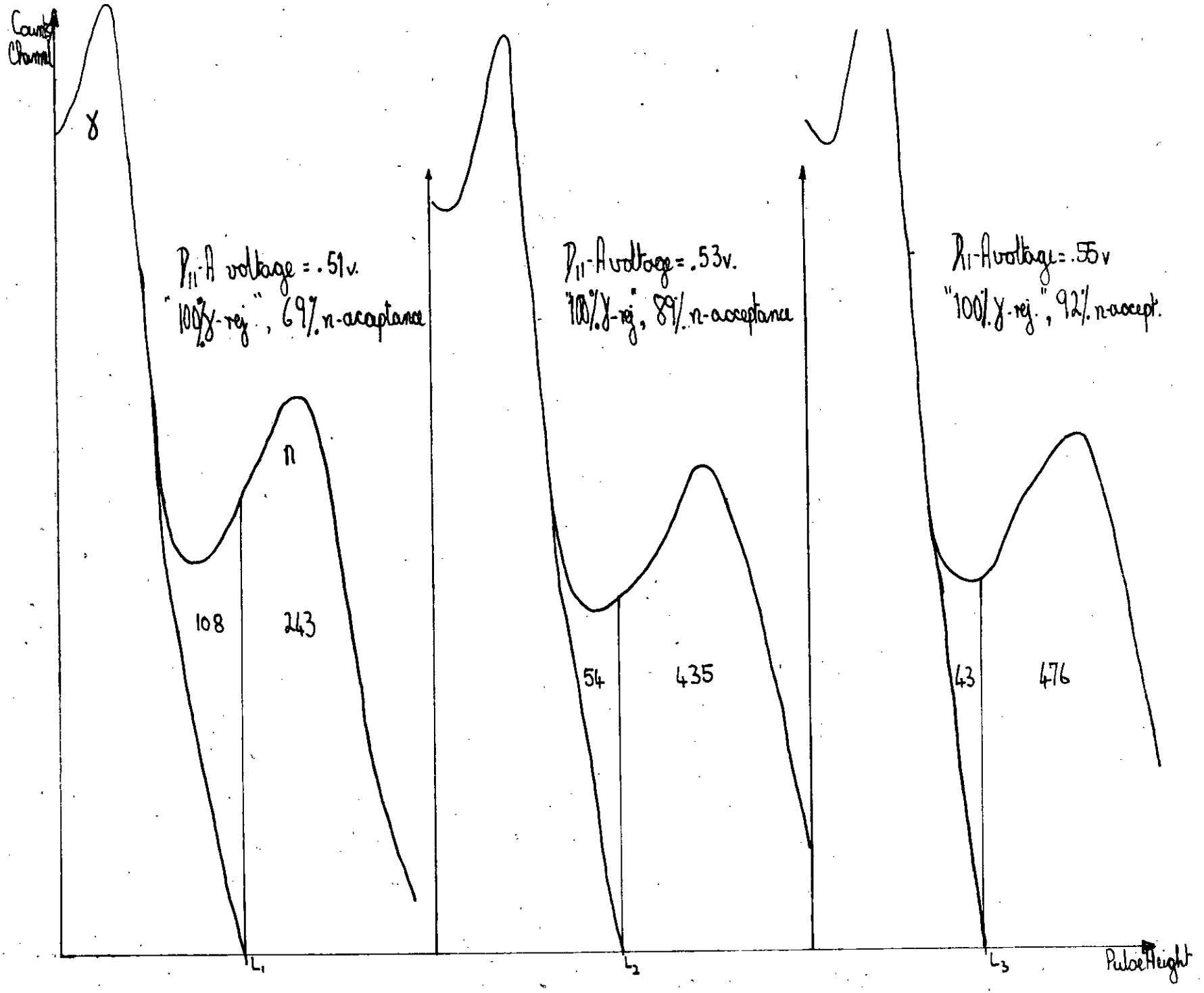

Fig. 44: To demonstrate the zero-gamma bias position.

gamma peaks may be obtained from Figure 45 which shows the superposition of the Owen pulse height distributions for a gamma-neutron source and a Pitchblende source, this latter being chosen because the gamma energy range stretches up to 2.6Mev. On the basis of such extrapolations, one may deduce the gamma rejection ratios obtained with a discriminator level set at various points in the gamma-neutron valley. These were checked in practice by finding the proportion of Pitchblende gamma pulses which exceeded the various discriminator levels, the output of the Owen discriminator being passed to a scaler for a set time and compared with the number of pulses accumulated by the Analyser in the linear spectrum over the same period of time. For the low count rate concerned errors due to dead time were negligible ($<5\%$). These gamma-acceptance ratios are shown in Figure 46 for various 'Owen' discriminator settings. The gamma-neutron flux in this case was from the 1Mev. Cockroft-Walton accelerator at the High Voltage Laboratory of the department. A mono-energetic beam of neutrons (3.5Mev) was obtained by the $^{2}H\ (d,n)^{3}He$ reaction, bombarding a deuterium target with deuterium ions accelerated through a potential of about 800kv. The ineffectiveness of the Batchelor (79) technique in this connection is associated with the absence of high energy gamma-rays from the set's radiations. The detector was a side-bulb 2" NE213 scintillator mounted horizontally on a 6097B phototube. The optimum saturation voltage was about half a volt, and 1.2volts in a second 6097B tube used.

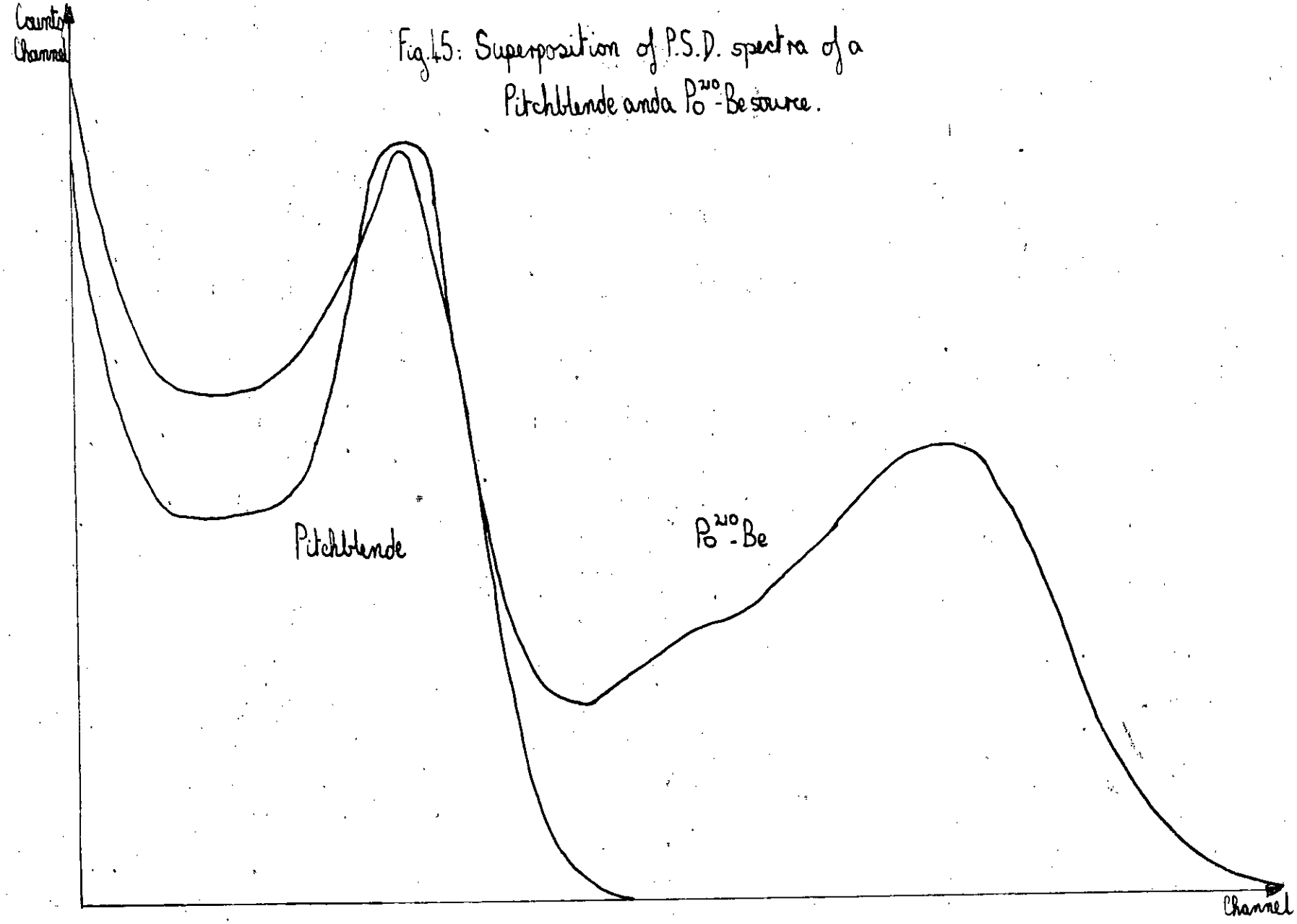

Fig. 4.5: Superposition of P.S.D. spectra of a Pitchblende and a Po^{210}-Be source.

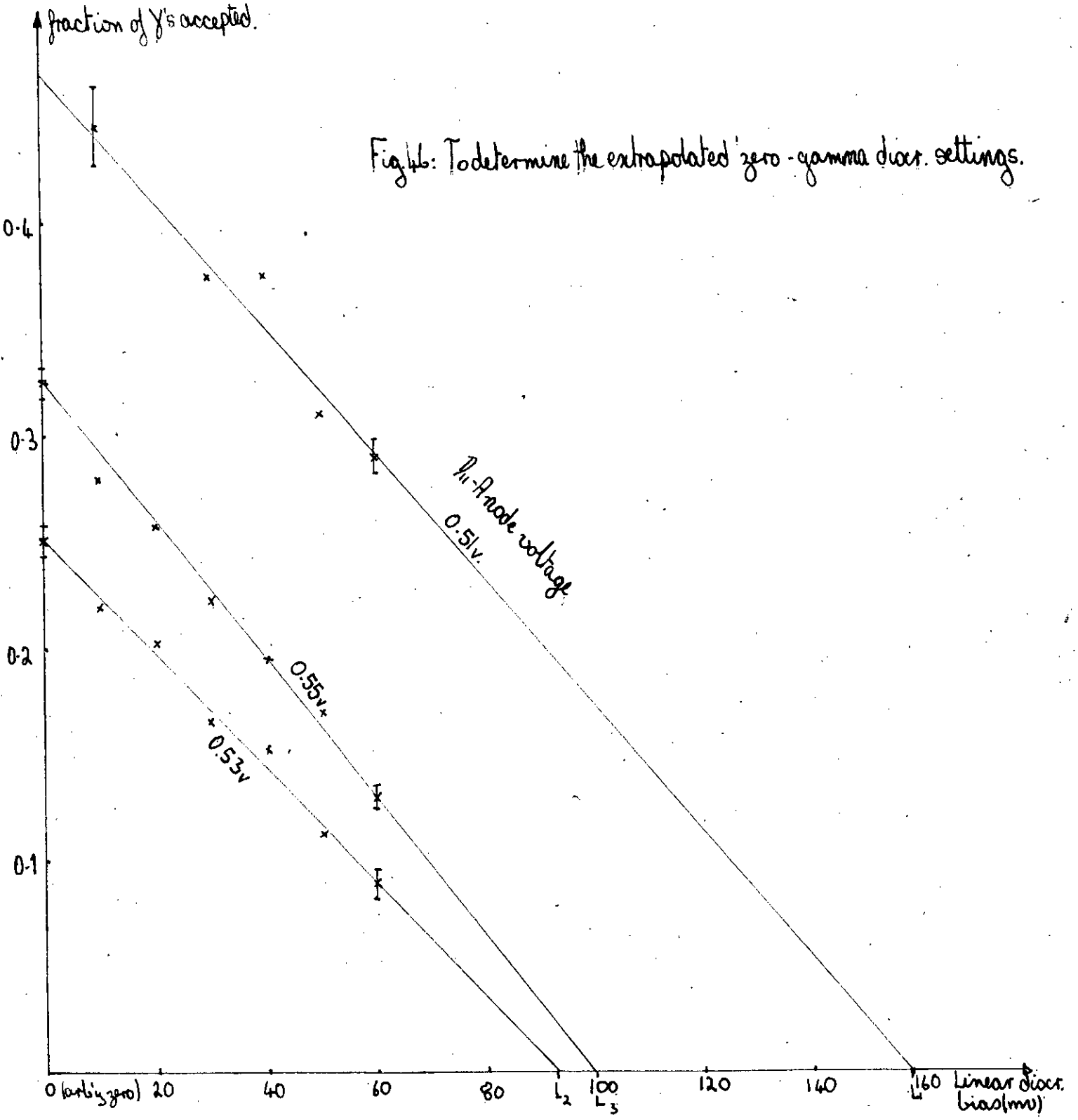

Fig 46: To determine the extrapolated 'zero-gamma discr. settings.

Similar differences in best dynode-anode voltage were observed in ten stage RCA tubes by Tanaka (142); Owen (7) who also used a 6097B tube found a setting of 4v. anode-last dynode was the best.

With a saturation voltage of 0.55 volts and the discriminator bias set slightly lower (by 28mv.) than shown, 99.9% gamma rejection was obtained with an improved neutron acceptance of 96%. The slightly higher saturation voltage also gave more gain. The good quality of this discrimination may be partly due to the fairly mono-energetic nature of the neutron source and the small proportion of high energy gammas. The indications were that the discrimination was very sensitive to the gamma discriminator bias position and hence for a wider range of energies distinctions would not be drawn so efficiently.

3-2.3 Source dependence.

In order to determine the relation, if any, between source and pulse shape discrimination performance a comparison was made (fig.47) of the spectra obtained with a Po^{210}-Be source and the H.T. set acting as source. The scintillator used was NE213 on the 6097B tube. The data were collected at slightly different rates - difficulty was encountered in adjusting the set and position of the detector to obtain the required intensity of radiation while still keeping the required proportions of gammas and neutrons. These adjustments were performed so that the sole difference between the two sources was in the energy range of the radiations detected. Under these conditions it was surprising

Fig. 47: To illustrate source dependence for the Owen technique.

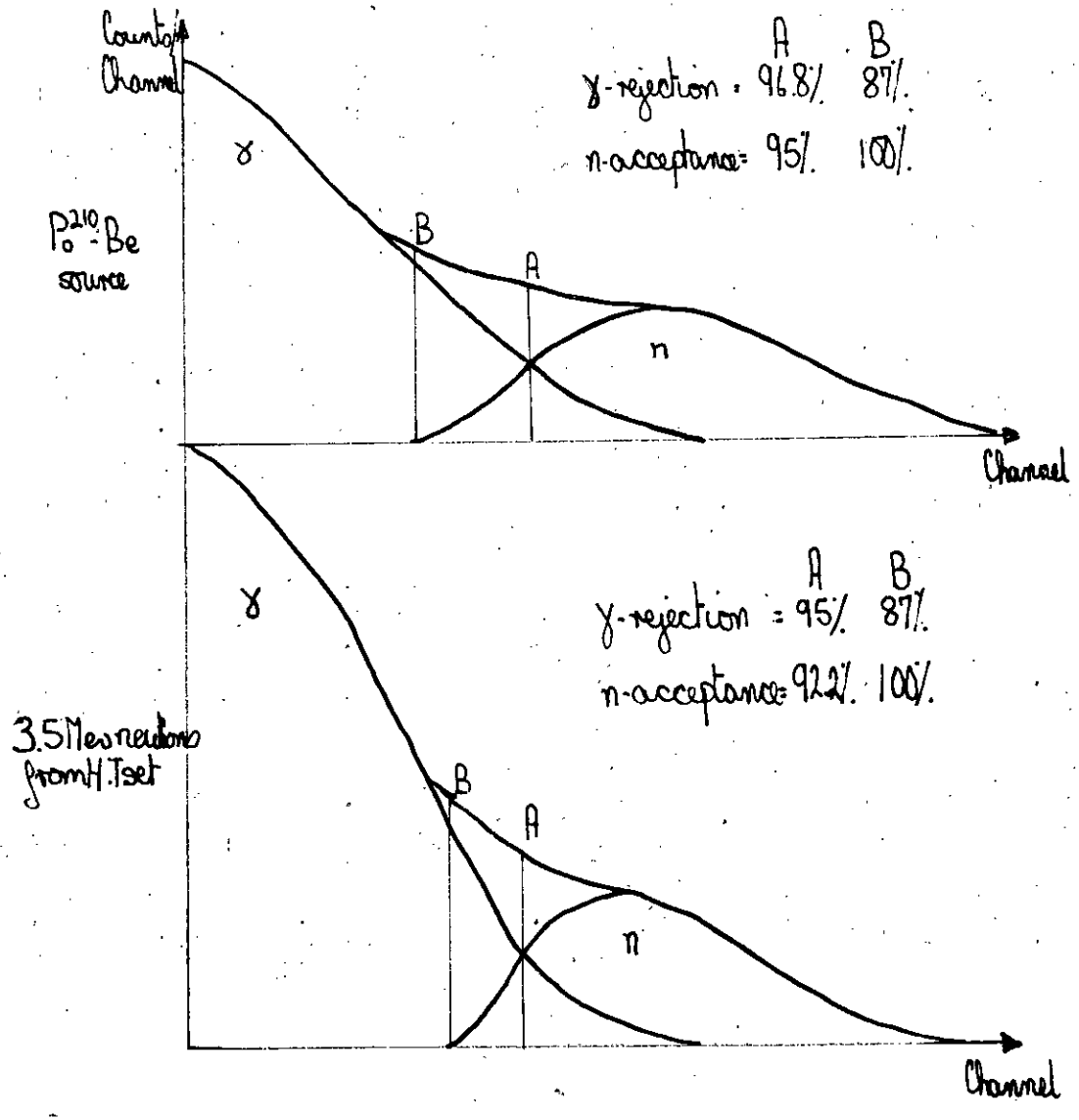

to note very little difference in the spectra obtained particularly as the neutron energy from the set was 3.5Mev and that from the source extended up to 10Mev. However, it is later shown (Sect.3-2.5) that the degree of discrimination in NE213 is largely dependent on the proportions of low energy neutrons and of gammas up to 1Mev in energy. It would thus appear to be a satisfactory explanation of the similarity of the pulse shape discrimination spectra if it is suggested that the neutron and gamma contributions are also similar for the two sources over this above mentioned energy range.

3-2.4 Scintillator and Tube Comparisons.

The convenience of the Po^{210}- Be source facilitated a series of tests on the liquid scintillators (Table 7). A number of headings require explanation: the dimensions are the face diameters of the different scintillators; the delay is that applied to the logic output of the 'Owen' discriminator to remove high energy gammas (fig.23); the figure-of-merit has been defined (Sect.1-2.1) and these values correspond to a threshold at 400kev equivalent electron recoil energy; the Owen voltage is the anode-last dynode voltage, the value being obtained from an earlier calibration of the 10k ohm potentiometer across this stage. These last optimum voltages were found to be much the same except for sample C of NE213 scintillator which also produced significantly poorer discrimination. This was the oldest sample of NE213 tested and it has been suggested (144) that at the time of its

preparation (1953) the essential process of de-oxygenisation was not performed so thoroughly. Aging was dismissed (144) as a highly unlikely cause. Also worth note was the noticeably superior performance of a side-bulb sample of NE213 - this also worked best at slightly weaker saturation.

Table 7: Comparison of performance with various scintillators on the 6097B phototube.

Scintillator	Delay	Figure-of-merit	Owen volts
2" NE213 A	0.6μs	1.24	1.12
	0.9μs	1.19	
2" NE213 B	0.4μs	1.43	1.20
	0.9μs	1.28	1.28
1" NE213 C	0.35μs	1.14	0.72
2" NE213 D	0.9μs	1.25	1.12
2" NE218 D	0.9μs	1.04	1.12
2" NE218E D	0.9μs	1.25	1.12

A = bubble free encapsulation, B = side-bulb cell, C = old sample D = standard cell.

At a later date a further series of tests was performed with a different range of scintillators, the performance in each case being compared with that obtained with a 56AVP tube. The two scintillators mentioned above which required different 'Owen' voltages were omitted from this comparison and the voltage fixed at 1.12volts for the 6097B, and the corresponding optimum voltage for the 56AVP was 3.6volts. Care was taken to minimise the

exposure to light during changes of scintillator; adopting this procedure, half an hour on H.T. sufficed to guarantee stability and low dark current. In this case the 'linear' discriminator threshold was set by the first Compton edge of the Na^{22} spectrum, a Compton electron recoil energy of 340kev, for a count rate of about 4,000cps. The table (8) gives the mean peak-to-valley ratio for both the gated and ungated pulse discrimination spectra and for the case of the 6097B, the figure-of-merit of the ungated spectrum; the figure-of-merit is also given at 1 and 2Mev electron recoil energy.

Table 8: Comparison of performance with various scintillators on the 6097B and 56AVP phototubes.

Scintillator	ungated P/V	gated P/V	bidimensional 1Mev	M	2Mev
56AVP					
NE213 D		3:1	2.5		2.75
NE218 D	3:2	30:1	2.1		2.2
NE218E D		3:1	2.45		2.0
NE230		12:1	1.0		1.0
NE232			0.7		0.8
KL360	2:1		2.0		1.5
6097B					
	P/V	P/V	M		
NE213 D	3.5:1	7.5:1	1.27	0.8	1.64
NE218 D	2:1	1.8:1	1.0	1.0	1.0
NE218E D	2.5:1	4:1	1.16	1.0	1.6
NE230				0.77	1.0
NE232					
KL360	2.5:1	4:1	1.18	1.0	1.25

Misleading features of figures-of-merit.

The misleading nature of certain figures-of-merit (Sect.1-2.1) is exemplified by this table. Firstly, the peak-to-valley ratios are quoted because of the ease of visualising performance from such figures; they are a direct indication of the gamma rejection ratios obtainable (fig.3). The quality factor, M, is also quoted but it is immediately apparent, particularly for the 56AVP, that there is little correlation between M and the P/V ratios. In fact, M is only a reliable figure-of-merit when the pulse height distribution closely approaches a double gaussian - any departure from this, i.e. any skewness, gives a false impression of the discrimination obtainable (see fig.48,also (2)). Equally important is the energy range with which these figures are associated. Thus figures-of-merit quoted at 1 or 2Mev equivalent electron recoil energy are superior to those for energies above, say, 340kev which in fact represent some form of weighted mean of performances over discrete energy intervals above this threshold. Further significance may also be obtained from bidimensional displays (Sect.3-2.5).

Certain of these scintillators are of particular interest: the NE230 and 232 scintillators are based on deuterated solvents and KL360 (150) is a less well-known scintillator with P.S.D. properties similar to NE213. Although the deuterated scintillators are supposed to have longer phosphorescence decay times, (145) they have been thoroughly investigated (146) and shown to have

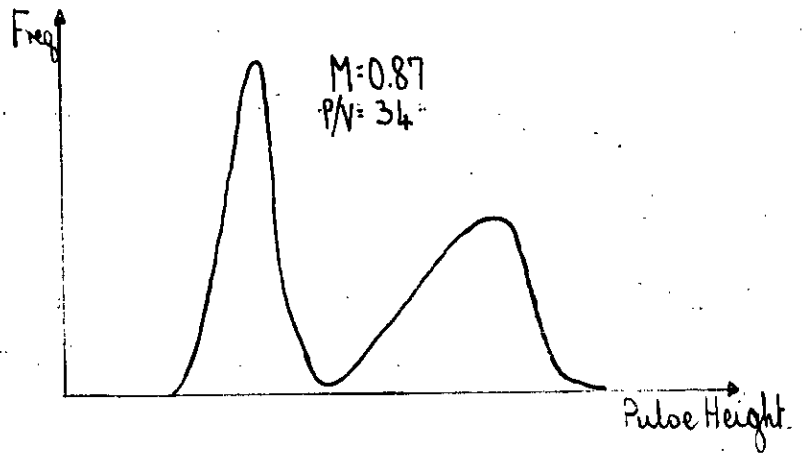

Fig. 48: To illustrate the misleading nature of figures-of-merit for skew P.S.D. distributions.

excellent P.S.D. potential particularly in charge comparison techniques (147-48). It is therefore surprising to note the inferior performance obtained in this case. No improvement was obtained despite a systematic trial of various saturation voltages and it was concluded that complete redesign of the dynode chain was required. As these deuterated samples only became available towards the end of this research, such alterations were not performed. A comparison of figures for the 6097B photomultiplier and the standard cells in Tables 7 and 8 shows as expected the superior performance obtained at the slightly higher threshold; the slight disparity in the case of NE213 is attributed to poor optical coupling in the earlier experiment.

One noteworthy distinction between the performance of the 56AVP and the 6097B is the degree of gamma-neutron separation in the ungated spectra. This is indicated by the P/V values - blanks indicate the absence of any valley between the gamma and neutron peaks.

At very low biases, i.e. 100kev and less, it would appear that the 6097B is far preferable to the 56AVP, but the situation is reversed for thresholds in the region of 400kev. This is illustrated by photographs (1) of the analysis displays. However, comparisons are misleading in this second case because the cross-over conditions in the faster tube are much more particle dependent and this leads to an implicit logic gating condition which is related to the 0.6 μs length of the discriminator pulses. A schematic explanation of this appears in Figure 49. As a consequence of this additional 'delay' gating

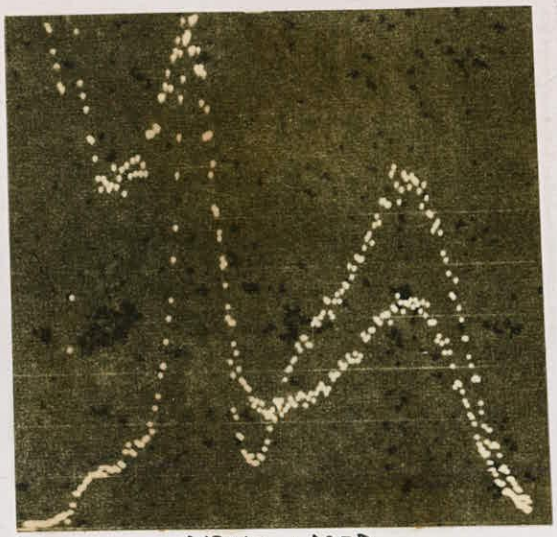

NE213, 6097B

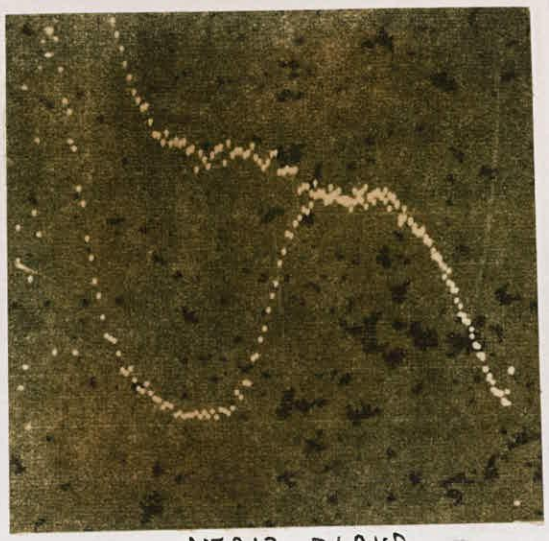

NE213, 56AVP

Photos 1: Ungated and gated Owen P.S.D. spectra.

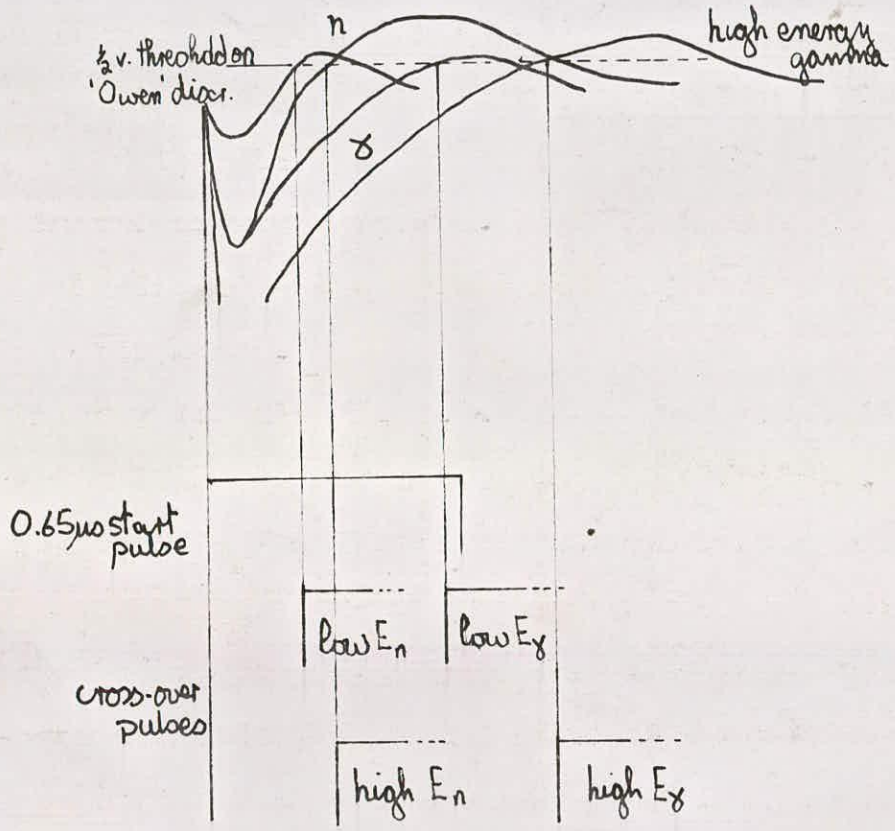

If the start pulse is delayed too much in order to count more gammas, weak neutron pulses are discarded.

Fig. 49: Implicit logic gating in the 56 AVP.

the figure-of-merit, M, is in general a poor guide and the alternative quality factors are more significant.

3-2.5 Interpretation with bidimensional displays.

A deeper understanding of the importance of the threshold may be obtained by reference to the so-called bi-dimensional display. This is explained by Figure 50 which shows this display to be a representation of the probability of occurrence of certain pulses as a function of saturated pulse height and corresponding equivalent electron recoil energy, the pulses analysed being those resulting from some P.S.D. technique. The efficiency of a technique is indicated by the distinction in pulse height between signals from different types of radiation, and the energy range over which this is attained.

Such bi-dimensional displays were obtained by photographing the bi-dimensional analyser screen with an exposure time of 10 seconds during a run. The 'flicker' photographs were thus obtained; in these the intensity of each spot indicates the frequency or probability of occurrence of a signal of a particular amplitude and with a particular associated electron recoil energy. The examples shown (Photograph 2), for NE213, underline the differences in performances obtained with the two tubes: in the 56AVP, the spurs are narrower and straighter, and tend to run parallel. Comparing these pictures it is easy to see that a straightforward pulse height analysis of these signals will produce entirely different results. In the ungated spectrum for

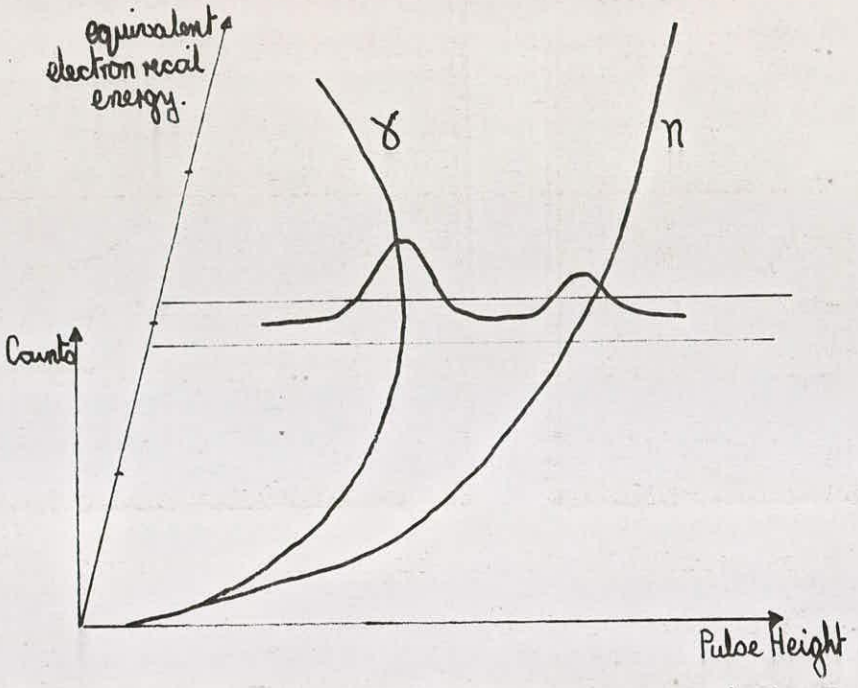

Fig. 30: Explanation of the bi-dimensional display.

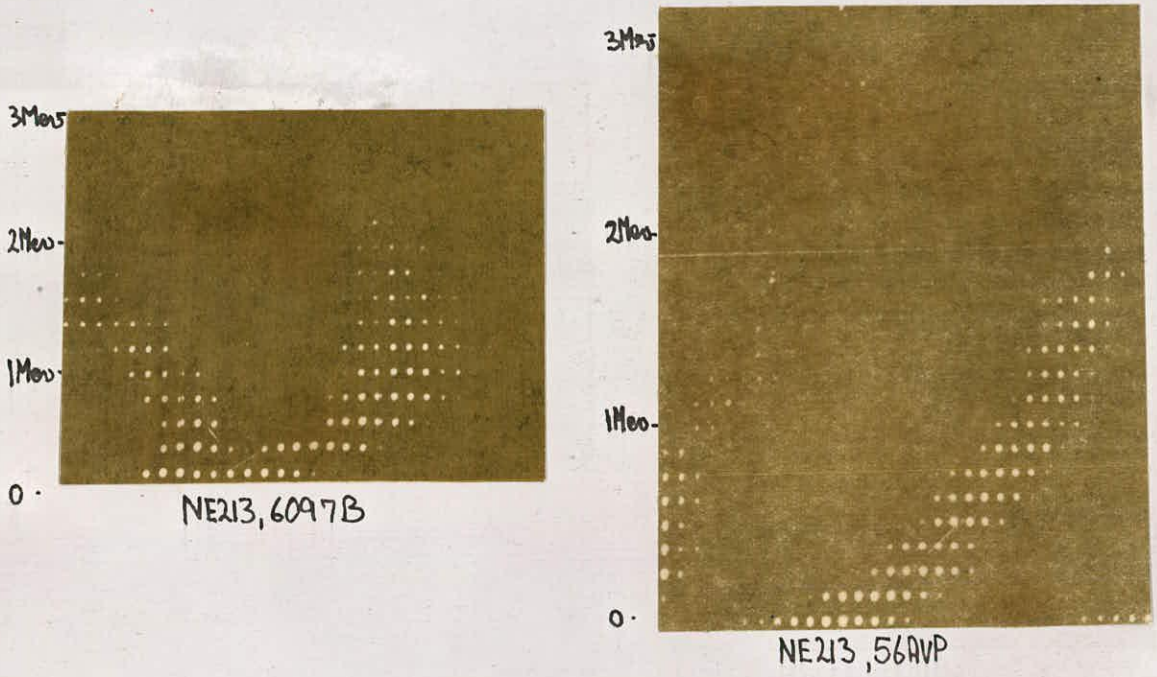

Photos 2: Comparison of bi-dimensional displays for two tubes.

the fast tube the pulse heights of the high energy gammas are similar to those of the low energy neutrons, whereas for the slow tube, although the separation of the spurs does not continue to so low an energy, the pronounced curvature of the spurs reduces considerably the occurrence of pulse heights like those at the intersection of the 'branches'. Similar curvature has been noted in a Dumont 6292 tube (15).

The bi-dimensional display (first applied successfully by Brooks (149)) is really a series of 'one-dimensional' displays at successive small energy intervals, and the superposition of these constitutes the normal one-dimensional display over a much larger energy range. The various parts of this latter display may therefore be correlated with the associated energy, according to the bi-dimensional display. Thus for the 56AVP it makes sense to refer to the right side of the gamma peak in the normal display (Photograph 1) as the high energy contribution and it may be appreciated that as the linear threshold is increased the gamma-neutron valley is widening just because the left 'low energy' side of the neutron peak is being eroded. The gamma-rays emitted from the Po^{210}- Be source used have an upper energy limit at 4.43Mev (from Be^{9} (α , n) C^{12*}). For the 6097B the situation is more complicated. In this case the valley is bounded on the left by the medium energy gammas and on the right by the low energy neutrons

The performance of the other scintillators may most easily be related to the degree of curvature in the 6097B bi-dimensional display. The pictures (Photograph 3) for KL360

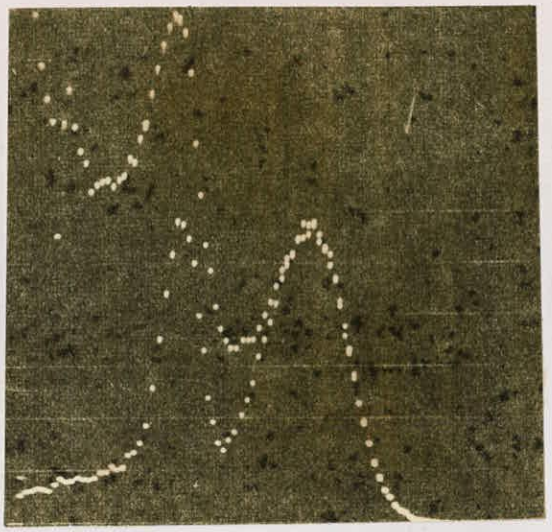

KL360, 6097B

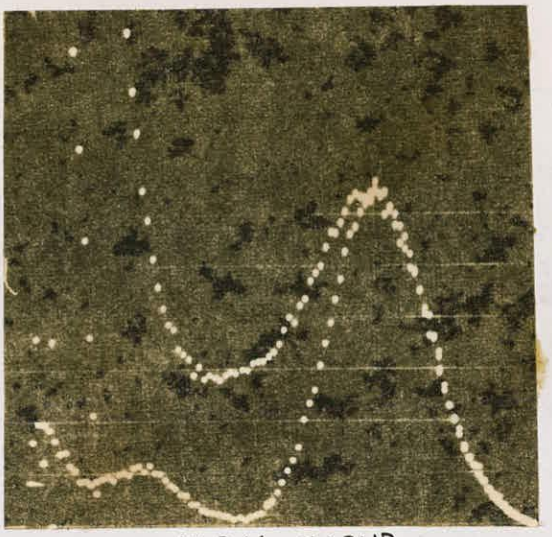

KL360, 56AVP

Ungated and gated Owen P.S.D. spectra

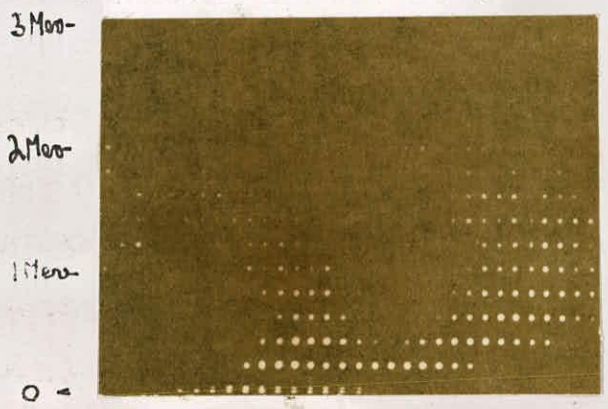

KL360, 6097B

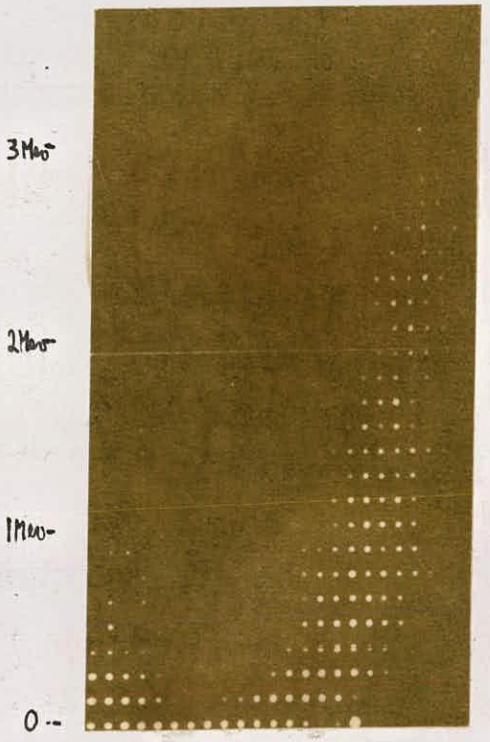

KL360, 56AVP

Photo 3. Interpretation of bi-dimensional displays with KL360

show this stronger curvature which appears to be reflected in more erect spurs in the case of the 56AVP. There are two main consequences of this effect. Firstly, with the 6097B the right-hand side of the valley in the one-dimensional display is bounded by both very high and low energy neutrons so that in this case applying a moderate threshold only slightly improves the valley and this improvement is due solely to the removal of low energy neutrons. With the 56AVP, the marked difference is the presence of a valley in the ungated spectrum. The reasons for this should be obvious from the bi-dimensional display. Although KL360 was chosen to illustrate these points, NE218 displays similar characteristics.

3-2.6 Special applications.

A series of tests was also carried out on experimental P.S.D. plastics. These samples were of identical size (1" x 1") and were compared under closely similar circumstances using a vertically mounted 6097B and 56AVP. For each scintillator the optimum setting of the Owen voltage was found, a linear spectrum recorded to derive a threshold at 500kev electron recoil energy, and using this both an ordinary gated and bi-dimensional analysis were performed. A comparison of findings indicated the best mode of scintillator preparation, special features of the bi-dimensional display, hopeful pulse shape discriminating plastics and any energy dependent behaviour. Samples of each plastic were prepared under N_2, CO_2 and vacuum; those prepared under CO_2 were found to

be consistently superior in discrimination properties. It was noted in early work on such scintillators, that the absence of unbound oxygen is crucial to the performance of the scintillator (149). The fact that the optimum Owen voltage was very similar for all these scintillators was taken as indicating that the decay time constants of the scintillators was also similar. Bearing in mind that the plastic scintillators have in general shorter decay times (151) it was expected that the best of these scintillators, labelled 3b/148, would show superior performance on the faster tube (Photograph 4). This was in fact the case. It was noted that the vacuum prepared sample of this plastic produced better discrimination at higher energies but deteriorated rapidly at the lower end. In general, the plastics varied quite widely according to their mode of preparation.

There are cases such as NE213 (Photograph 2) and 3b/148 (Photograph 4) where the resulting separation of gammas and neutrons is not such as to allow simple pulse height discrimination to accomplish the identification. Although slight integration at the input of the preamplifier was found to enhance the separation (82) it is not thought that any further improvement would be obtained by an effective integration on the dynode output (83,84). In cases where different curvatures occur in the proton branch of the bi-dimensional display, correction is possible by adding a proportion of a linear pulse to the processed pulse (58) but in the present case the correction must effectively tilt the 'branches'

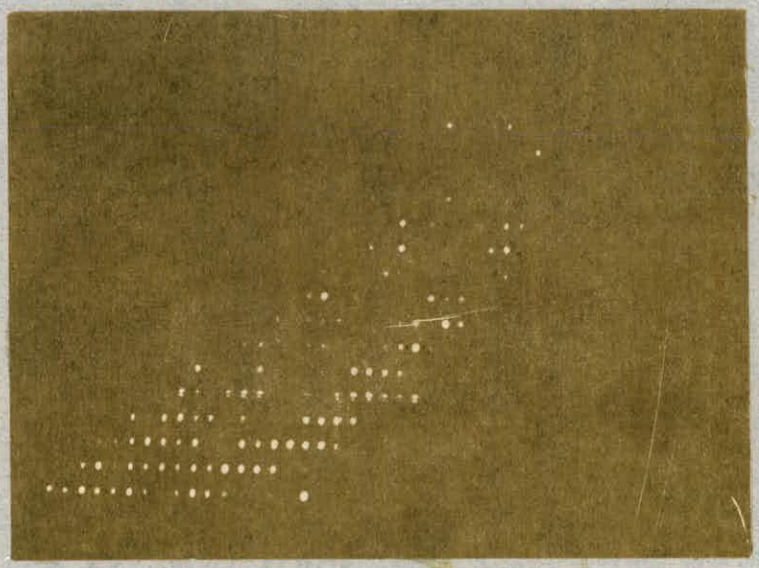

Photo.4: Bi-dimensional display

for 3b/148.

To a first approximation, such a correction might be obtained by adding to the processed pulse a pedestal proportional to (X - E) where X is some suitable ceiling energy about which the display is to tilt and E the energy associated with the processed pulse. Such a correcting signal could be obtained using the linear output and a difference amplifier. This manipulation was not attempted.

3-3 Light output and associated effects.

3-3.1 Light output of various scintillators.

While setting thresholds for the gating of the analyser, much data were amassed regarding the light output of the various scintillators. To make these strictly comparable the geometric conversion factors derived earlier (Sect.2-3.2) were applied and a 2" x 2" NE213 liquid scintillator was taken as standard. The scintillator was covered to a depth of 2mm. with NE560 (TiO_2) paint. Comparisons indicated a light output decrease of 20% when filter paper is substituted for paint, and of 30% when smooth foil is placed in contact with the scintillator surface. These figures were obtained to determine the advantage of painting over other forms of coating so that plastic scintillators on loan could be compared without treating their surfaces. The scintillators were mounted vertically, and the preamplifier used had an integrating time constant of 0.8μs. Table 9 lists these results and compares the figures with other sources.

Table 9: Light output of various scintillators quoted as a percentage of a standard NE213 cell.

Scintillator	Active Size (cm)	Light O/P	Corrected Light O/P	Accepted Light O/P (151)
NE218E D	ϕ4.3 x4.8	96±2	96±2	
NE218 D	ϕ4.3 x4.8	89±2	89±2	90
NE232	ϕ3.4 x2.6	95±2	85±6	
NE230	ϕ3.4 x2.6	86±2	74±6	77
NE213 C	ϕ3.5 x3.7	89±2	83±6	
NE213 B	ϕ4.3 x5.1	84±2	84±2	
KL360	ϕ4.6 x4.8	105±2	105±2	
NE102 C	ϕ5.08x5.08	42±2	42±2	
NE102A	ϕ4.6 x5.1	96±2	96±2	83
3a/148	ϕ2.6 x2.6	142±3	130±10	

B = side-bulb cell C = old sample D = standard cell

It should be noted that NE232 possessed what appeared to be a very slowly decaying phosphorescence. This manifested itself as a 'background' count three to four times higher than with other scintillators even several hours after removal from light. The figures for the older NE213 samples are rather surprising particularly as the larger specimen still gave excellent P.S.D. The light output of the small plastic sample is typical of those investigated and is particularly interesting as plastics normally have much lower light outputs. This measurement was taken shortly after receiving the samples; after a period of three months

nearly all the exposed surfaces had turned opaque. This effect was initially considered to be caused by oxygen poisoning from the air, but a recent paper (152) has attributed such an effect (over a much longer period) to exposure to natural light. These investigators remarked, however, that no change in scintillation decay times accompanied this surface clouding.

3-3.2 Optical coupling and effect on performance.

The scintillator-photocathode coupling suffers from a number of shortcomings, some of which have already been mentioned (Sect.2-3.2). For instance, the sensitivity variation on the 56AVP photocathode was shown to be quite appreciable. The magnitude of the effect was gauged from a light output comparison for a 1" diameter plastic scintillator placed at various positions on the tube face. The technique consequently averaged over local fluctuations whereas the measurements previously referred to gave a more precise mapping. Despite this smoothing effect the light output was found to be about 10% smaller for most positions at the cathode edge than at the centre and in one isolated case, 30% down. These measurements were repeatable to within ±2% indicating that the optical coupling was not an important variable. Taylor (49) has explained the importance of such variations in the timing technique of P.S.D.

It has also been pointed out (Sect.2-3.2) that when 2" scintillators are coupled to (nominally) 2" phototubes, there is a large areal mismatch in the coupling. In order to assess the

importance of these factors a very thin annulus of aluminium foil was arranged to screen the outer rim of the scintillator. It is worth noting that foil, when immersed in optical grease, suffers a large change in its reflective properties (117). This annulus, although only ¼" wide, reduced the effective area of the cathode of the 6097B tube by 20%, yet the light output decreased only 6%. This tends to indicate that the light is effectively concentrated more on the centre of the photocathode (153) or that the foil reduces to some degree the escape of light in the scintillator overlap

Table 10: The effect on P.S.D. performance of partially masking the scintillator.

Count rate		400cps		4,000cps	
	Threshold	200kev	400kev	200kev	400kev
No annulus	M	1.26	1.57	1.4	1.4
	P/V	9	70	8	60
Annulus	M	1.38	1.52	1.25	1.36
	P/V	3	30	2	25

The Table(10) indicates a noticeable deterioration in P.S.D. when the annulus is present. The two performance figures are given in each case for two count rates and above two thresholds. In general the 'peak-to-valley' ratios are a more reliable indicator of performance as the values of M are dependent on the peak shapes. A similar reduction in performance was noted by Reid and Hummel (9) using a charge comparison technique; in this case the light collected from NE218 was halved

by introducing an air gap between the scintillator and photocathode. It was also pointed out that this had some relevance to the performance of large volume scintillators.

3-4 Application of the Owen technique with a large diameter photomultiplier.

The application of Owen type P.S.D. with a larger tube was also investigated. Of particular interest in this context was deterioration associated with varying transit time in a 5" photocathode-scintillator combination, and the effect the light-guide has on the attainable performance. The photomultiplier used, an XP1040, was a fast tube with similar characteristics to the 56AVP, but with a 5" photocathode. NE213 liquid organic scintillator was used throughout: in a 2" diameter vertically mounted standard cell for test purposes; in a side-bulb 5" x 1½" encapsulation for direct coupling; and in a 12" x 2" bubble free cell coupled to the tube by a conical shaped perspex light guide, 5" in thickness. (Because of the larger areas to be coupled, paraffin was used for this purpose throughout).

3-4.1 The effect of the light guide and large scintillator volumes.

This light guide was selected as the result of earlier research aimed at producing uniform sensitivity over the whole area of a large scintillator (154). This is particularly important in the measurement of P.S.D. where the validity of energy thresholds relies on the absence of any relation between pulse height and the site in the scintillator of the energy transfe

Table 11: Light output comparison to determine the uniformity of a large scintillator-light guide combination.

Post'n of beam Collimated	Source	Case	Pulse heights (volts)	% of light OP at centre
Centre	Na^{22}	A	1.22 3.54	
	Y^{88}	A	2.36 4.92	
	Y^{88}	B	2.40 5.46	
	Cs^{137}	C	3.75	
¼ out	Cs^{137}	C	3.90	104
	Y^{88}	A	2.20 4.84	93 98
½ out	Y^{88}	B	2.24 5.02	92 92
	Cs^{137}	C	3.75	100
¾ out	Cs^{137}	C	3.55	93
Edge	Na^{22}	A	1.12 3.38	92 95
	Y^{88}	A	2.28 5.00	96 102
	Y^{88}	B	1.80 4.02	75 80
	Cs^{137}	C	3.40	87
Uncollimated	Y^{88}	A	1.23 2.74	
	Y^{88}	D	0.48 1.09	

A = on 12" sc'r ; B = on 2" sc'r ; C = on 12" sc'r(from15

D = on 5" sc'r centrally placed on light guide.

The first tests checked the conclusions of this earlier paper and extended the measurements. The results were obtained for a collimated beam of gamma-rays, ½" x 1½" in size, incident on the face of the cell, the rest of the scintillator being shielded by 4" of lead. Table 11 gives the pulse heights associated with the Compton edges of the Na^{22} and Y^{88} spectra for a beam at the centre, 3" and 5½" out, and the percentage alterations from the value at the centre, the amplifier being kept at the same gain throughout so that intercomparisons may be performed. The third section lists the pulse heights recorded in the earlier paper (154) in this case for a collimated beam of gammas from a Cs^{137} source. The fourth section of the table shows the pulse heights recorded when the 2" standard cell was vertically mounted on the light-guide at similar sites to those at which the collimated beams were incident.

The present measurements indicate a greater degree of uniformity than was originally attributed to this light guide. In fact the original figures followed more closely the performance obtained by Koechlin (113) for a more tapered cone. The results for the 2" scintillator indicate a much poorer light collection from the edge of the guide. Large scintillators produce larger pulses for events at their edges unless some adjustment is made to correct for this. This phenomenon is presumably related to the neighbouring reflective surfaces which enhance the light collection. There is no such explanation for the lower light output of the 5" scintillator; it is tempting to assume that this, like the other older NE213 samples, has a lower intrinsic light output.

Further light output tests with the 2" scintillator directly coupled to the tube showed a high degree of cathode uniformity. These measurements averaged over local variations in the same way as described earlier (Sect.3-3.2). Within the limitations of the technique the response was found to be completely uniform over the central half of the cathode, dropping by only 8% as the edge was approached.

It is interesting to note that in recent papers involving the use of large scintillators (49,155) the light output function derived differed from results based on smaller scintillators. These disagreements are understandable on the basis of Kuijper's excellent paper (107) in which he produced an equation taking geometrical and other effects into account. With this he was able to point out errors in Batchelor's (79) earlier efficiency calculations. The cause of these errors appears to be the deformation of pulse heights by varying degrees of attenuation and changes in effective bias levels for distant scintillations, a vertical variation as opposed to the lateral variation accounted for above. Such considerations were taken into account in Verbinski's neutron light output calibration (156).

3-4.2 P.S.D. with and without the light guide.

The P.S.D. obtained with the 5" scintillator directly coupled to the tube was very similar to that found with the 56AVP. However, the performance when the light guide was used resembled that obtained with the 6097B (Photograph 5). The explanation for this may be seen from Figure 51 to lie in the spread of transit

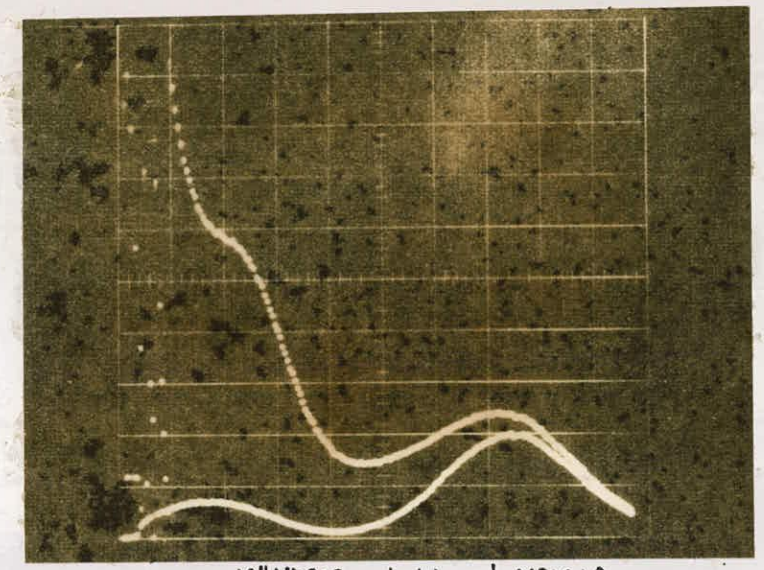

12" NE213 on light guide, XP1040

Photo 5: Ungated and gated Owen P.S.D. spectra

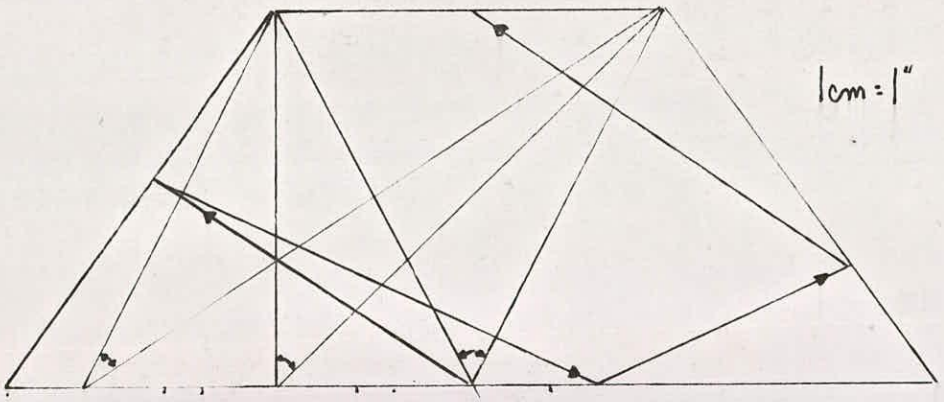

Fig. 51: Light guide showing solid angles and possible light transit paths.

times for photons passing from the scintillator to the photocathode. This spread was calculated to be of the order of 7ns. An attempt to calculate the resulting change in the dynode pulse shape failed because the angular distribution of light emission of the scintillator was insufficiently understood. The result of such an increase in transit time spread may be seen from Lewis and Wells (157) to be similar to an integration of the pulse. The requirements for optimum saturation were consequently rather different and an 'Owen' voltage of 3.46 volts was selected in this case as opposed to the 2.60 volts required for the directly coupled scintillator.

Table 12: The effect on P.S.D. performance of the location of the scintillation.

		Overall	Centre	7cm out	14cm out
12" cell on light guide	M =	1.04	0.65	0.66	0.70
	P/V=	9.8	2.78	3.03	4.54
2" cell on light guide	M =		0.79	0.69	0.66
	P/V=		7.4	5.4	3.8

Table 12 shows the performance figures from a series of experiments. These were performed for a linear bias of 300kev electron recoil energy and to obtain good statistics the counts were over 1000seconds or longer. The first entries refer to the performance for a collimated beam of neutrons and gammas from a Po^{210}- Be source incident on a half inch square of the 12" scintillator. In addition to the four inches of lead used for the

light output experiment the scattered neutrons were further moderated by a 12" x 10" cylinder of paraffin wax. For each measurement a background count was taken for the same period and the difference taken to obtain the data displayed. The bias level was reset at each position so that the figures depend only on the effect of the site of scintillations on the pulse shape. The measurements were repeated for the 2" scintillator at various points on the face of the light guide. Apart from the absence of any shielding or collimation and 5000 second counting periods, the procedure was identical with that above.

It is obvious from this latter experiment that if the excitations are limited to a small area, the discrimination deteriorates towards the edges. This is understandable since the transit time spread is a function of the solid angle subtended by the cathode face. This angle is decreased by two thirds in moving the 2" scintillator from the centre to the edge of the light guide (fig.51). When the larger scintillator was used the light liberated by the excitations traversed greatly varying path lengths and the resultant smearing of the scintillation pulse shape caused a marked deterioration in particle discrimination. Thus only in the neighbourhood of the wall where the light may be scattered preferentially towards the photocathode does the performance approach that of the smaller cell. When the whole of the larger scintillator was exposed to the gamma-neutron source the figure-of-merit, M = 1.04 and P/V = 9.8. These figures are far superior to those for collimated beams. The difference arises from the

smaller light output measured when the whole of the 12" scintillator is irradiated with Y^{88} gamma-rays. The threshold based on this Y^{88} spectrum corresponds to a higher bias for local excitations to that used for the collimated beam from the neutron-gamma source.

The P.S.D. obtained for the directly coupled scintillator has already been referred to as being similar to that obtained with other fast tubes. It was therefore meaningless to attribute normal quality factors to these displays and instead the gamma rejection ratios are quoted (Sect.3-2.4). Performing similar extrapolations to those described earlier (Sect.3-2.2) the rejection ratio for the Po^{210}- Be source above a threshold of 300kev electron recoil energy was better than 99.99%. As before, no improvement was found on applying the timing requirements as suggested by Batchelor (79). A qualitative description of the timing relationships of the signals appears in Figure 32. To check on this point the pulses were lengthened from 0.65μs to 1.5μs to allow for a much wider range of cross-over times but no significant difference in the gated spectrum was noted. The ungated spectrum showed a pronounced gamma-neutron valley which was not observed with the 56AVP.

3-5 Cross-over timing on the 'Owen' pulse.

3-5.1 For the XP1040 photomultiplier.

The best delay between linear and 'Owen' discriminator pulses for the larger tube was established by a process of trial and error, the degree of fit to the ungated spectrum being used

as a guide in this selection (Photograph 6). To determine this, the 'Owen' and linear discriminators were used to gate the linear spectrum. Even when the 'Owen' discriminator is set at its minimum bias of 0.45 volts, most of the gamma pulses are inhibited. Figure 52 shows the linear spectra obtained for three relative delays between the discriminators. The first (optimum) delay is energy independent; the second corresponding to a 0.25μs delay of the 'Owen' discriminator pulse shows a rapid cut-off above 1Mev - this may be attributed to the later cross-over of 'Owen' pulses for higher energy radiation while the higher energy linear pulses will tend to trigger the linear discriminator earlier; the third corresponding to a 1.5μs delay of the linear pulse displays a peculiar valley at 600kev - the tentative explanation for this is that intermediate energy pulses have 'Owen' cross-overs which are slightly earlier, and therefore their discriminator pulses do not coincide with the critically delayed linear pulses. This last arguement is partly vindicated by the fact that the 'valley' disappears when the bias of the 'Owen' discriminator is raised to about 3 volts, corresponding to a further delay in this discriminator pulse (cf Sect.3-2.4).

In order to obtain a more quantitative understanding of the time relations of the gamma and neutron cross-overs in the 'Owen' pulse a time analysis was performed on the signals. Figure 53 shows the circuit used. The start of the time-to-amplitude converter was obtained from the negative leading edge of the amplified 'Owen' pulse. A 'LeCroy' discriminator triggering

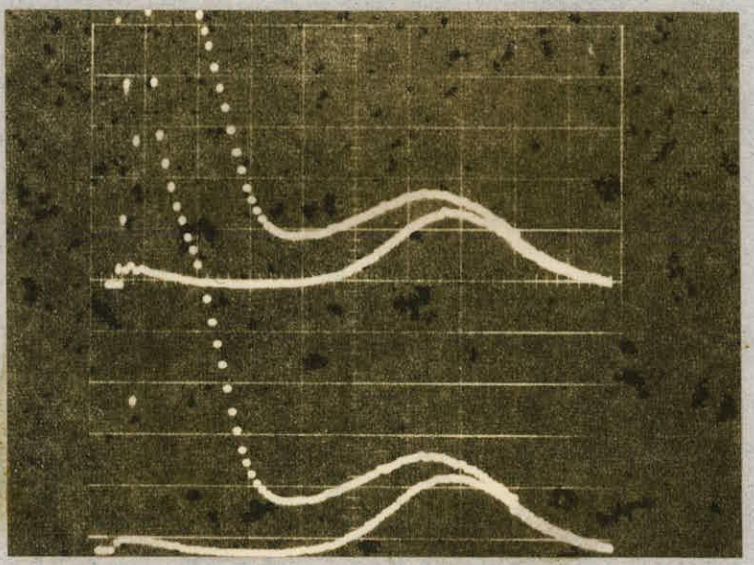

Photo.6: Varying degrees of fit to ungated spectrum.

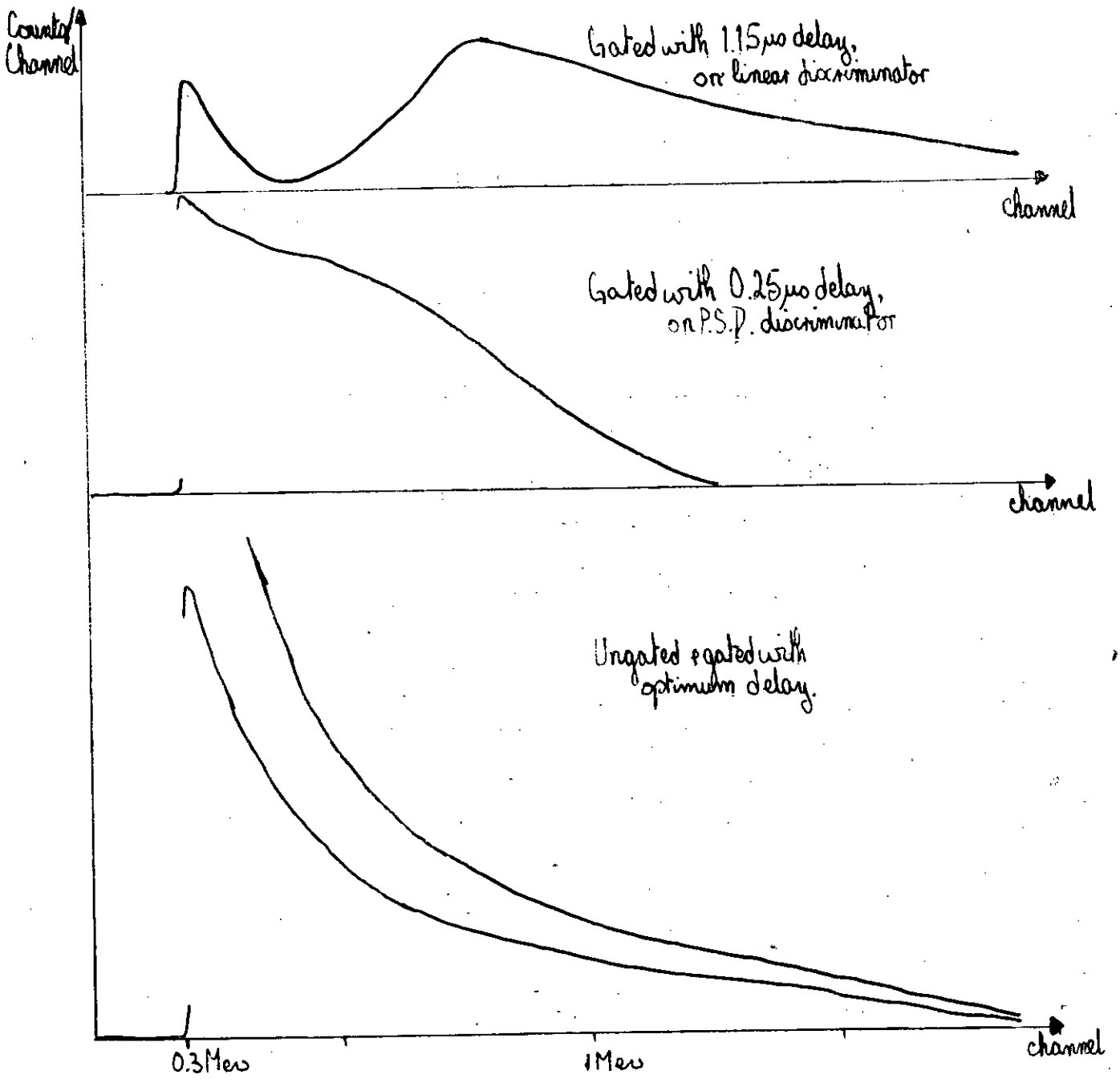

Fig. 52: Ungated and gated Linear spectra with various delays.

at -150mv. was used to obtain this pulse. A zero cross-over discriminator operating on an inverted output of the amplifier provided the stop pulse to the converter. Care was taken that the amplifier did not saturate on the negative going pulse, because saturation effects the reproduction of the point of zero cross-over. Figure 54 shows the time relation of the cross-overs, the source in this case being Po^{210} - Be. The neutron peak is to the left since these pulses cross over first. The scale here is 4ns/channel and the application of an energy threshold to gate the analyser did not appreciably improve the display. Also shown is the time spectrum for a gamma source, Y^{88}. It is evident that this technique may be used for P.S.D. in its own right.

3-5.2 For the 6097B photomultiplier.

In the case of the 6097B tube, difficulty was encountered in getting sufficiently large signals at the voltages at which it was operated. Figure 55 gives the circuit finally settled on. The typical wave forms as given by an oscilloscope at the dynode outputs show no sharp distinction between the cross-overs as found for the fast tubes and this is probably to be expected for the 6097B with its poor time resolution. The timing properties were further investigated by performing a bi-dimensional analysis to determine the variation in cross-over times with energy. The linear signal was shaped and applied to the 'Y' converter and the time-to-analog converter fed to the

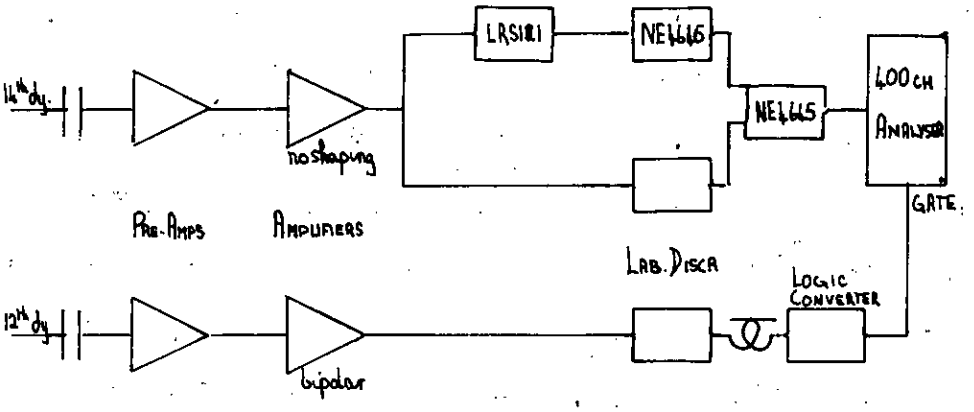

Fig. 53 'Owen' cross-over timing circuit for the XP1040.

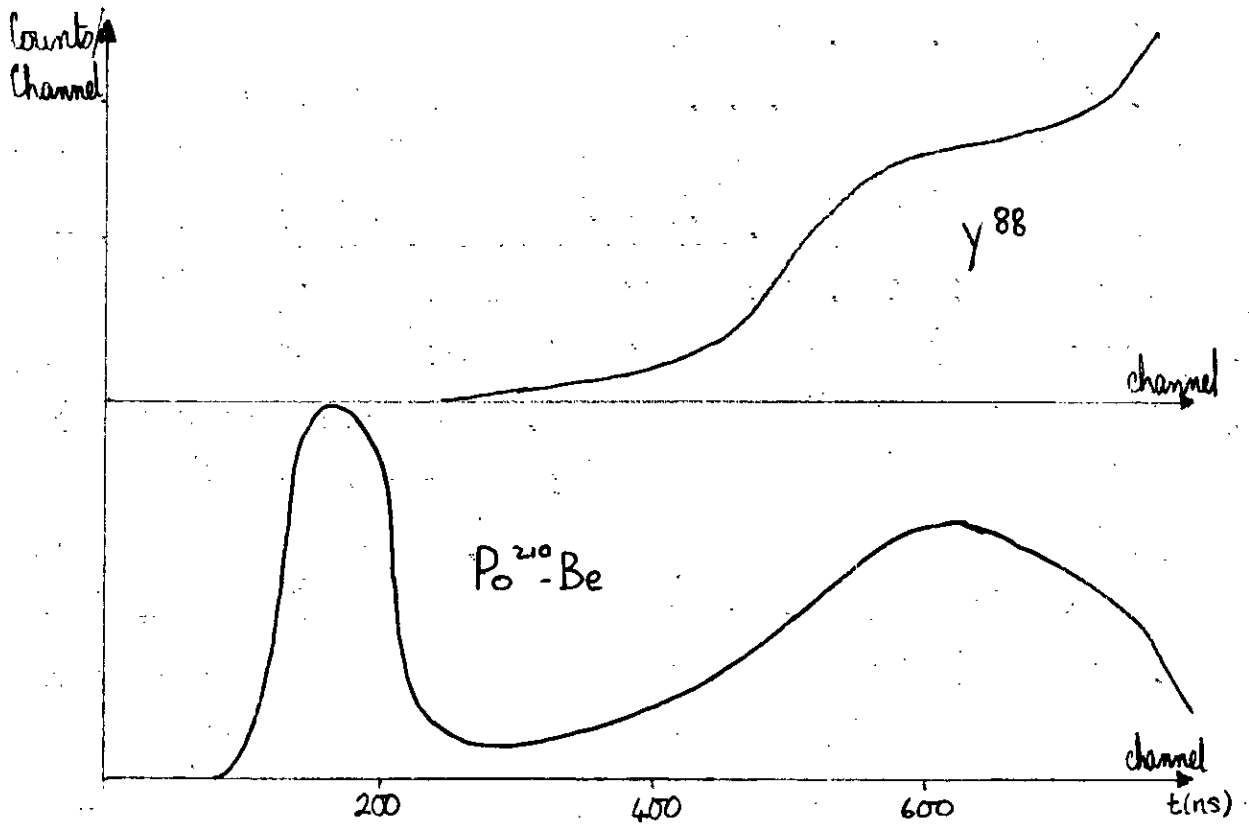

Fig. 54: Cross-over time analysis for two sources with the XP1040

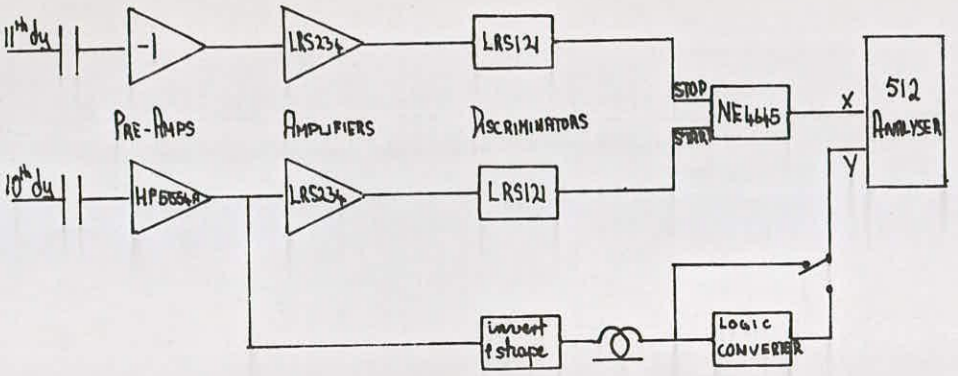

Fig. 55: 'Owen' cross-over timing circuit for the 6097B

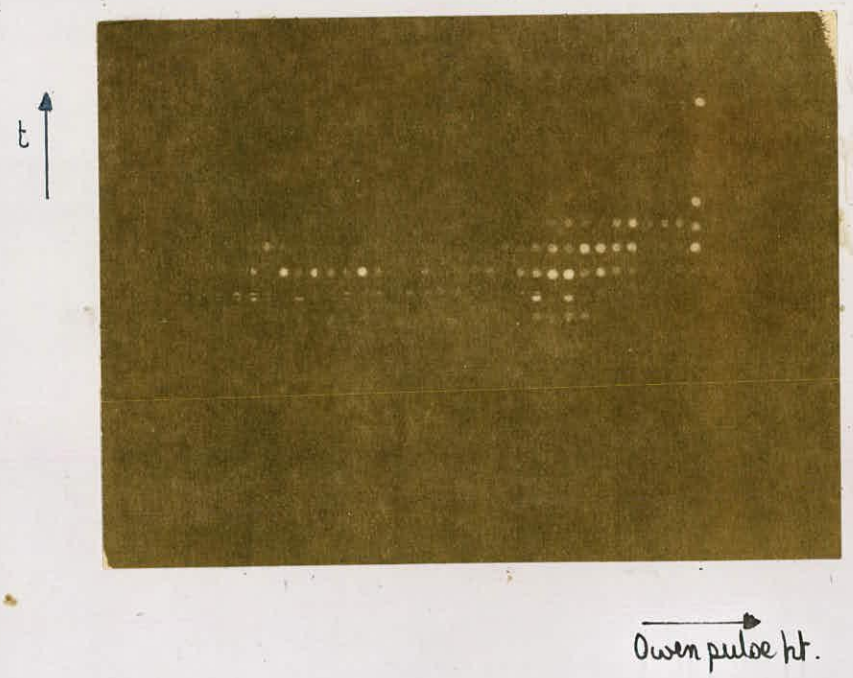

Photo 7: Bidimensional analysis of cross-overs for the 6097B

'X' converter. The display (Photograph 7) fails to show any marked separation as a function of energy.

3-5.3 For the 56AVP photomultiplier.

Inspection of the saturated output dynode pulses showed the standard cell of NE218 to give the best defined cross-overs (Photograph 10) and this scintillator was therefore used. The 56AVP gave the best cross-over time separation of the three tubes. The availability of larger pulses simplified the analysis and the circuitry (fig.56). The display, even for the case of the ungated spectrum (Photograph 8), has a very good peak-to-valley ratio although the appearance may be slightly enhanced by the fact that lower energy gammas will not trigger the cross-over discriminator. However, every neutron pulse with sufficient energy to trigger the start discriminator (Sect.3-5.1) will trigger the cross-over discriminator and thus the technique has by far the best performance for neutron identification down to a threshold dictated by the scintillator used. A very simple adjustment, delaying the discriminator pulse in the second channel by 1.1μs, reversed the roles of the start and stop pulses. This produced the mirror image of the first display (Photograph 9). The obvious advantage of this lies in the ease of gamma rejection by setting an integral discriminator bias in the 'valley'.

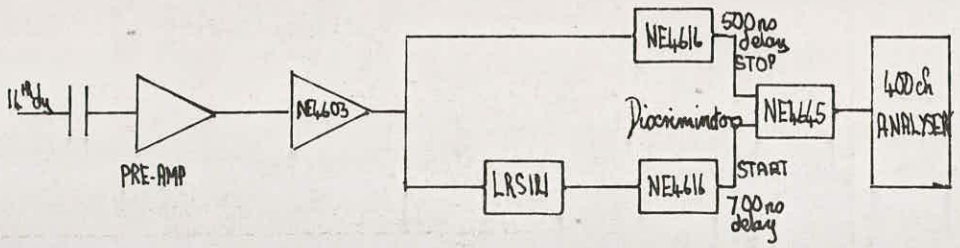

Fig. 56: 'Owen' cross-over timing circuit for the 56AVP

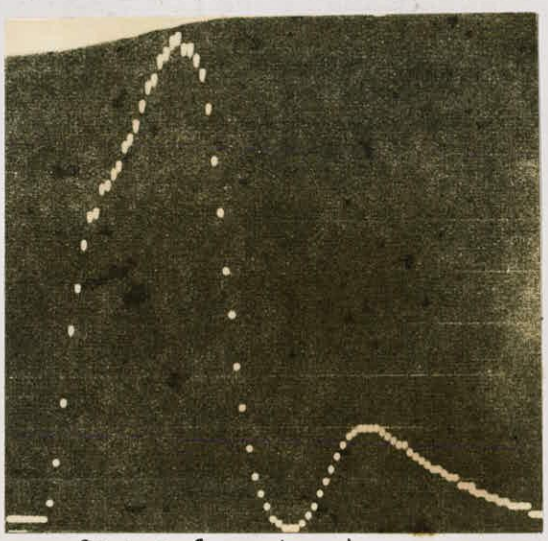

Photo. 8: Circuit as above

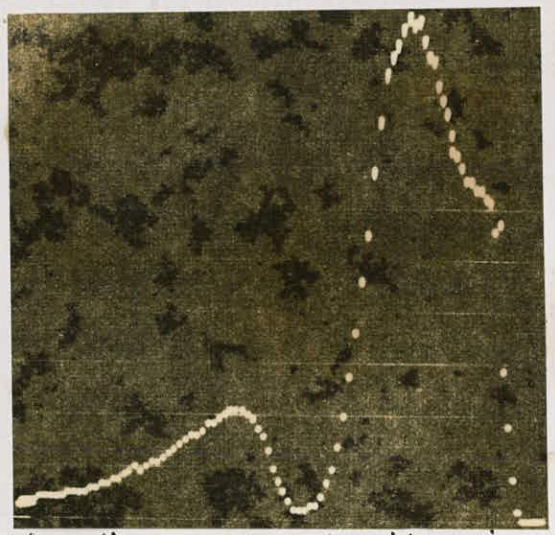

Photo. 9: With additional 1.1 μs delay on 'START'.

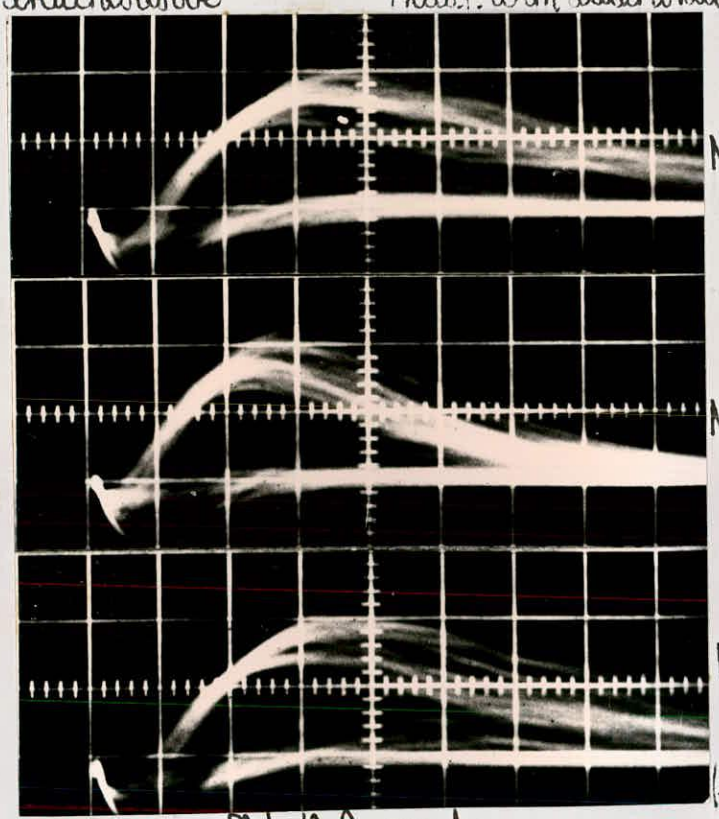

Photo. 10: Owen pulses

3-6 Count rate dependence.

One final experiment was performed on Owen P.S.D. This was to determine the dependence on counting rate. Previous feasibility studies involving the use of the large scintillator tube combination had found a rapid deterioration above 75,000cps counting rate.

3-6.1 The effect on the linear output.

The first tests were to determine the effect on overall gain of increasing the count rate. The detector was pladed horizontally and a strong gamma source positioned on the axis of the detector at various measured distances from the centre of the scintillator.

Table 13: Overall Gain changes with Count rate.

Source	Range at centre	Compton Edge Channel	Count rate (cps)	Dead time.
Na^{22} (0.2mCi nominal)	50cm	19	3,500	58%
	25cm	21	10,000	80%
	12½cm	20¾	20,000	89%
	6cm	18½	40,000	93%
	1cm	17	45,000	95%
Cs^{137} (1mCi nominal)	60cm	29	52,000	98%
	50cm	32½	70,000	98%
	43cm	38	90,000	98%
	40cm	44	110,000	98%

Table 13 gives the results obtained. The count rate given refers to the number of pulses from energy events greater than 340kev, and the Compton edge channel is the reference point at the 72% peak height corresponding to 340kev for the Na^{22} source and 480kev for the Cs^{137} source. The dead time of the analyser was fixed at 32 s so that the selection of pulses was completely random, i.e. not count rate dependent. (Under these circumstances the analyser had a maximum analysing rate of 14,000 pulses per second).

The results indicate an increase in overall system gain which is directly proportional to the count rate. The effects noticed when the source is less than 15cm. from the scintillator are associated with local rather than general excitation of the scintillator i.e. the gamma source is effectively collimated and this phenomenon has been described before (Sect.3-4.2). The result of this general increase in light output is that in thresholds set at, say, 340kev decrease to ~300kev at 70,000cps, and ~260kev at 90,000cps with a consequent deterioration in the appearance of the gated P.S.D. spectrum.

3-6.2 The effect on P.S.D.

A second series of tests attempted to find any other source of deterioration in the Owen discrimination performance. To accomplish this, the count rate was increased, but changes in the effective threshold (set at 340kev) were adjusted for by alteration of the 'linear' discriminator. The changes which occur to the pulse shape spectrum are shown in Table 14 and Photograph 11.

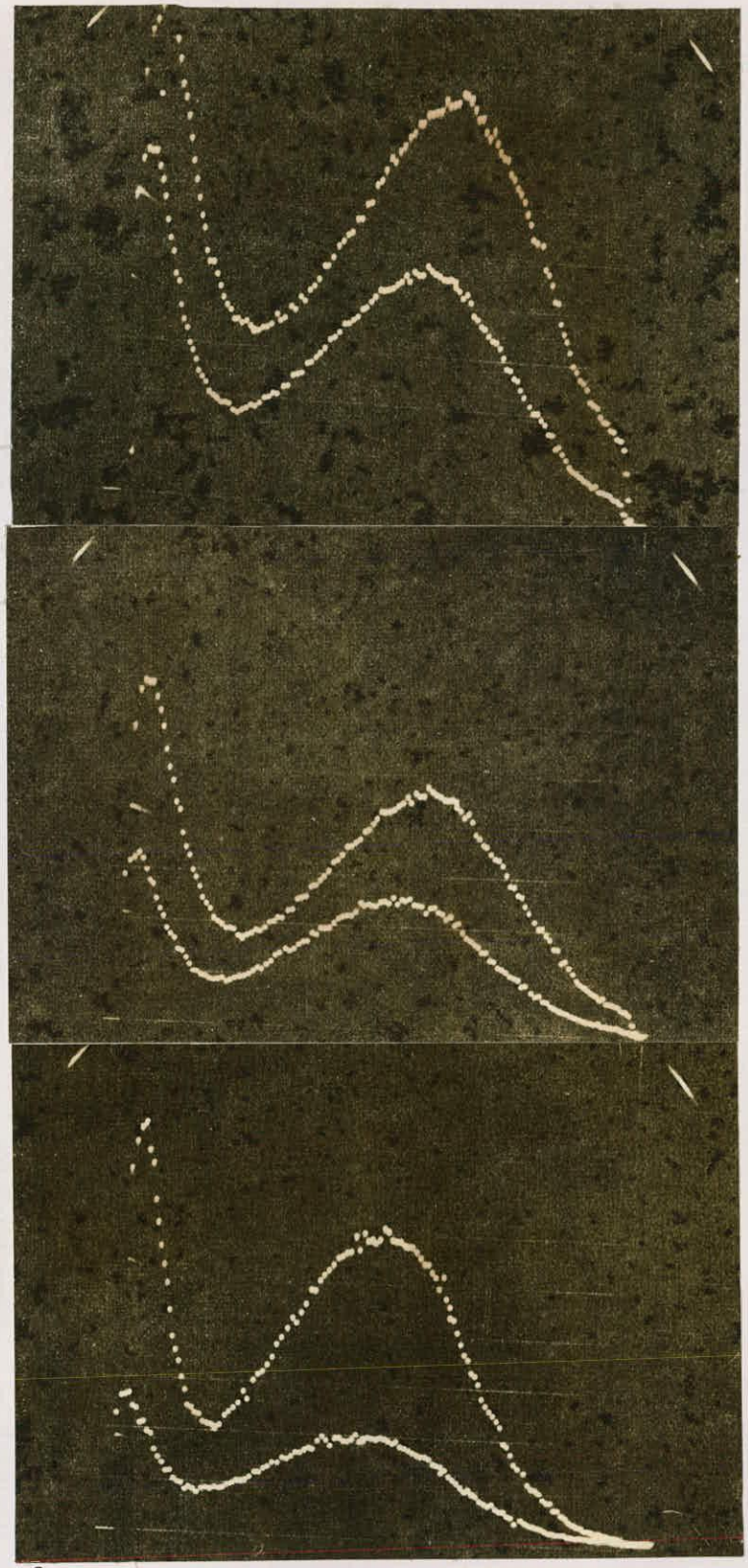

Photo. 11: The effect of count rate on Owen P.S.D..

Table 14: The effect of Count rate on P.S.D.

Source	Count rate (cps)	Channel nos. (80mv/ch +0.5v.) Neutron peak	Valley	P/V
Po^{210} - Be + Na^{22}	500	59	23	2
	1500	62	25	3
	3000	67	26	2½
	16000	72	30	2½
	18000	77	32	2

Care was taken to maintain a constant pro rata contribution by gamma-rays and neutrons at all stages and as a result of earlier findings, sources were never closer than 15cm. to the scintillator. The results indicate a progressive increase in pulse height as the count rate increases - there is a 0.7v. shift in the position of the valley for an increase from 500 to 20,000cps. Although the quality of discrimination has not deteriorated, any integral discriminator set to reject gammas in such a pulse height distribution would have to be continuously reset as the count rate altered, or a decreased gamma rejection ratio would have to be accepted.

The cause of this shift is associated with the increase in pulse sizes as at the linear output and dealt with above. The problem would therefore be best dealt with at source by adjusting the tube H.T. supply to obtain a constant pulse height energy relationship. This would keep the energy threshold constant and reduce the shift described above. Such a correction was not tried.

3-7 Conclusions.

In conclusion, justification has been found for Owen's (7) recommendation of slow tubes, particularly down to low energies. However, the results obtained by Owen and also by Brooks and Pringle (149) with the 6097B tube are not in a form allowing comparison with my own findings. The same applies to Tanaka's report (142); he used ten stage RCA and Du Mont unfocussed tubes. Fast tubes only show superior performance to the slower tubes above a certain threshold which is to some extent dependent on the scintillator. The quality of discrimination produced in the present work is superior to that in many previous papers concerned with the saturation technique but tallies closely with that obtained by Broek (77) who used a 6810A RCA tube and stilbene.

The superiority of Owen cross-over timing methods has been stressed, especially as regards the low neutron energy thresholds to which the system works. Equally good performance has been obtained by Fabiani (86) using NE213 and 6810A RCA tube, but the results obtained by Hsu (85) appear to be inferior though lack of detail makes comparison difficult. All circuits using this technique exclude the low energy gamma pulses which would otherwise destroy the good discrimination obtained. The deterioration in discrimination can only originate in signal noise and pile-up. Tanaka (142) has shown in fact the signal-to-noise ratio is four times larger in the linear than in the saturated pulse because the small noise pulses are less reduced by the space charge effect.

No grounds have been found for the commoner criticisms of this technique. It is easy to set up the Owen voltage and there is no deterioration for count rates up to 70,000cps. The shifts associated with magnetic fields and higher count rates can in most cases be guarded against. The only difficulty encountered was in determining the absolute gamma rejection attainable but at the extremely low gamma miscounting rates obtained this difficulty will be found with any technique.

CHAPTER 4.

Pulse shape discrimination by the timing technique.

4-1 Description of the timing technique.

The zero cross-over timing method of discriminating was also considered. A variety of techniques have been described in the review and a mathematical justification for some of these appears in the Appendix. The results reported here relate to a unit devised by Davie (132) and applied in combination with a variety of scintillators and the two types of photomultiplier. Much of the detail refers to modifications performed on the P.S.D. circuitry either to alter the shape of the pulse or to improve the efficiency with which the timing information was extracted. Also discussed are the various criteria by which the value of these adjustments were judged.

The circuit (fig.57) was originally designed to work off the same principle as Roush's (11) i.e. to affect a timing from start to zero cross-over of a once integrated and differentiated dynode pulse. A linear pulse was required in order that the shape be not distorted by saturation and therefore a single dynode output was used for both the linear output, and the P.S.D. unit; this technique, as pointed out by Forte (36), is not susceptible to inter-stage gain changes as are those methods which derive 'start' and cross-over pulses from separate outputs. The shaped pulse was limited and amplified before passing to a

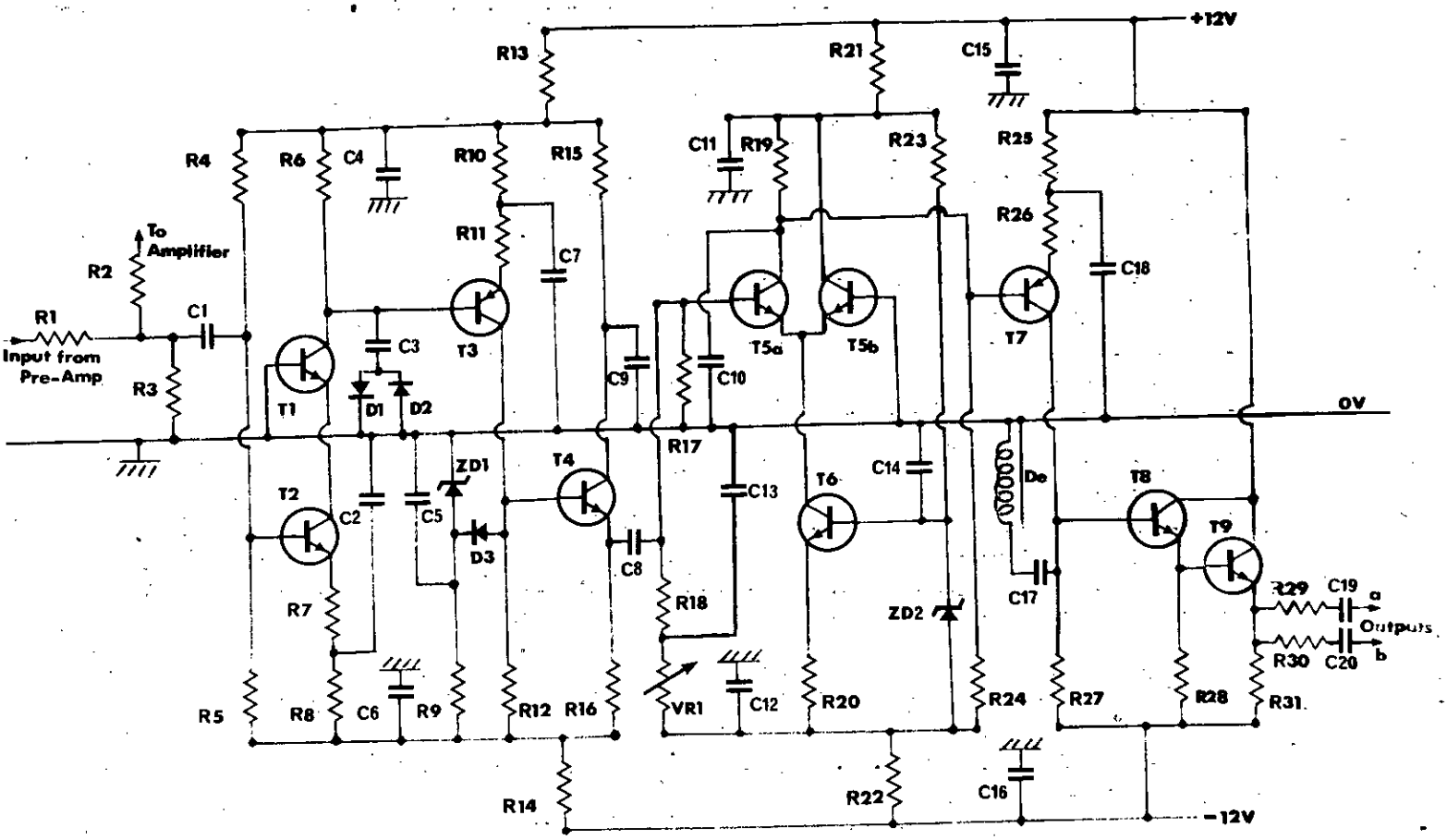

PULSE SHAPE DISCRIMINATION UNIT

Fig. 57

'long-tailed pair' (158) which charged up a capacitor for the time that this pulse exceeded an adjustable threshold. The amplitude of the voltage pulse from the capacitor being proportional to the time required, this pulse was suitably shaped for multi-channel analysis.

4-2.1 Application with a slow tube.

The tenth dynode of the 6097B, previously shown to be linear up to 1,350 volts, did not provide sufficiently large signals and further amplification was required before input to the unit (fig.58). A charge sensitive preamplifier (133) with low noise characteristic was used. However, the pulse shape discriminator was designed to accept only positive signals as provided by a conventional compound common emitter preamplifier. Therefore an inverting input stage (fig.59) was added. The preamplifier used performed a 100μs integration (effectively infinite for pulses with ~½μs decay times) and this represented a sharp departure from the normal procedure of initially integrating with RC≃ 400ns. Thus to provide a zero cross-over, double differentiation was required, the first differentiation illustrated as occurring in the inverting input stage. (Further details on such techniques appear in Section 1-4.3).

The first tests were concerned with finding the best combinations of tube EHT and preamplifier gain, the aim being to keep the noise generated to a minimum. This accomplished, the effect of the input transistors T_2 and T_3' was enquired into (T_3' was placed

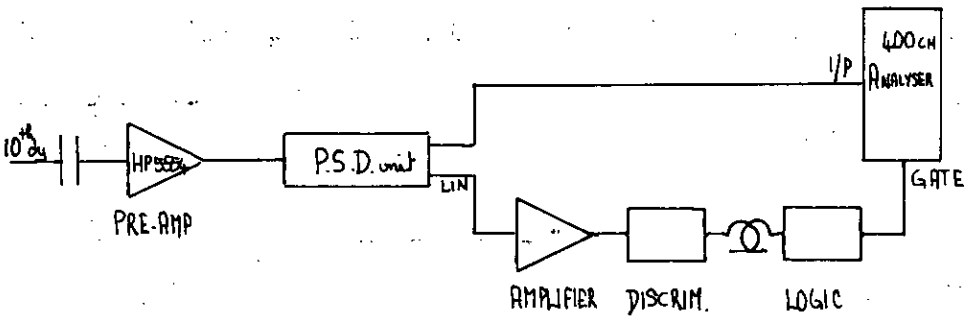

Fig. 58: Block Diagram of gating process for P.S.D. display.

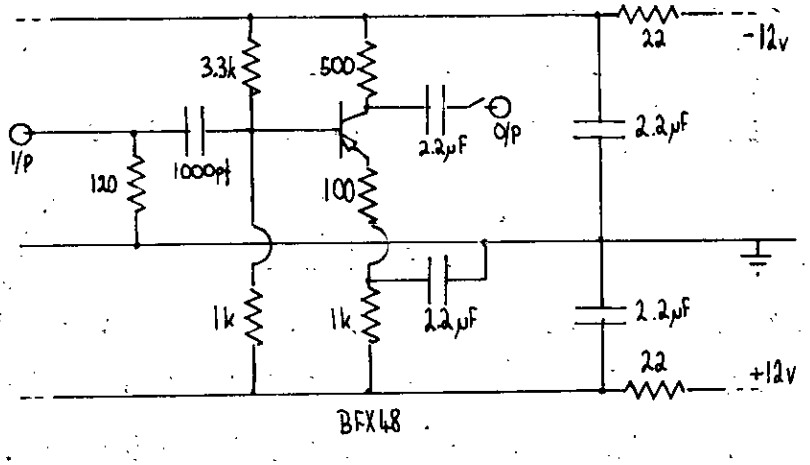

Fig. 59: Inverting input stage for use with the charge sensitive preamplifier.

in the second stage in a similar position to T_2). Their presence was intended to reduce the Miller effect associated with the ~2pf. capacitance of the transistor base-collector junction. The presence of this capacitance in the second stage would create undesirable integration with the 1.8k resistor. However, the removal of T_2 and T_3 produced no detectable worsening in the overall discrimination.

Table 15: An example of the analysis performed.

With Transistor in input stage:

Preamplifier gain	Channel Neutron peak	Channel Gamma peak	FWHM Neutron	FWHM Gamma	M (±0.14)	FWHM ratio (±0.14)
10 x 1	82	91	3.9	6.0	0.91	1.54
10 x 2	80	90	4.3	7.6	0.84	1.77
10 x 4	81	92	4.3	8.1	0.89	1.88
10 x 8	81	92	5.1	7.8	0.85	1.53
Without Transistor in input stage:						
10 x 1	82	92	3.8	6.4	0.89	1.69
10 x 2	81	92	4.7	7.6	0.89	1.62
10 x 4	82	92	4.6	6.3	0.92	1.37
10 x 8	79	90	6.3	9.6	0.70	1.56

Table 15 presents an example of the analysis performed. The comparison is in terms of the previously defined quality factor, M, for an energy threshold of 400kev. M was derived for various settings of gain, with and without the additional transistor in the input stage and no significant changes were noted.

Although not obvious from this table, the setting of 10 x 2 gain was found best for minimising noise contributions. The other conclusion of importance relates to the FWHM ratio for the neutron and gamma peaks. It is apparent that the value of this ratio depends strongly on the electronics settings. This is contrary to the findings of Reid and Hummel (9) that this ratio is a constant characteristic of a given scintillator.

Roush has pointed out (11) that the quality of P.S.D. is dependent on the 'steepness' of the pulse at the zero cross-over as well as on the difference in cross-over times for neutron and gamma pulses. It may therefore be appreciated that for a given type of shaping the response of the time-to-amplitude converter is of some importance. In the converter used, a BFY74 and BZY88 acted as diode compensated constant current generator for the 'long-tailed pair' (159). The adjustable ratio $\frac{10k}{10k+33k+1M(\text{var.})}$ controlled the threshold at which all current is switched from passing through the right-hand to the left-hand member of the dual transistor. Thus, the response of the converter depends on the switching speed and gain - bandwidth product of the transistor used.

In practice this threshold was adjusted at about 100mv. Using an oscilloscope this setting was fixed above the level of small positive overshoots caused by unavoidable integrations at earlier stages in the circuit. Further improvement was obtained on suitably terminating unused outputs, and adhering to the best gain settings found earlier.

4-2.2 Optimising and performance rating.

For this particular type of shaping an attempt was made to find the best time constants for the two differentiations, i.e. in the inverting stage and at the input stage of the discriminator unit. Figure 60 shows the crossing time spectra obtained for a fixed electron recoil energy threshold of 500kev using various capacitances as indicated in the two stages. Capacitance was adjusted in preference to resistance in order that input impedance and gain should remain unchanged. These results were obtained for a standard NE213 scintillator (ϕ 2" x 2½") with a 100mCi Po^{210}- Be source positioned 15cm off axis to give count rates of about 1 kcps. Under these conditions (d) was chosen as optimum for the consistency with which this shaping produced good P.S.D. The RC time constant in each stage was 350ns. Further runs were performed with the input shaping capacitor changed to 200, 600, and 800pf. by turn, but inferior results were obtained.

As in the previous tests the peaks appeared symmetrical and the quality factor, M, was considered on its own to be a sufficient criterion by which to judge performance.

Using these same shaping parameters, and other experimental conditions, a further comparison was carried out using two standard cells of NE218 and NE218E of the same dimensions. In each case the 500kev threshold, derived from a linear Na^{22} spectrum, was adjusted to take account of the different light outputs of the scintillators.

Fig. 60: Pulse height distribution graphs for pulse shaping optimisation.

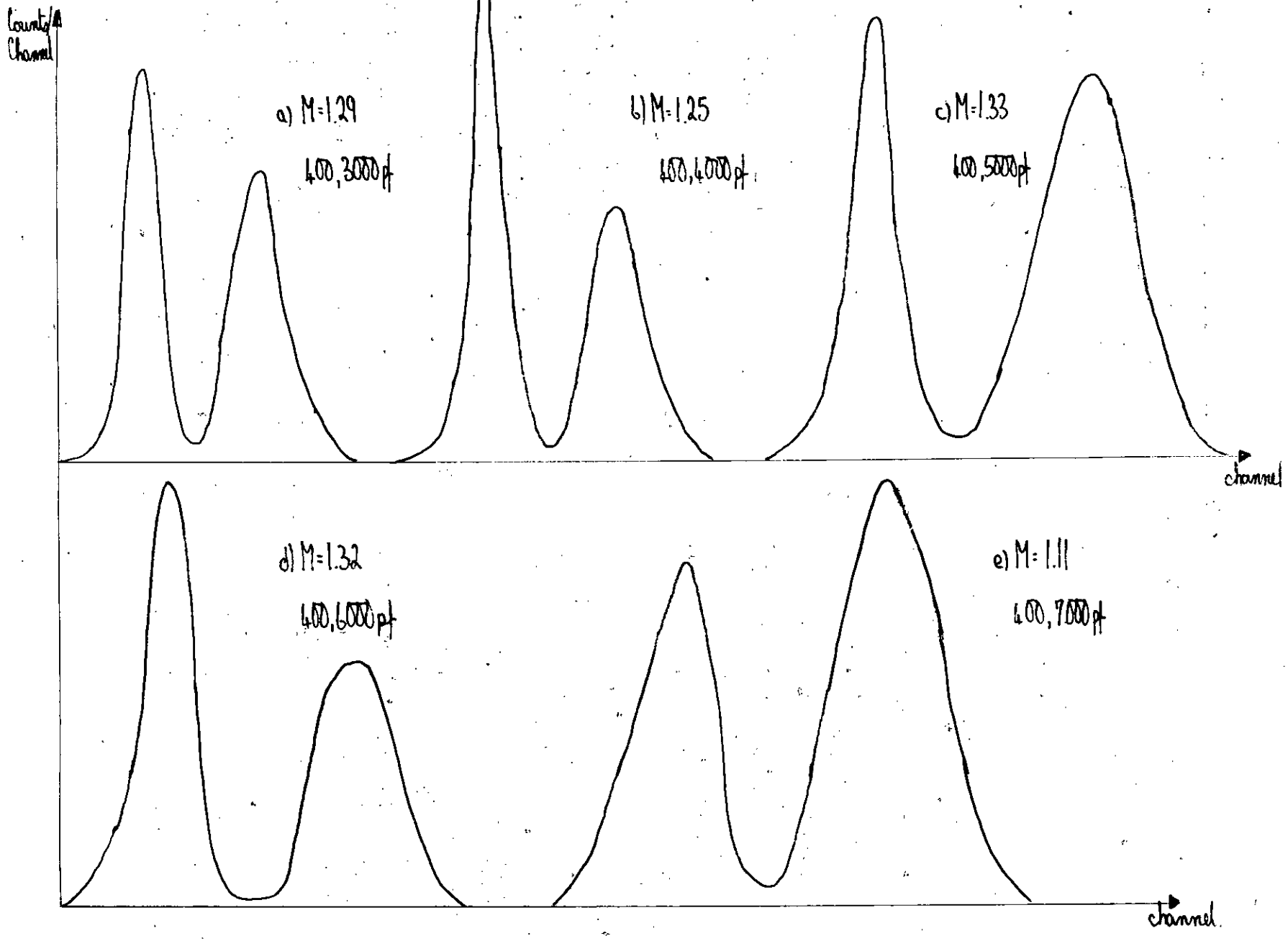

Table 16: P.S.D. performance with the 6097B tube using the timing technique.

Scintillator	P/V	Neutron acceptance	Gamma rejection	M
NE213	22.5:1	99.89%	99.89%	1.30
NE218	4.5:1	97.98%	97.32%	0.88
NE218E	16.6:1	99.97%	99.97%	1.16

Table 16 lists the results obtained for the three scintillators, the acceptance and rejection ratios being obtained by a similar extrapolation procedure to that described earlier (Sect.3-2.2). These results indicate that NE213 and NE218E produce discrimination of a similar quality, but taking the gamma, neutron proportions as the most reliable guides, NE218E may be taken as slightly superior (See Sects.1-2.1 and 3-2.4)

4-2.3 Source dependence.

In keeping with the course of experiments followed earlier (Sect.3-2.3) comparisons of performances for different sources were also carried out. Figure 61 shows the results obtained with this timing technique with (A) the Po^{210}- Be source and (B) the radiations from the H.T. set under similar conditions to those reported before. In this case the counting rate was 1 kcps for both sources above an energy threshold of 400kev. A comparison indicates a slightly superior performance in terms of peak/valley ratio, and acceptance and rejection values, for the

Fig 61: To illustrate source dependence for the timing technique.

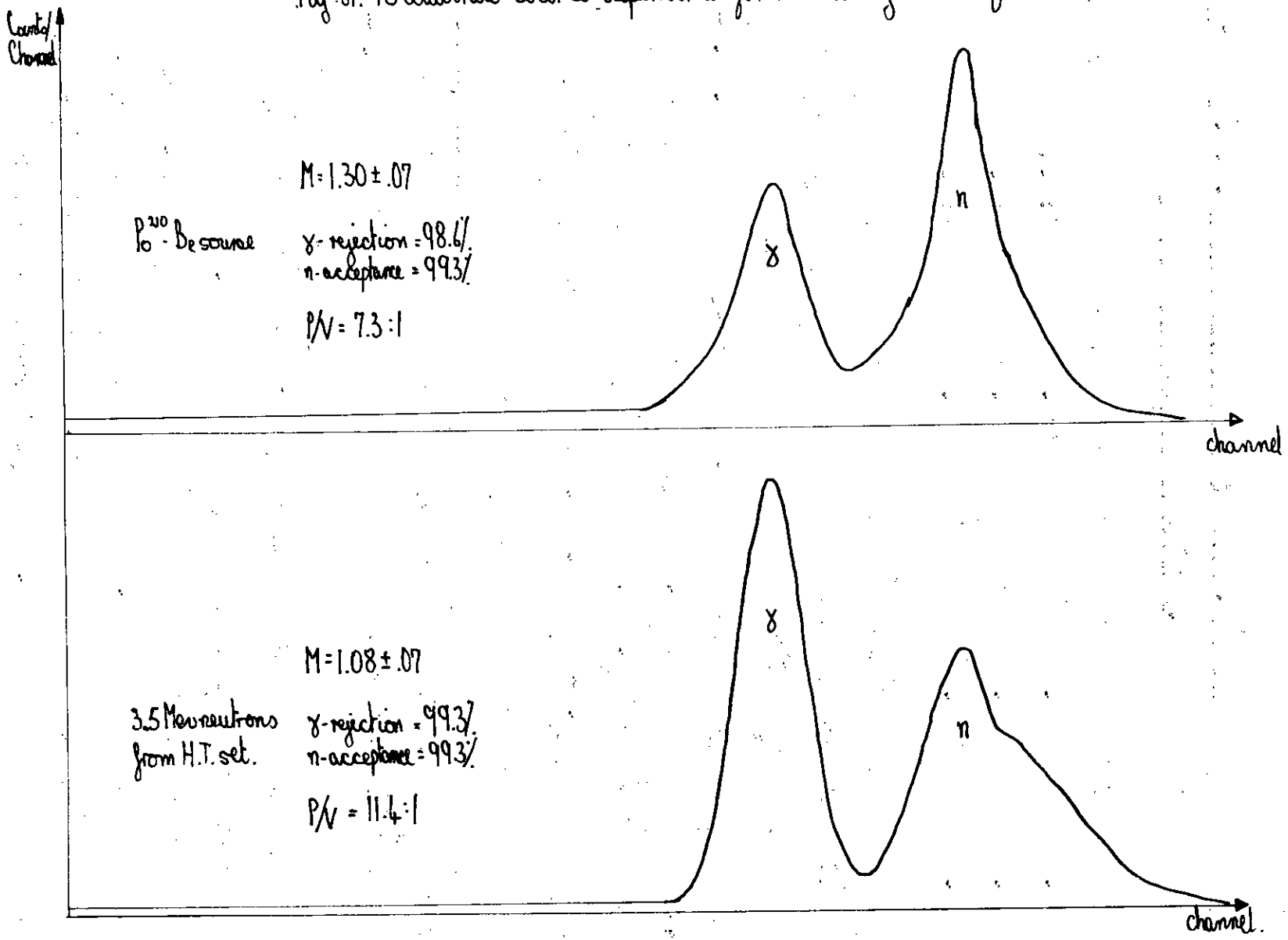

'monoenergetic' beam. A contrary conclusion might be drawn from the quality factor, but the low value of M for the H.T. set is caused by the peculiar shape of the neutron peak. The cause of this has not been established. The deterioration for higher energy ranges is associated with a similar curvature of the bi-dimensional display to that described before (Sect.3-2.5).

4-2.4 Delay-line shaping.

Alternative forms of pulse-shaping were also investigated. Firstly delay-line shaping was substituted for the first differentiation, the RC input network being removed and the 50ohm output of the charge sensitive preamplifier matched by the cable used to shape the pulse. Since only 100ohm cable was available in sufficient length, two shorted cables were used in parallel to avoid ringing (fig.62). After reference to Roush's paper (11) 300ns lengths were used giving a clipping at 600ns. An attempt to remove the pedestal on the clipped pulses by capacitive coupling (160) was abandoned lest it was degrading any distinctive feature of the waveform.

In a second investigation, the order of this shaping was reversed. The inverting stage was returned to its original form and the differentiation in the input stage was replaced. 330ohm cable matched at input was used as shown in Figure 63 to again provide a 600ns clipping. At best only very poor discrimination was obtained by either of these methods for a large range of differentiation constants (fig.64)

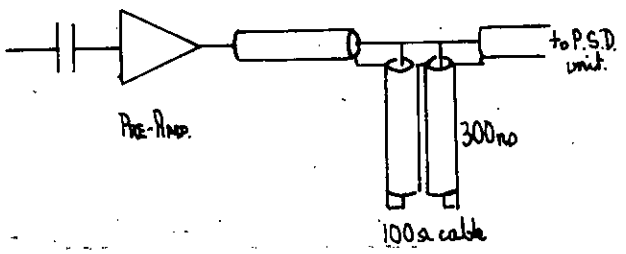

Fig. 62: DL shaping at pre-amp o/p.

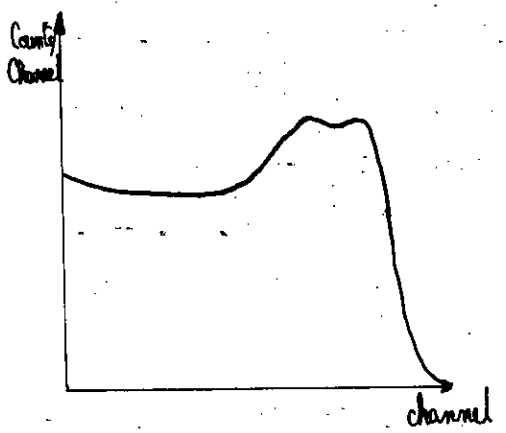

Fig. 64: Sketch of best performance obtained

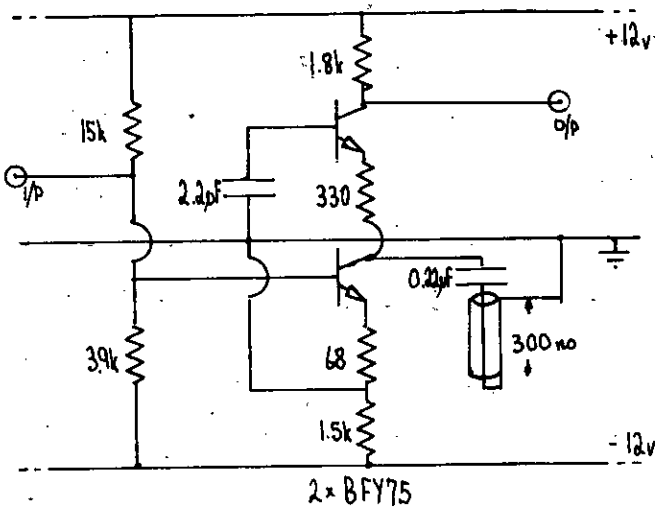

Fig. 63: P.S.D. input stage; DL shaping.

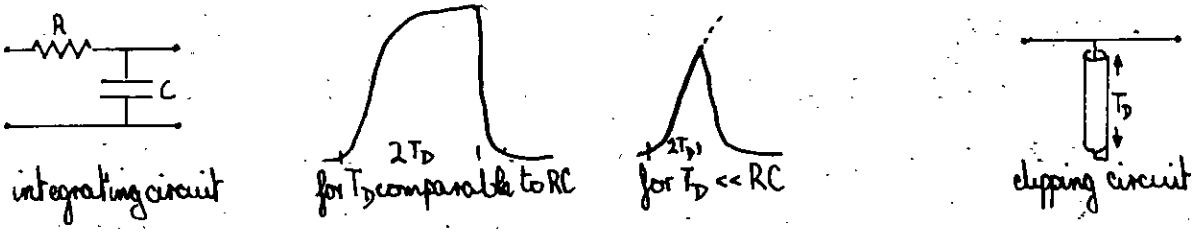

Fig. 65: The effect of adjusting the clipping time to much less than the integration time constant.

A possible explanation for the failure of these techniques may lie in the very long integration time constant of the preamplifier. As is shown in Figure 65 when the time constant is short or comparable with the clipping time the result is an inverted copy of the leading edge, but if an appreciable proportion of the integration is yet to occur when the pulse is clipped, the result is somewhat different and the eventual zero cross-over may not occur at a significant part of the pulse. It is worth noting however that the part of the pulse which is most significant i.e. particle dependent, depends on the type of tube used.

One marked disadvantage of the system described was the smallness of the dynode output pulses. Little was gained by changing the final stage resistor in the voltage divider and using the eleventh dynode output in preference to the tenth, as the output voltage was still limited by the deliberately saturation prone characteristics of this dynode chain.

4-3.1 Application with a fast tube.

The 56AVP with its larger current delivering capacity did not suffer from this problem. The linear output did suffer from the pick-up distortion and it was obvious that the final dynode should be used to reduce this to an acceptable level. Great improvement in P.S.D. performance was obtained when this dynode was used with the 10k variable resistor over the final stage replaced by 420k ohm in order to maintain the tapered voltage distribution referred to earlier (Sect.2-1). Under these conditions

the photomultiplier produced a linear output at the 14th dynode above 1,700volts but since the conventional preamplifier used limited at higher voltages, this value of EHT was not exceeded. Using this voltage preamplifier the integrating time constant could be adjusted to suit, and in the present application this was set to give a decay time constant of 400ns. By viewing the output pulses with an oscilloscope and adjusting components to obtain this value account was taken of stray capacitance in the voltage divider, in the short linking cable, and at the input of the preamplifier.

4-3.2 Design features and modification of the pulse shape discriminator.

In accordance with Roush's findings for the NE213 scintillator, a differentiating time constant of 400ns was also selected. Thus with the shaping set to suitable values, a systematic series of tests and substitutions was carried out on the P.S.D. unit to obtain improved performance. The performance was assessed using the Po^{210}- Be source, and the standard NE213 cell.

The differentiation constant is more precisely given as $(R + r_e)C$ where r_e is the emitter resistance of T_2. Since r_e is inversely proportional to the current drawn through T_2 for large pulses this resistance will decrease from, say, 5 to 4ohm, which for R = 100ohm represents a ~1% decrease in the differentiation constant. It is easy to visualise how this might be used to remove the curvature from the bi-dimensional display.

This curvature (Photograph 12) has been referred to by many researchers (58,59) and appears to be a characteristic of the particular scintillator. Figure 66 shows how the smaller pulses which are not so strongly differentiated will cross later than otherwise and hence the curvature may be compensated for.

Tests were performed for various values of R, adjusting C to keep RC constant, and noting the corresponding peak/valley ratios of discrimination spectra. On the basis of these the combination of 100ohm and 4,000pf. was selected as optimum.

The bi-dimensional display still shows an 'elbow' (fig,66) associated with low energy pulses which prevents discrimination down to such energies. This limitation is associated with the clipping diodes, the function of which is to prevent saturation in T_1 by shorting to earth all pulses larger than $\pm$0.6v. However this technique results in small pulses seeing a large load -1.8k in parallel with diodes - and large signals seeing the same until they reach 0.6v. when they are shorted. The larger pulses inevitably return to zero later than they should. An attempt was made therefore to make the small pulses also return slightly later by applying a very weak integration. For this purpose a small 1 - 10pf. variable capacitor was placed across the diodes. The bi-dimensional display was used to determine the best setting of the trimmer for reducing this 'elbow'. This was about 3pf. because at higher values the integration adversely affected the display in the high energy region. However the improvement was so marginal that it was not pursued.

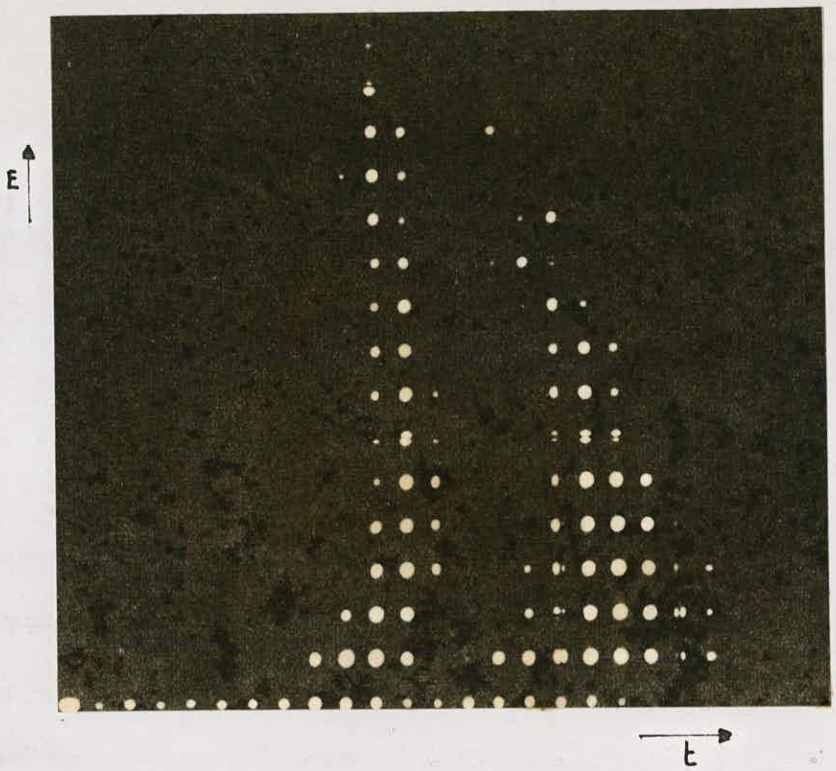

Photo.12: Bidimensional display for the timing technique (RC shaping).

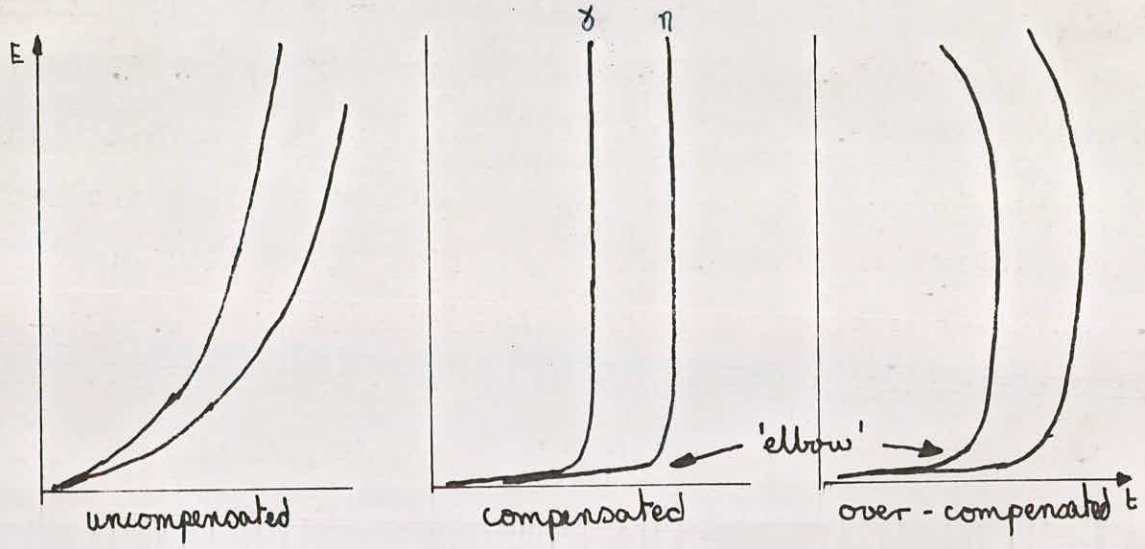

Fig.66: Bidimensional displays showing counteraction of pulseshape vari with energy.

Attempts to improve the clipping by the use of faster Ge diodes also failed. The smaller clipped pulses required further amplification and this was not easily available in the following stage. The final solution adopted was the use of a single diode (1N916) to clip the negative timed pulse and, since with no discharge path to earth it would charge up, a 10k ohm resistor was placed in parallel with the diode.

Additional precautions of a general nature were also taken. Heavy braiding was substituted for the earth line of the circuit which was mounted on 'Verobord'. The output stage, a compound common emitter, was separately de-coupled and small resistors placed on supply lines as it was known this output drew large surges of current from the supply and could feed back to earlier stages.

Consequent performance.

After these modifications had been performed a comparison of scintillators was performed. The results appear in Table 17 and an example (for NE213) in Figure 67. As with previous comparisons the tube H.T. was adjusted to obtain the same thresholds by reference to Na^{22} spectra. The count rate for the gamma-neutron source was maintained at 1 kcps.

Fig. 67: P.S.D. spectra with RC shaping.

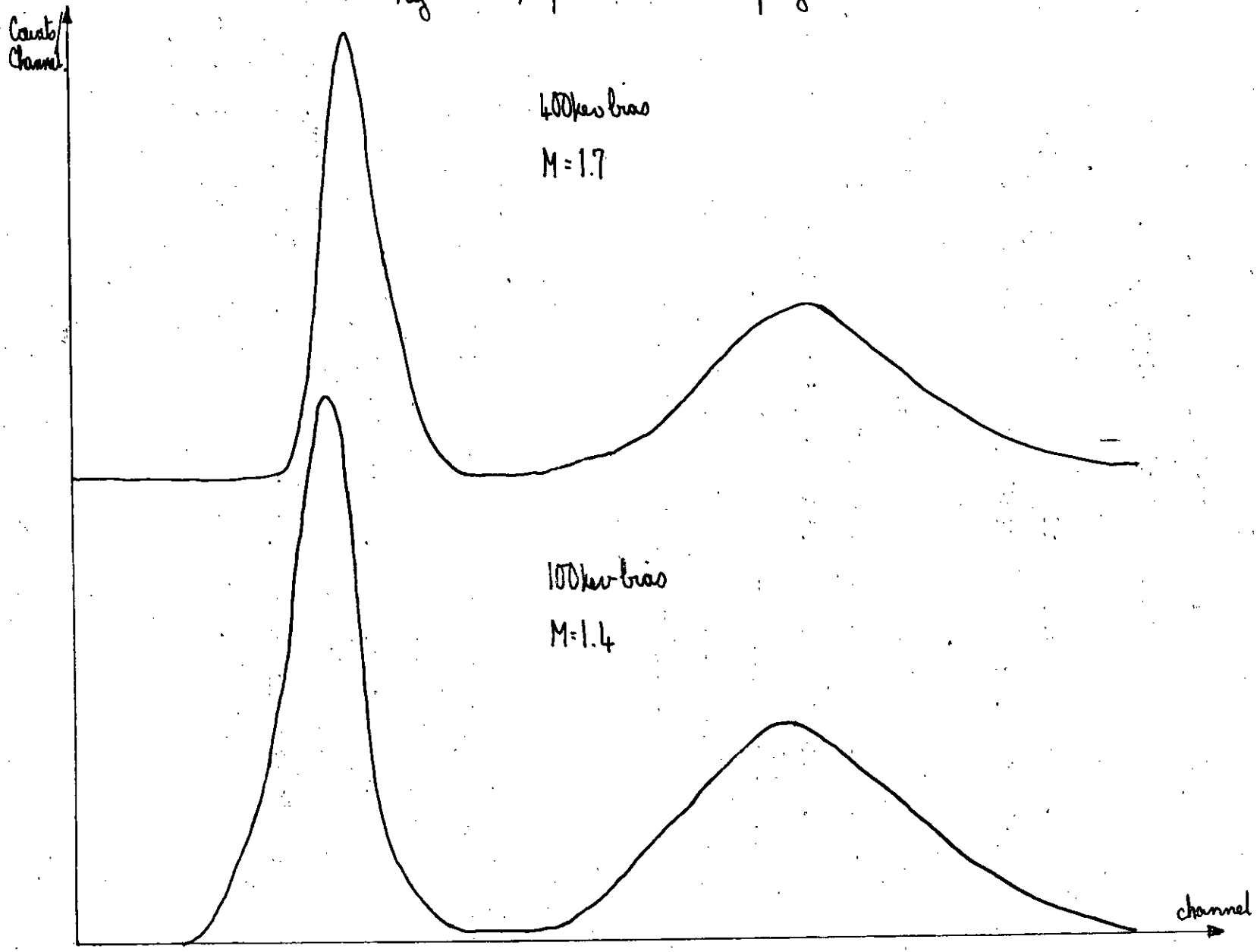

Table 17: P.S.D. performance with the 56AVP tube using the RC timing technique.

		M		P/V	
		equivalent electron recoil energy thresholds.			
Scintillator	Cell size	100kev	400kev	100kev	400kev
NE213 D	ϕ2" x2"	1.4	1.7	41.5	175
NE218 D	ϕ2" x2"	0.9	1.3	9.5	15.5
NE218E D	ϕ2" x2"	1.2	1.45	57.5	70
NE230	ϕ1½"x1"	0.5	0.7	1.5	2.5
NE232	ϕ1½"x1"				
KL360	ϕ2" x2"	1.1	1.2	10	14

D = standard cell.

In general, the performance is remarkable for the values obtained at low energy thresholds. It is noted from McBeth's article (2) that quality figures of 1.5 or better represent complete separation of radiations. However this technique does not appear tolerant of scintillators suspected of having different delay times and in this the figures for the last three scintillators are not truly representative.

4-3.3 Delay-Line and other forms of shaping.

Alternative forms of pulse shaping were also considered. Again refering to Roush's paper (11) it was found that unless

substantial re-designing was carried out, a simple RLC network to perform P.S.D. would require an inductance of 15μH! This was not attempted. Details in this paper relating to delay-line shaping are limited to stilbene, but extrapolating from the parameters for stilbene and NE213 in the case of RC - CR shaping tentative conclusions were reached: time constants of 1μs and 500ns were initially selected for the integration and delay-line clipping. It was also decided to incorporate a variable attenuator into the input of the unit to obtain the best timing from the converter.

4-3.4 Optimising and performance rating.

A systematic search for the best shaping parameters was then commenced. The circuit used is shown in Figure 68. With two preamplifiers in parallel attached to a single dynode output, there was complete freedom to adjust shaping parameters and attenuation. The non-inverting preamplifier was used as the linear output from which to derive a constant recoil electron energy threshold at 100kev, this being checked whenever adjustments of the preamplifier integration time constants could have changed the effective load seen by the dynode output. The second preamplifier was used in the inverting mode, the output impedance being very closely matched by the 100 ohm variable length clipping delay-line. The input impedance of the inverting stage was effectively infinite, the gain of this stage being adjusted to suit the P.S.D. unit. The performance of the assembly was judged by comparisons of figures-of-merit for spectra gated at a 100kev

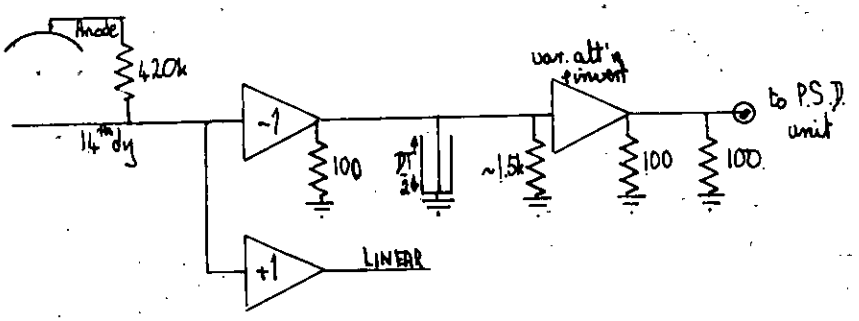

Fig. 68: Circuit for delay-line shaping.

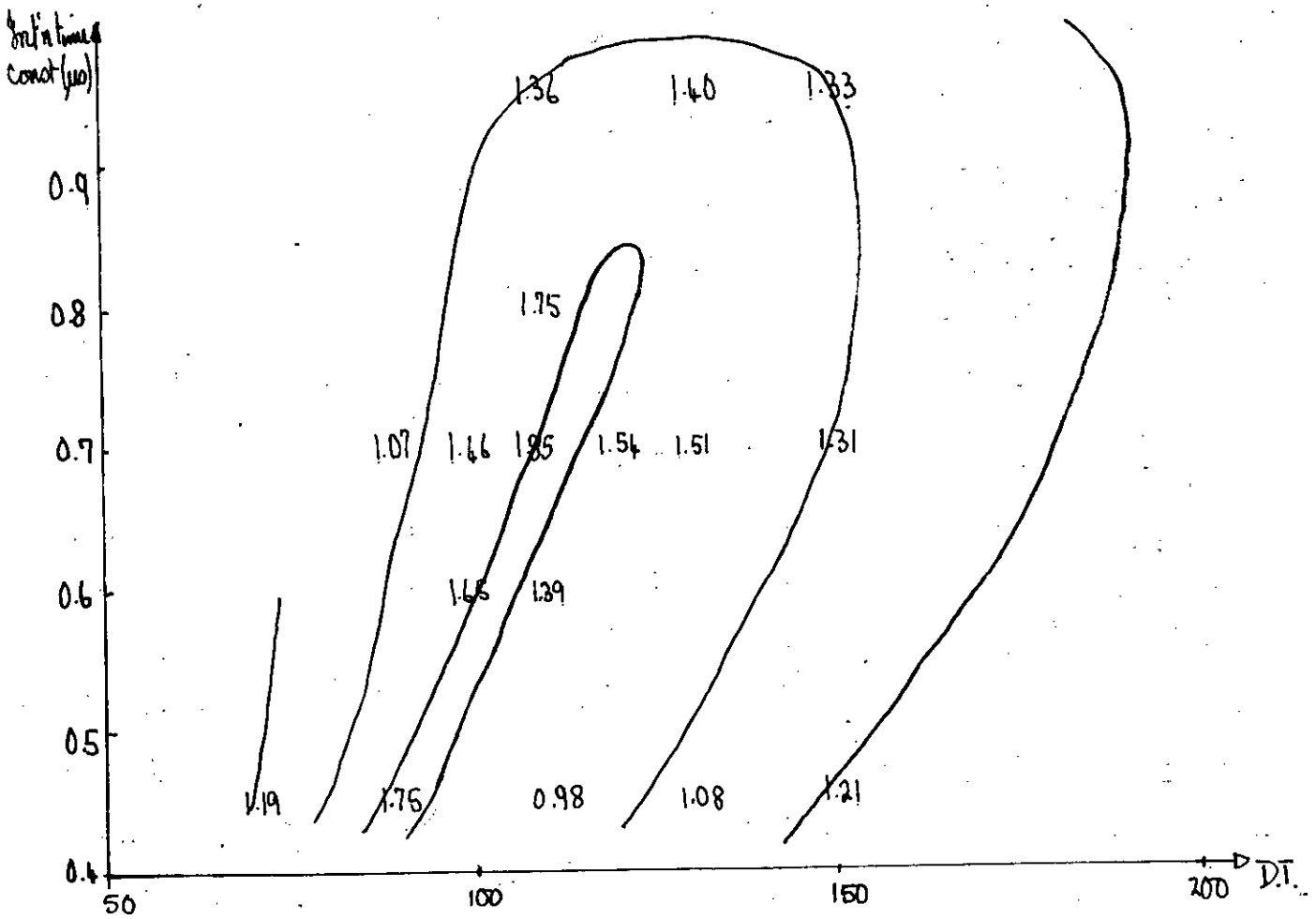

Fig. 69: Contour map of 'M' for delay-line shaping.

threshold, the standard NE213 cell and Po^{210}- Be source being used throughout.

The results of this experiment are displayed in a contour map of integrating time constants versus clipping delay line lengths (fig.69). Small inconsistencies in this graph were attributed to after-pulses occurring about 140ns after the main pulse commenced. On the basis of this graph, an integrating time constant of 0.65μs (as observed at the preamplifiers output) and a clipping time of 110ns were used.

Table 18: P.S.D. performance with the 56AVP tube using the DL timing technique.

		M		P/V	
		equivalent electron recoil energy thresholds			
Scintillator	Cell size	100kev	400kev	100kev	400kev
NE213 D	ϕ 2" x2"	1.85	2.05	31.5	140
NE218 D	ϕ 2" x2"	1.29	1.37	8.7	23
NE218E D	ϕ 2" x2"	1.82	2.00	15	150
NE230	ϕ 1½"x1"	0.95	1.03	4.2	4.9
NE232	ϕ 1½"x1"				
KL360	ϕ 2" x2"	1.50	1.65	13.5	38

D = standard cell.

With these shaping parameters a comparison of scintillators was performed, the quality factors in Table 18 being given for

thresholds of 100 and 400kev. In each case the H.T. was adjusted to obtain the same overall gain i.e. so that the threshold discriminator did not require adjustment and the signal sizes entering the P.S.D. unit were identical. An example of the spectra obtained is given for NE213 (fig.70).

4-4 Conclusions.

Comparing this DL shaping with the RC shaping considered earlier the above method appears to be more satisfactory for the deuterated and Koch-Light scintillators. The obvious advantage for the standard (D) cells lies in the flat bottomed valley, which in the case of NE213 (fig.70) is ~300mv wide. Thus the setting of the discriminator for gamma rejection is not crucial, and small changes due to temperature or power supply drift are of little consequence. Also it may be assumed that with this short 110ns clipping the count rate capability is correspondingly enhanced.

A comparison of Tables 16 and 17 indicates that the 56AVP photomultiplier is clearly superior to the 6097B when used in timing techniques of P.S.D. However in contrasting these performances note should be made that due to the limitation in pulse size in the smaller tube rather different methods were used in the two cases. With the slow tube where double differentiation was used, the optimum shaping constants were found to be similar to the integration and differentiation constants used for the fast tube, both providing a zero cross-over about 500ns after the pulse started. Table 19 compares the various figures-of-merit in

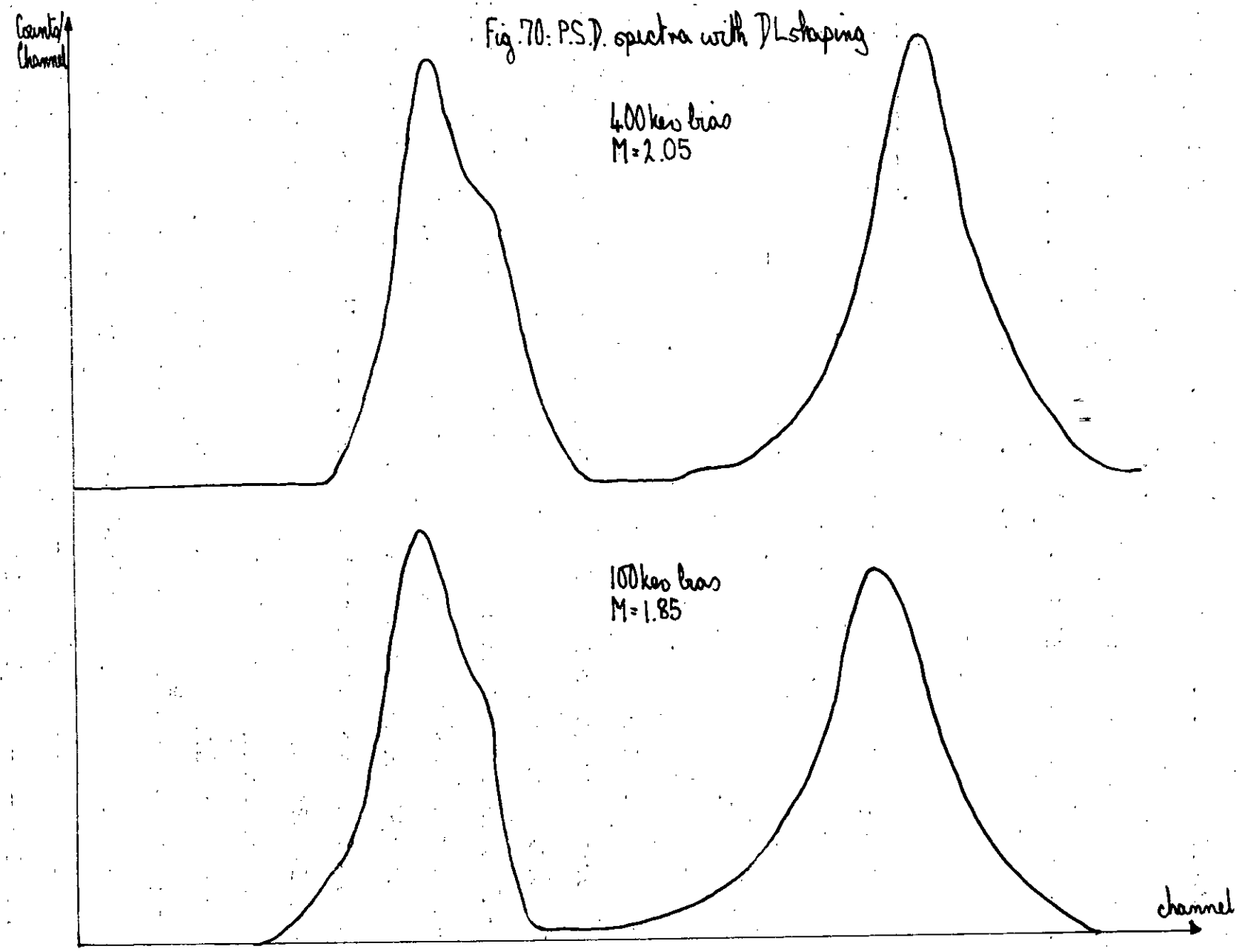

Fig.70: P.S.D. spectra with DL shaping

the two cases, for NE213. As would be expected in this applicati the fast tube is definately superior. Table 18 would indicate tha delay-line shaping techniques deserve more attention.

Table 19: Comparison of tubes for the timing technique.

Expt'l Details	P/V	Neutron acceptance	Gamma rejection	M
		6097B above 500kev		
NE213 D(2"x2") Po^{210}- Be source 1,000cps	22.5:1	99.89%	99.89%	1.30
		56AVP above 100kev.		
	41.5:1	99.86%	99.90%	1.4
		56AVP above 400kev.		
	175:1	99.97%	99.98%	1.7

A comparison with standards of discrimination by the timing technique obtained by other researchers may be made using Table 3. The performance of both RC and delay-line shaping with the 56AVP and NE213 is as good or superior to anything produced before. The one exception to this is the work of Bucher (58)(Sect1-4.3

The performances of the two tubes in the Owen technique have already been dealt with. Considering the results obtained for each tube with the two techniques one sees little difference in performance from the slow tube (Tables 7&16 8&17) but a marked improvement in using the 56AVP with the timing technique. However in certain applications sufficient discrimination over a wider energy range may be obtained using the most economical combination of components, and without any stringent requirements on the associated

electronics. It is worth repeating that the base of the gamma-neutron valley in this Owen technique is at least 1v. wide (fig,43).

The timing technique based on the Owen technique also deserves further attention. From the investigations carried out it is concluded that this little-used technique, when applied to a fast tube inherits the attributes of both the other methods dealt with. Both the precision of the timed cross-over and the sharp distinction of radiations associated with the Owen technique play their part in making this an excellent method of P.S.D. In general terms, it appears that the Owen technique depends less critically for its functioning on the characteristics of the scintillators. Certainly when the plastics referred to earlier (Sect.3-2.6) were used with the timing technique absolutely no discrimination was observed. Presumably after careful re-designing of the photomultiplier dynode chains, suitable shaping parameters could be found for these scintillators just as they were determined for NE213.

CHAPTER 5.

Possible Improvements.

The source of P.S.D. in the liquid organic scintillator is understood (5,162) but since the chemical features associated with these characteristics are not known, the production of better discriminating scintillators is largely a matter of trial and error. However, recent advances suggest r.f. stimulation of the scintillator as a means of shaping the fluorescence pulses to eliminate noise and enhance the neutron-gamma separation (162).

Separation may be further enhanced if some well-defined relation between fluorescence spectra and incident radiation can be found. The research into the decay time versus wavelength relations (163-165) has not shed any new light on the subject, but recent work by Langenscheidt (166) implies that spectral filters or cathodes with selected spectral responses may preferentially detect the desired radiation. Such a technique was used by Hrehuss (167) for alpha-gamma discrimination in CsI(Tl).

In timing applications where a fast tube is used, the findings of Bengston (168) suggest that increasing the efficiency of the photocathode is the simplest way of improving time resolution. Taylor,(49) thinking more in terms of photon detection efficiency, reasoned that a change to a superior photocathode should halve the energy threshold at which acceptable discrimination might be obtained. An alternative method of obtaining higher timing resolution may be provided by the hybrid photomultiplier proposed by Chevalier

(169,170). Reduction in the transit time spread may be achieved by the use of larger voltages over parts of a conventional photomultiplier as suggested by Brest (171).

In the Owen technique it appears likely that in some photomultipliers the geometry or spacing of the anode and last dynode may be specially suitable for producing the optimum filter for P.S.D. Only a careful survey of many tubes could establish this.

The sampling technique suggested by Tojo has many desirable properties. Apart from complete freedom to make the most of pulse shape differences, there is the advantage of ease of adjusting for other scintillators with unknown characteristics. This appears to be a great disadvantage of the timing technique and to a lesser extent of the Owen technique as well.

APPENDIX 1.

Field conditions due to Space Charge.

The avoidance of space charge saturation in the final stage of a photomultiplier has been extensively treated elsewhere (172). The simpler treatment here verifies the effect of the space charge on field distributions assumed earlier.

From Maxwell's first equation and the definitions of charge density and potential:

$$E = -\frac{dV}{dx} \tag{1}$$

$$\rho = \epsilon \frac{dE}{dx} \tag{2}$$

$$V = \frac{J}{\rho} \tag{3}$$

The last dynode-anode current variation may be associated with V_o, the average velocity for electrons leaving the dynode. When this is zero, there are equal numbers of electrons leaving and returning to the dynode. Thus the electron velocity at various points with associated V(x) is:

$$V = \left[-\frac{2q}{m}V + V_o^2\right]^{\frac{1}{2}} \tag{4}$$

Re-writing (2) in terms of potential and velocity:

$$-\frac{d^2V}{dx^2} = \frac{J}{\epsilon V}$$

and substituting from (4)

$$\frac{d^2V}{dx^2} = \frac{J}{\epsilon}\left[-\frac{2q}{m}V + V_o^2\right]^{-\frac{1}{2}}$$

giving V as a function of x alone.

Solution:-

Let $\frac{d^2V}{dx^2} = p\frac{dp}{dV}$ where $p = \frac{dV}{dx}$

$$pdp = \frac{J dV}{\epsilon\left(\frac{-2qV}{m} + v_0^2\right)^{\frac{1}{2}}}$$

and $$\frac{1}{2}p^2 = \frac{2J}{\epsilon}\frac{\left(\frac{-2qV}{m} + V_0^2\right)^{\frac{1}{2}}}{-2q/m} + \text{Constant, by integration.}$$

When $x = 0$, $V = 0$ and $-p = E_0 = -\left(\frac{dV}{dx}\right)_0$

$$\text{Constant} = \frac{1}{2}E_0^2 + \frac{mJv_0}{q\epsilon}$$

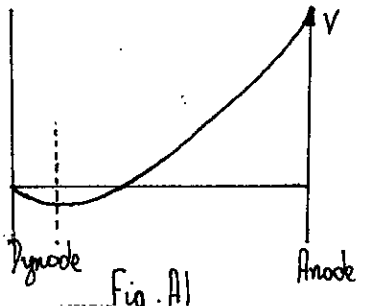

Fig. A1

Accordingly there must be a point given by:

$$\frac{Jm}{q\epsilon}\left(\frac{-2qV}{m} + v_0^2\right)^{\frac{1}{2}} = \frac{1}{2}E_0^2 + \frac{mJv_0}{q\epsilon} \qquad (5)$$

at which $p = \frac{dV}{dx} = 0$ - a minimum (fig.A1') corresponding to a virtual dynode and also the maximum space charge density.

Re-writng (5) as:

$$V = -\frac{m}{2q}\left(\left(\frac{q\epsilon E_0^2}{2Jm} + v_0\right)^2 - v_0^2\right)$$ it may be seen that as v_0 increases, reflecting closely the variation in the current pulse, V becomes more negative and the space charge more positive.

This mechanism thus serves as a velocity filter. Under idealised conditions the effect of varying v_0 and varying space charge repulsion may cancel out these conditions being obtained by the best choice of dynode-anode voltages and geometries. It is equally probable that suitable adjustment of these parameters will make the system very sensitive to low intensity changes in dynode current.

APPENDIX 2.

Theory of Owen pulse height and zero cross-over discrimination.

Since it has been shown experimentally (17) that the fast component of the scintillation is particle independent, the P.S.D. theory should be applied from the point at which the slow component becomes operative. Let t = 0 at this point in time and the corresponding voltage of the Owen pulse by $V = -V_0$ (fig.22).

Considering the last dynode circuit (fig.41).

$$C\frac{dV}{dt} + \frac{V}{R} = I_2 - I_1 = (\delta - 1) I_s \exp(-t/\tau_s) \qquad (1)$$

where $I_1 = I_s \exp(-t/\tau_s)$ and $I_2 = \delta I_1$

I_s is the initial value of the slow component of the current pulse.

τ_s is the decay time of the slow component.

δ is the multiplication factor at the last dynode (assumed constant

Taking the integrating factor exp (t/RC), eq.(1) becomes:

$$\frac{dV}{dt}\exp(t/RC) + \frac{V}{RC}\exp(t/RC) = \frac{(\delta-1)I_s}{C}\exp t\left(\frac{1}{RC} - \frac{1}{\tau_s}\right)$$

or

$$\frac{d}{dt}\left(V\exp(t/\tau)\right) = \frac{V_s}{\tau}\exp t/\tau_a \qquad (2)$$

where $V_s = R I_s (\delta - 1)$, $\tau_a = (\tau^{-1} - \tau_s^{-1})^{-1}$, and $\tau = RC$.

Integrating (2) $\quad V\exp(t/\tau) = \frac{\tau_a V_s}{\tau}\exp t/\tau_a + G$

and since $V = -V_0$ when $t = 0$ $\quad G = -\left(V_0 + \frac{\tau_a V_s}{\tau}\right)$

$$V = \frac{\tau_a V_s}{\tau}\exp t\left(\frac{1}{\tau_a} - \frac{1}{\tau}\right) - \left(V_0 + \frac{\tau_a V_s}{\tau}\right)\exp(-t/\tau)$$

When $V = 0$, $t = t_o$

$$\exp t_o/\tau_a = \left(V_o + \frac{\tau_a V_s}{\tau}\right) \Big/ \frac{\tau_a V_s}{\tau}$$

$$t_o = \tau_a \ln\left(\frac{V_o}{V_s}\frac{\tau}{\tau_a} + 1\right) \qquad (3)$$

Re-express V as:-

$$V = \frac{\tau_a V_{as}}{\tau} \exp\left(-t/\tau_s\right) - \left(V_o + \frac{\tau_a V_s}{\tau}\right) \exp\left(-t/\tau\right) \qquad (4)$$

When $\frac{dV}{dt} = 0$, $V = V_p$

$$\frac{dV}{dt} = -\frac{\tau_a V_s}{\tau \tau_s} \exp\left(-t/\tau_s\right) + \frac{1}{\tau^2}\left(V_o\tau + V_s\tau_a\right) \exp\left(-t/\tau\right)$$

$= 0$ when $V = V_p$ and $t = t_p$ (value at maximum of overswing)

$$\exp t_p\left(-\frac{1}{\tau_s} + \frac{1}{\tau}\right) = \tau_s\left(\frac{V_o\tau}{\tau_a V_s \tau} + \frac{V_s\tau_a}{\tau_a V_s \tau}\right) = \frac{\tau_s}{\tau_a}\frac{V_o}{V_s} + \frac{\tau_s}{\tau}$$

and

$$t_p = \tau_a \ln\left|\frac{\tau_s}{\tau_a}\frac{V_o}{V_s} + \frac{\tau_s}{\tau}\right|$$

Substituting in (4)

$$V_p = \frac{\tau_a V_s}{\tau}\left(\frac{\tau_s V_o}{\tau_a V_s} + \frac{\tau_s}{\tau}\right)^{-\tau_a/\tau_s} - \left(V_o + \frac{\tau_a V_s}{\tau}\right)\left(\frac{\tau_s V_o}{\tau_a V_s} + \frac{\tau_s}{\tau}\right)^{-\tau_a/\tau}$$

$$= \frac{\tau_a V_s}{\tau}\left(\frac{\tau_s V_o}{\tau_a V_s} + \frac{\tau_s}{\tau}\right)^{-\tau_a/\tau_s} - \frac{\tau_a V_s}{\tau_s}\left(\frac{\tau_s V_o}{\tau_a V_s} + \frac{\tau_s}{\tau}\right)\left(\frac{\tau_s V_o}{\tau_a V_s} + \frac{\tau_s}{\tau}\right)^{-\tau_a/\tau}$$

$$= \frac{\tau_a V_s}{\tau}\left(\frac{\tau_s V_o}{\tau_a V_s} + \frac{\tau_s}{\tau}\right)^{-\tau_a/\tau_s} - \frac{\tau_a V_s}{\tau_s}\left(\frac{\tau_s V_o}{\tau_a V_s} + \frac{\tau_s}{\tau}\right)^{-\tau_a/\tau_s}$$

$$= V_s\left(\frac{\tau_s V_o}{\tau_a V_s} + \frac{\tau_s}{\tau}\right)^{-\tau_a/\tau_s}\left(\frac{\tau_a}{\tau} - \frac{\tau_a}{\tau_s}\right) = V_s\left(\frac{\tau_s V_o}{\tau_a V_s} + \frac{\tau_s}{\tau}\right)^{-\tau_a/\tau_s} \qquad (5)$$

From (5):

$$\frac{T_s}{T} + \frac{T_s}{T_a}\frac{V_o}{V_s} = \left(\frac{V_s}{V_p}\right)^{T_s/T_a}$$

and

$$1 + \frac{T}{T_a}\frac{V_o}{V_s} = \frac{T}{T_s}\left(\frac{V_s}{V_p}\right)^{T_s/T_a}$$

Substituting in (3):

$$t_o = T_a \ln \frac{T}{T_s}\left(\frac{V_s}{V_p}\right)^{T_s/T_a}$$

$$= T_a \ln \frac{T}{T_s} + T_s \ln\left(\frac{V_s}{V_p}\right) \qquad (6)$$

Equations (5), (3), and (6) appear as equations (1), (2) and (3) on P. 45

APPENDIX 3.

Theory of zero cross-over timing techniques.

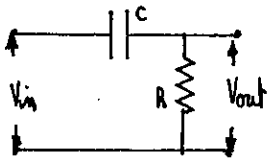

For a differentiating circuit as shown:

$$\frac{dV_{out}}{dt} + \frac{V_{out}}{RC} = \frac{dV_{in}}{dt} \qquad (1)$$

If $$V_{in}(t) = V_0 \exp(-t/\tau)$$

where τ is the decay time constant of the input voltage pulse, them for (1) the Complementary Function is:

$$V_{out} = A \exp(-t/RC)$$

To determine the Particular Integral let:

$$V_{out} = H \exp(-t/\tau)$$

and substitute in (1)

$$-\frac{H}{\tau}\exp(-t/\tau) + \frac{H}{RC}\exp(-t/\tau) = -\frac{V_0}{\tau}\exp(-t/\tau)$$

$$\therefore \quad H = \frac{V_0}{\tau}\left(\frac{\tau RC}{RC-\tau}\right)$$

the Particular Integral is $$V_{out} = \frac{V_0 RC}{RC-\tau}\exp(-t/\tau)$$

the General Solution is $$V_{out} = \frac{V_0 RC}{RC-\tau}\left(\exp(-t/\tau) + A\left(\frac{RC-\tau}{V_0 RC}\right)\exp(-t/RC)\right)$$

and since $V_{out} = V_0$ at $t = 0$ $$V_0 = \frac{V_0 RC}{RC-\tau}\left(1 + \frac{A(RC-\tau)}{V_0 RC}\right)$$

$$\therefore \quad A = \left(\frac{RC-\tau}{RC} - 1\right)\frac{V_0 RC}{RC-\tau}$$

$$= -\frac{V_0 \tau}{RC-\tau}$$

the General Solution becomes:

$$V_{out} = \frac{V_0 RC}{RC-\tau}\left(\exp(-t/\tau) - \frac{\tau}{RC}\exp(-t/RC)\right)$$

Providing $RC \neq \tau$, when $V_{out} = 0$

$$\exp t_0\left(\frac{1}{RC} - \frac{1}{\tau}\right) = \frac{\tau}{RC}$$

$$t_0 = \frac{RC\tau}{\tau - RC} \ln \frac{\tau}{RC}$$

This indicates that t_0, the time of zero-crossing, is dependent only on the pulse decay constant and the shaping parameters.

ACKNOWLEDGEMENTS.

I wish to thank Professor N.Feather, F.R.S. for the facilities provided for this research. I am particularly grateful to Dr.R.B.Galloway, my supervisor, for his guidance, interest and advice throughout these studies and also to Dr.D.G.Vass and Mr.H.Davie for many helpful suggestions and interesting discussions on particular aspects of the work.

The research could not have been performed without the willing co-operation of Nuclear Enterprises Ltd. who loaned most of the scintillators investigated, or without the assistance provided by Mr.D.Aliaga-Kelly, Mr.W.Morton and many others of that firm.

I am extremely grateful to Mr.H.J.Napier for his help in diverse ways, in particular for maintaining and operating the H.T. set, and also to Messrs. G.Turnbull and D.G.P.Green for their willing assistance.

REFERENCES.

1 - Owen,R.B. Trans. of I.R.E. on Nuclear Science 9/3 (1962) 285

2 - McBeth,G.W. et al. Koch-Light Labs. Ltd., Booklet '71 "Pulse Shape Discrimination with Organic Scintillators". Nucl. Instr. &. Methods to be published.

3 - Sabbah,B. et al. Nucl. Instr. &. Methods 58 (1968) 102.

4 - Birks,J.B. "Theory and Practice of Scintillation Counting". Pergamon Press (1964).

5 - Horrocks,D.L. etal. "Organic Scintillators and Liquid Scintillation Counting, Proceedings of the International Conference on". (July 1970) San Francisco, California University.

6 - Horrocks,D.L. Applied Spectroscopy 24 (1970) 397

7 - Owen,R.B. Nucleonics 17/9 (1959) 92

8 - Gatti,E. et al. Nucl. Instr. &. Methods 30 (1964) 213

9 - Reid,W.B. et al. Can. Nucl. Tech. 5 (1966) 36

10 - Bucher,W.P. et al. Rev. Sci. Instr. 38 (1967) 1259

11 - Roush,M.L. et al. Nucl. Instr. &. Methods 31 (1964) 112

12 - Taylor,I.J. et al. Nucl. Instr. &. Methods 88 (1970) 267

13 - Johnson,F.A. Nucl. Instr. &. Methods 58 (1968) 134

14 - Jones,D.W. Nucl. Instr. &. Methods 62 (1968) 19

15 - de Vries,L.J. etal. 1962 Nuclear Electronics Conference (Belgrade)305

16 - Kastner,J. et al. Trans. of I.E.E.E. on Nuclear Science 17 (Feb.1970) 144

17 - Sjölin,P.G. Nucl. Instr. &. Methods 37 (1965) 45

18 - Williamson,T.A. Trans. of I.E.E.E. on Nuclear Science 14 (Feb.1967) 103

19 - Owen,R.B. Trans. of I.R.E. on Nuclear Science 5 (Dec.1958) 198

20 - Brooks,F.D. Nucl. Instr. &. Methods 4 (1959) 151

21 - Jackson,H.E. et al. Rev. Sci. Instr. 36 (1965) 419

22 - Yarom,A. et al. 1968 Nuclear Electronics Conference (Versailles) Art.9.

23 - Elron PSD -N-1: Elron Electronic Industries, Haifa, Israel.

24 - Johnson,P.A. et al. Nucl. Instr. &. Methods 93 (1971) 417

25 - Jones,D.W. Trans. of I.E.E.E. on Nuclear Science 15 (June 1968) 491

26 - Doolin,V.A. et al. Nucl. Instr. &. Methods 82 (1970) 178

27 - Omel'yanenko,A.A. Instr. &. Exper. Tech. 16 (1970) 87

28 - Daehnick,W. et al. Rev. Sci. Instr. 32 (1961) 666

29 - Richter,J.M. "Scattering of Fast Neutrons in Light and Medium Nuclei". M.Sc. Thesis, Ohio University, (1965)

30 - Mendell,R.B. et al. Rev. Sci. Instr. 34 (1963) 1356

31 - Co-nuclear NE 5553

32 - Bertin,A. et al. Nucl. Instr. &. Methods 68 (1969) 24

33 - St.Onge,R.N. et al. Trans. of I.E.E.E. on Nuclear Science 15 (1968) 264

34 - St.Onge,R.N. et al. Nucl. Instr. &. Methods 69 (1969) 25

35 - Horrocks,D.L. Progress in Nuclear Energy Ser. IX Anal. Chem. 7 (1966) 21 Pergamon Press

36 - Forte,M. et al. 1962 Nuclear Electronics Conference (Belgrade) 277

37 - Nadav,E. et al. Nucl. Instr. &. Methods 33 (1965) 289

38 - Orman,P.R. Nucl. Instr. &. Methods 21 (1963) 121

39 - Kowalski,E. "Nuclear Electronics", Springer-Verlag (1970)

40 - Schweimer,W. Nucl. Instr. &. Methods 39 (1966) 343

41 - Fülle,R. et al. Nucl. Instr. &. Methods 35 (1965) 250

42 - Mathe,Gy. Nucl. Instr. &. Methods 39 (1966) 356

43 - Tietsch,R.A. et al. Trans. of I.E.E.E. on Nuclear Science 14 (Feb.1967) 131, 406

44 - Soucek,B. et al. Nucl. Instr. &. Methods 50 (1967) 71

45 - Brady, F.P. et al. Nucl. Instr. &. Methods 81 (1970) 280

46 - Alston,W.J. et al. Nucl. Instr. &. Methods 35 (1965) 155

47 - Kozlowski,T. Nukleonika 13 (1968) 999

48 - Wakuba,Y. et al. Nucl. Instr. &. Methods 71 (1969) 133

49 - Taylor,I.J. et al. Nucl. Instr. &. Methods 88 (1970) 277

50 - Kahane,J. et al. Rev. de Phys. Appl. 4 (1969) 257

51 - Gatti,E. et al. Energia Nucleare 17 (1970) 34

52 - Alexander,T.K. etal. Nucl. Instr. &. Methods 13 (1961) 1244

53 - Peele,R.W. et al. N.R.C. Nucl. Sc. Report 40, 146

54 - Landis,D. et al. N.R.C. Nucl. Sc. Report 40, 143

55 - Miller,T.G. Nucl. Instr. &. Methods 63 (1968) 121

56 - Cialella,C.M. et al. Nucl. Instr. &. Methods 60 (1968) 269

57 - Trans. of I.E.E.E. on Nuclear Science 13 (Feb.1966) 394

58 - Bucher,W.P. et al. Rev. Sci. Instr. 39 (1968) 165

59 - Heistek,L.J. et al. Nucl. Instr. &. Methods 80 (1970) 213

60 - Burrus,W.R. et al. Nucl. Instr. &. Methods 67 (1969) 181

61 - McBeth,G.W. et al. Nucl. Instr. &. Methods 93 (1971) 99

62 - Bell,R.E. Nucl. Instr. &. Methods 42 (1966) 211

63 - Jones,D.W. et al. Nucl. Instr. &. Methods 59 (1968) 309

64 - Bass,R. et al. Nucl. Instr. &. Methods 30 (1964) 237

65 - Gedke,D.A. et al. Nucl. Instr. &. Methods 55 (1967) 377

66 - Gedke,D.A. et al. Nucl. Instr. &. Methods 58 (1968) 253

67 - McDonald,W.J. et al. 1968 Nuclear Electronics Conference (Versailles) Art.56

68 - Kuchnir,F.T. et al. Trans. of I.E.E.E. on Nuclear Science 15 (Junel968) 107

69 - Kimbara,S. et al. Nucl. Instr. &. Methods 67 (1969) 261

70 - Kimbara,S. et al. Nucl. Instr. &. Methods 70 (1969) 173

71 - Furuta,Y. Nucl. Instr. &. Methods 84 (1970) 269

72 - Ortec 458

73 - Johnson,F.A. Nucl. Instr. &. Methods 78 (1970) 1

74 - Gatti,E. et al. 1962 Nuclear Electronics Conference (Belgrade) 275

75 - Adam,A. et al. Rev. de Phys. Appl. 4 (1969) 262

76 - Donati,S. et al. Electronics and Electron Physics 26 (1969) 306

77 - Broek,H.W. et al. Rev. Sci. Instr. 31 (1960) 1063

78 - Litherland,A.E. et al Phys. Rev. Lets. 2 (1959) 104

79 - Batchelor,R. et al. Nucl. Instr. &. Methods 8 (1960) 146

80 - Kaman Aircraft Corporation.

81 - Hahn,O.J. et al. Nucl. Instr. &. Methods 27 (1964) 323

82 - Johnson,F.A. Can. Jour. Phys. 41 (1963) 793

83 - Doke,T. et al. Nucl. Instr. &. Methods 57 (1967) 163

84 - Hiramoto,T. et al. Nucl. Instr. &. Methods 58 (1968) 167

85 - Hsu,T.H. Nucl. Instr. &. Methods 39 (1966) 8

86 - Fabiani,F. et al. Supl. al Nuovo Cimento 111 (1965) 187

87 - Tojo,O. Nucl. Instr. &. Methods 50 (1967) 38

88 - Lush,H.J. Jour. Sci. Instr. 42 (1965) 597

89 - Mullard Photomultiplier Tubes, Mullard Bulletin 23/007/D/E - 4 - 1963.

90 - Belletini,G. et al. Nucl, Instr. &. Methods 21 (1963) 106

91 - Gibson,W.A. Rev. Sci, Instr. 37 (1966) 631

92 - Stump,R. Rev. Sci. Instr. 25 (1954) 1132

93 - Flagge,B.d'E. etal. Rev. Sci. Instr. 26 (1955) 619

94 - Hendrick,R.W. Rev. Sci. Instr. 27 (1956) 240

95 - Kane,J.V. Rev. Sci. Instr. 28 (1957) 582

96 - Galloway,R.B. etal. Nucl. Instr. &. Methods 43 (1967) 55

97 - Jung,H. et al. Nucl. Instr. &. Methods 65 (1968) 178

98 - Looten,A. Nucl. Instr. &. Methods 71 (1969) 141

99 - Beckman

100 - RCA Photomultiplier Manual, Technical Series PT-61

101 - Vass,D.G. — Ph.D. Thesis, Edinburgh University '66

102 - Ashkin,J. et al. — Nuovo Cimento 13 (1959) 1246

103 - Galloway,R.B. et al. — Private communication.

104 - Walter,G. et al. — Trans. of I.E.E.E. on Nuclear Science 11 (June 1964).44

105 - Flynn,K.F. et al — Nucl. Instr. &. Methods 27 (1964) 17

106 - Bertolini,G. et al. — Trans. of I.E.E.E. on Nuclear Science 13 (June 1966) 119

107 - Kuijper,P. et al. — Nucl. Instr. &. Methods 42 (1966) 56

108 - Wasson,M.McN. — A.E.R.E. - R. 4244 (1963)

109 - Schuttler,R.J. — O.R.N.L. 3888 U.C. - 34 (1966)

110 - Ohgushi,A. — Jour.Nucl.Sci.&.Tech. 7 (1970) 466

111 - Toms,M.E. — Trans. of I.E.E.E. on Nuclear Science 17 (Junel970) 107

112 - Evans,R.D. — Handbuch der Physik 34 (1958) 218

113 - Koechlin,Y. — Jour.dePhys.etRad. 16 (1955) 849

114 - Harris,C.C. et al. — Trans. of I.R.E. on Nuclear Science 5 (Nov.1956) 87

115 - Crabb,D.G. et al. — Nucl. Instr. &. Methods 45 (1966) 301

116 - Kilvington,A.I. et al — Nucl. Instr. &. Methods 80 (1970) 177

117 - Ankenbrandt,C.M. et al. — Rev. Sci.Instr. 34 (1963) 647

118 - — Dow Corning,20-057; SISS Silicones France

119 - Kaiser,W.C. et al. — Trans. of I.E.E.E. on Nuclear Science 11 (Junel964) 29

120 - Heath,R.L. — N.A.S. N.S. 3107 Chem. (1962)

121 - Chery,R. — Jour.dePhys.etRad. 21 (1960) 679

122 - Rohde,R.E. — Trans. of I.E.E.E. on Nuclear Science 12 (Feb.1965)

123 - Paul,J.M. Nucl. Instr. &. Methods 89 (1970) 285

124 - Birth,G.S. Appl. OPtics 10 (1971) 687

125 - Bonitz,M. et al. Nucl. Instr. &. Methods 29 (1964) 309,314

126 - Morton,G.A. et al. Trans. of I.E.E.E. on Nuclear Science 14 (Feb.1967) 443

127 - Brochure P001 (fP70)

128 - Charpak,G. Nucl. Instr. &. Methods 48 (1967) 151

129 - Charpak,G. Nucl. Instr. &. Methods 51 (1967) 125

130 - Engstrom,R.W. etal. Nucleonics 10 (April 1952) 58

131 - Pietri,G. Acta Electronika 5 (1961) 7

132 - Davie,H. Ph.D. Thesis, Edinburgh University (1971)

133 - Hewlett Packard, 5554A

134 - Wadey,W.G. Rev. Sci. Instr. 27 (1956) 910

135 - Matveev,U.V. etal. Instr. &. Exper. Tech. 2 (1963) 116

136 - Leybold Cat. No. 555 58

137 - Leybold Bulletin 23E

138 - Krackhardt,R. "Vacuum Tube Electronics", Merrill Books ('66)

139 - Lavioe,L. et al. Rev. Sci. Instr. 40 (1969) 1350

140 - Suhami,A. et al. Nucl. Instr. &. Methods 30 (1964) 141

141 - Radiospares, 25 turn, 5% tolerance.

142 - Tanaka,O. Mitsubishi Denki Laboratory Reports (1963) 101

143 - Van der Zwan,L. Can. Jour. Phys. 46 (1968) 1527

144 - Ewer,M. Private communication.

145 - Berlman,I.B. etal. Trans. of I.E.E.E. on Nuclear Science 11 (June 1964) 27

146 - Smith,D.L. et al. Nucl. Instr. &. Methods 64 (1968) 157
147 - Czirr,J.B. Nucl. Instr. &. Methods 72 (1969) 23
148 - Czirr,J.B. Nucl. Instr. &. Methods 88 (1970) 321
149 - Brooks,F.D. et al. Trans. of I.R.E. on Nuclear Science 7 (Junel960) 35
150 - Koch-Light Labs. Ltd.
151 - Nuclear Enterprises Catalogue (1970) 4
152 - Golutvina,I.G. etal. Instr. &. Exper. Tech. 17/1 (1970) 95
153 - Mortinez,P. et al. Rev. Sci. Instr. 31/9 (1960) 974
154 - Galloway,R.B. et al. Nucl. Instr. &. Methods 83 (1970) 35
155 - Bertin,A. et al. Nucl. Instr. &. Methods 91 (1971) 649
156 - Werbinski,V.V. etal. Nucl. Instr. &. Methods 65 (1968) 8
157 - Lewis,I.A.D. et al. "Millimicrosecond Pulse Techniques", London Pergamon Press 1959
158 - Delaney,C.F.G. "Electronics for the Physicist", Penguin Books 1969.
159 - Herbst,L.J. "Discrete and Integrated Semiconductor Chapman and Hall 1969. Circuitry" P.34.
160 - Nowlin,C.H. et al. Rev.Sci.Instr. 36 (1965) 1830
161 - NE4603
162 - Short,A.M. et al. Appl. Phys. Let. 14 (1969) 303
163 - Amaldi,V. et al. Nucl. Instr. &. Methods 91 (1971) 477
164 - Miller,T.G. et al. Nucl. Instr. &. Methods 84 (1970) 147
165 - Miller,T.G. et al. As in (5) P.479
166 - Langenscheidt,E. Nucl. Instr. &. Methods 91 (1971) 237
167 - Hrehuss,G. Nucl. Instr. &. Methods 8 (1960) 344
168 - Bengstron,B. et al. Nucl. Instr. &. Methods 81 (1970) 109

169 - Chewlier,P. Nucl. Instr. &. Methods 50 (1967) 346

170 - Nussli,J. Phillips Tech. Rev. 30 (1969) 236

171 - Brest,J.D. et al. Rev. de Phys. Appl. 4 (1969) 299

172 - Leuba,P. Jour. de Phys. et Rad. 16 (1955) 298

JAN 1989